HEAT TRANSFER IN

FOAM INSULATION

by

Mark Anthony Schuetz

S.B. Massachusetts Institute of Technology, Cambridge
(1979)

Submitted to the Department of
Mechanical Engineering
in Partial Fulfillment of the
Requirements of the
Degree of

MASTER OF SCIENCE

at the

MASSACHUSETTS INSTITUTE OF TECHNOLOGY

December 1982

Massachusetts Institute of Technology

Signature of Author_____
Department of Mechanical Engineering
October 29, 1982

Certified by_____
Thesis Supervisor

Accepted_____
Chairman, Mechanical Engineering Department Committee

HEAT TRANSFER IN FOAM INSULATION

by

MARK ANTHONY SCHUETZ

ABSTRACT

A combined experimental, theoretical study has been performed on the heat transfer through foam insulation. A model is presented for conduction through the gas/solid structure with simultaneous radiation heat transfer. The model is easy to apply and requires a minimum number of experimentally determined properties. Some data is compared to the model's predictions.

Conduction through the solid is found to be a strong function of the percentage of the solid in struts versus membranes. Published conduction models do not take this factor into consideration and are therefore found seriously inaccurate for real foam. Upper and lower limits are placed on the conduction through real foam.

Published radiation models based on opaque cell walls are experimentally proven inaccurate. Polyurethane foam cell walls are found to be 80% transparent or higher, on average, over the infrared portion of the spectrum.

The extinction coefficient is analytically shown to be both necessary and sufficient for predicting radiation in most practical foam applications. A simple technique is presented for measurement of this property.

The absorption coefficient, scattering coefficient and phase function were measured for a polyurethane foam sample and for a glass fiber insulation sample. From these results the simple technique is shown to overestimate the extinction coefficient by approximately 11% for foams, and by 60% for glass fiber insulations. Radiation is shown to account for approximately 25% of the total heat transfer in foams. The error introduced by the simple technique results in an error of 2.5% for the overall heat transfer in foam. Recommendations are provided for improvement of the simple technique measurement accuracy without excessively increasing the complexity. The improved technique is expected to be applicable to glass fiber insulations as well as foams.

Addition of strongly absorbing particles is experimentally shown to decrease the overall heat transfer through foams by 6%.

ACKNOWLEDGEMENTS

TABLE OF CONTENTS

LIST OF TABLES

—

LIST OF FIGURES

LIST OF FIGURES (con't.)

—

a	absorption coefficient
A	area
b	center to center spacing
d	cubical cell "diameter"
D	depth
e_b	blackbody emissive power
i	summation index
I	intensity
j	summation index
k_f	overall foam conductivity
k_g	conductivity of gas
k_s	conductivity of solid
k_{s+g}	solid plus gas contribution
k_{r+s}	radiation plus solid contribution
K	extinction coefficient
l	length of bridge
L	overall foam thickness
n	number of paths
	or: index of refraction
N_{cr}	conduction-radiation number
q_c	conduction flux —
q_r	radiative flux
q_T	total flux
R	resistance
s	pathlength
S^2	strut cross-sectional area
t	wall thickness
T	temperature
T_*	arbitrary reference temperature
W	width
x	cartesian coordinate
y	cartesian coordinate
z	cartesian coordinate
α	angle defined in Figure 2-20
β	angle defined in Figure 2-20
γ	angle defined in Figure 2-20
$\hat{\epsilon}$	porosity
ϵ	emissivity
λ	wavelength
	or: constant length or area parameter

NOMENCLATURE

ϕ	azimuth (conduction)
Φ	phase function
ρ	density
ξ	arbitrary angle
ψ	azimuth (radiation)
σ	Stefan-Boltzmann constant
σ_S	scattering coefficient
θ	polar angle
τ	optical thickness
$\Delta\omega_L$	solid angle of laser beam
ω_o	incident beam solid angle
ω_s	albedo for scatter
Ω	solid angle

Subscripts

a	air
c	conduction
f	foam
g	gas
L	laser
LL	lower limit
M	measured
o	incident
r	radiation
s	solid or scatter
T	total
UL	upper limit
λ	spectral
$\perp$	perpendicular

1. BACKGROUND AND INTRODUCTION

Foam insulations have come to represent a large industry in the United States as well as in other countries. Foams have grown in popularity due to their superior thermal and mechanical properties compared to other insulations. The use of foam insulation is expected to expand in the future as energy saving becomes more important in people's thinking and as new and better foams are developed for new applications.

When a closed cell foam is blown with a low conductivity gas such as R-11 or R-12 (freon gas), the overall thermal conductivity of the foam is approximately two-thirds the conductivity of stagnant air with no radiation. In contrast, open celled foams and glass fiber insulations have overall conductivities from 1.3 to 2.0 times the conductivity of stagnant air. Unfortunately, when closed cell foam is left exposed to the atmosphere, the blowing agent (often R-11) diffuses out while oxygen, nitrogen and water vapor diffuse in. The gas in the cells is thus a mixture of oxygen, nitrogen, water and R-11. Over a period of a few years the foam conductivity rises to a level approximately equal to the conductivity of stagnant air. This process is called "aging" and clearly represents a substantial insulation performance degradation.

At the Massachusetts Institute of Technology, research on foam insulation is ongoing in the areas of aging and heat transfer modeling. This study is concerned with the heat transfer modeling question. One motivation for attempting to model the heat transfer through foam is to relate the gas diffusion results of the other researchers (Doug Reitz, Leon Glicksman) to data on overall thermal conductivity changes with time. Chapter 6 presents a model for predicting overall foam conductivity during aging. Given gas concentration profiles for each of the gases and given the thermal conductivity measured at a time when the gas composition is known, the model predicts overall foam conductivity within 0.5%.

One further motivation for understanding the heat transfer problem is to develop foams with lower thermal conductivities at the time of foaming. Once the heat transfer mechanism is properly understood, development work to produce better foams may be pursued in a more mechanistically directed way than has been possible in the past. Some early successes from this new approach are presented in Chapter 7.

1.1 Problem Statement

The motivation of this study is to develop lower conductivity foams and to provide the heat transfer model which is required for the aging studies ongoing at MIT. In a broad sense, the problem is therefore to predict the overall thermal conductivity under a wide range of conditions. Empirical correlations are not useful because they cannot provide the insight which is desired.

In order to achieve these goals, the authors have undertaken the problem of developing a physically realistic model for heat transfer through foamed materials. This development requires theoretical and experimental research to correctly understand the three important contributors to heat flow: conduction through the gas, conduction through the solid, and radiation. It is also necessary to be able to estimate the effects of interactions of these three contributors. It was anticipated that a simple model requiring a minimum number of measured properties could be developed, based on the proper understanding of the basic heat transfer mechanisms.

While it would be possible to solve the integro-differential equation of radiative transfer simultaneously with the conduction equation, this would require knowledge of certain material properties (absorption and scattering coefficients, phase function) which are not reported in the literature. Techniques for the experimental determination of these properties are not found in the literature either. No one has developed an experimental technique which fully characterizes the material's radiation properties.

The problem therefore entails experimental determination of the material's radiation properties as well as development of a model in which to use the experimental results. As will be seen in succeeding chapters, the experimental results themselves provided the physical insight required to determine which simplifications to the general radiation theory are accurate and thus applicable.

A pure conduction model is also required for the foamed structure. The solid has a much higher conductivity than the gas, but only occupies a small percentage of the volume. We will show in Chapter 2 that the previously published models for this conduction problem are inaccurate for the real foam geometry.

1.2 Review of the Literature

A recent review of the foam heat transfer literature was published by Valenzuela and Glicksman (1). They show that convection within the cells is negligible. An expression developed by Doherty (3) is used for the effective conductivity of the medium in the absence of radiation along with an expression for the effective "radiation contribution" which assumes that cell walls are opaque in the infrared. This combined model is shown to underestimate the data for overall foam conductivity by approximately 25%. They identify the major source of the discrepancy to be poor modeling of the radiation heat transfer.

Conduction Literature

The majority of the foam heat transfer literature use the models which Valenzuela and Glicksman (1) showed to be inaccurate, or other models in a similar vein. For example, Baxter and Jones (15) correctly point out that the conduction problem is analogous to electrical conduction in a composite medium and that the theoretical results of Kerner (34), and others apply. The conduction model which Baxter and Jones adopt may be shown to predict essentially the same results at low

densities as the equation proposed by Russell (2). Also, when the equation proposed by Doherty,et al. (3) is modified for three dimensional bubbles (rather than the two dimensional case he presents), his equation also produces the same result at low densities. Unfortunately, none of these equations are accurate for real foam. These expressions would be correct if the foam consisted of bubbles with uniform wall thickness throughout. In real foam, a considerable portion of the solid material builds up in the corners of bubbles. This results in rigid, stick-shaped elements called struts. We will show in Chapter 2 that the presence of struts significantly decreases the calculated conduction heat transfer.

Radiation Literature

The treatment of radiation by previous authors in the foam literature must be re-examined. Norton (17) dismisses radiation entirely without giving an explanation as to why it may be dismissed. Papers by Skochdopole (18), and Doherty, et al. (3) both state that the radiant heat flux in foams may be estimated by treating the cell walls as opaque. As will be seen in Chapter 4, cell walls in foams are at least 80% transparent over the wavelength range of interest.

The heat transfer literature dealing with the general problem of simultaneous radiation and conduction in a homogeneous medium is more applicable to the problem of heat transfer in foam than are many references specifically addressed to radiation in foam. Viskanta (11) formulated and numerically solved the case of simultaneous conduction

and radiation in absorbing and isotropically scattering gray materials. Fine, et al. (12) also numerically solved this case and furthermore showed for sufficiently optically thick media that this problem may be solved within 0.5% with a greatly simplified model based on the Rosseland diffusion approximation. See Hottel (20) for a clear derivation of the Rosseland diffusion approximation. We will show experimentally that the conditions for this simplified model are met in polyurethane foam, except for the requirement of isotropic scattering. Glass fiber insulation will be shown to be sufficiently optically thick also, but nonisotropic scattering and highly non-gray behavior makes the simplified model less accurate for glass fiber insulation.

The most general case - a nongray medium which conducts, absorbs, emits and nonisotropically scatters - has been numerically solved by Houston (14) and by Koram (33). Their research was directed toward the problem for glass fiber insulation and therefore the solutions are for values of the radiation parameters found in that insulation.

The nonisotropic scattering case is the most difficult problem to solve. Accordingly, various approximations may be found in the literature including the two flux approximation by Larkin and Churchill (21) and the linear anisotropic scattering approximation by Dayan and Tien (22). Probably the best available solution to the nonisotropic scattering problem is the P-1 approximation presented most clearly by Lee and Buckius (23). This approximation provides a simple way to modify the scattering coefficient so the nonisotropic scattering problem

may be simulated with an equivalent isotropic scattering problem.

Aging Literature

The other literature relevant to this work is the foam literature concerning aging. The approach of Norton (17), and of Brandreth (24) has been to measure an effective diffusion coefficient for each of the gases diffusing through the foam. Experiments have shown that the effective diffusion coefficient changes considerably from foam to foam. However, once an effective diffusion coefficient is found, the mass transfer - heat transfer analogy_ may be applied to the diffusion problem. Newman (25), (19) gives the series solution to the problem of transient diffusion in a slab. Alternatively, the same results could be read from graphs prepared from this series solution for the analogous heat transfer problem. Rohsenow (26) explains the heat/mass transfer analogy and presents some charts. Arpaci (27) gives more detailed charts and furthermore explains how multidimensional problems (i.e. edge diffusion in slabs) may be solved by using the product of results read from the one-dimensional charts. Arpaci also gives solution charts for cylindrical and spherical geometry problems. Gas concentration in foams may thus be determined from the charts for the most common geometries once the diffusion coefficient is known for each gas in the foam. The key element in this process of predicting gas composition with age is the prediction of the effective diffusion coefficient. The remainder of the work is well documented mathematics.

Once the gas composition is known throughout the foam, this information is used to calculate an effective foam thermal conductivity. Norton (17) calculates the mole fraction of the average gas composition and uses this to predict the overall conductivity of the foam. This approach may not be accurate for all cases. This approach will be accurate whenever the gas composition is nearly uniform (initially, and during the "plateau" when the oxygen and nitrogen diffusion are nearly complete) but will not be accurate whenever significant oxygen and nitrogen concentration gradients cause a large variation of gas composition from the foam core to the surface. An accurate alternative which is as easy to apply as Norton's approach is presented in Chapter 6.

Concerning the thermal conductivity of gas mixtures, some authors have used a linear combination of mole fraction times pure component thermal conductivity in order to estimate cell gas mixture thermal conductivity. Bretsznajder (8) shows that the linear model for the conductivity of a gas mixture only applies when the gases in the mixture are nonpolar and have approximately equal molecular weights. Because the freons have much higher molecular weights than oxygen and nitrogen, other models are required. Reid (6) and Tsederberg (7) both present a correlation by Lindsay and Bromley which would be expected to hold for freon - oxygen - nitrogen - water vapor mixtures. Peters, et al. (5) give data for freon - nitrogen mixtures which agrees well with the Lindsay - Bromley correlation. The linear model for mixture conductivity deviates from the data by 35%.

In succeeding chapters, it will be shown that the prevailing models presented throughout the foam literature overestimate solid conduction, overestimate gas conduction during aging, and drastically underestimate radiation. As will be seen in Chapter 7, the improved understanding gained in this study has helped identify promising development work as well as provide immediate fruit in the quest for lower conductivity insulations.

1.3 Approach

The general approach in this work has been to examine the most general problem statement, perform limit analyses and experiments which examine the basic processes involved, and simplify the problem, based on the experiments.

The specific approach to the conduction problem was to make simplifications, but keep track of whether the simplifications will be increasing or decreasing the heat transfer. In this way upper and lower limit models for gas plus solid conduction were developed which illuminate the physical process, as well as provide a sufficiently accurate conduction model. Since low conductivity foams are typically produced at densities on the order of 2.0 pcf (32 kg/m^3), the conduction analyses ignore the results at densities over 5.0 pcf (80 kg/m^3). This restriction allows some simplifying approximations to be used.

For radiation heat transfer the approach has been more experimental than theoretical. While several authors noted in the previous section have solved complex conduction-radiation heat transfer equations, very few have performed experiments designed to measure the appropriate radiation parameters. Accordingly, three experiments were performed in this work. The first proves the opaque cell wall radiation models to be incorrect. The second shows that the medium is optically thick and nearly gray. It also provides a convenient technique for measurement of the extinction coefficient, the one property which must be measured for the simplified radiation model _developed in Chapter 3. The third experiment is unique in the literature because it directly measures the absorption coefficient, scattering coefficient, and phase function. These measurements may be compared to scattering theory results, or may be used directly in the general nonisotropic scattering radiation analysis. The results are also used to estimate the error inherent in the simple technique for extinction coefficient measurement.

Finally, we used the knowledge gained over the course of our reseach to reduce heat transfer in a low density foam. The approach entails adding strongly absorbing particles to reduce the radiation contribution. Since this simultaneously increases conduction, an estimate of the best trade-off was made. As seen in Chapter 7, the result was a 6% reduction in thermal conductivity compared to a control foam with no particles.

2. CONDUCTION HEAT TRANSFER IN FOAMS

The conduction chapter is divided into four sections. The first section, Introduction to Conduction, provides the motivation and the technical basis for the approach taken. Section 2.2, Two Dimensional Limit Models, develops the concepts in upper and lower limit modeling which are extended in section 2.3, Three Dimensional Limit Models. The recommended conduction model is presented in section 2.3, followed by the Conduction Conclusions, section 2.4.

2.1 Introduction to Conduction

This section presents the conduction problem as the authors faced it. The second part, Basis for Limit Models, explains the basic limit modeling techniques used in this work.

2.1.1 Background

In the absense of radiation, conduction through the foam structure would account for 100% of the heat transfer. Valenzuela and Glicksman (1) have shown conclusively that convection is negligible in freon blown foams for cell sizes below approximately 1.5 mm (0.059 in). With other gases such as air, the cutoff diameter is even larger. Even with radiation, conduction through the solid/gas structure accounts for approximately 75% of the total heat transfer in low density freon blown foams, and approximately 90% of the total in high density foams, and in open celled foams. Therefore, an accurate conduction model is required if we are to predict foam thermal conductivity.

Aging of freon blown closed cell foams is characterized by dilution of the low conductivity freon gas with oxygen, nitrogen, and water vapor from the atmosphere. The thermal conductivity of the gas mixture is raised, thus increasing the overall foam thermal conductivity. In order to quantify the changes in overall foam conductivity given a mass transfer model for the gases, it is important to correctly understand the conduction problem.

Various published aging studies implicitly or explicitly make the following assumptions: 1.) The change in foam conductivity is equal to the change in space mean gas conductivity, 2.) The change in foam conductivity is equal to the change in conductivity of the average gas composition, 3.) The conductivity of the gas mixture may be expressed as the summation of the mole fractions of each component times the pure component conductivity. In succeeding chapters we will show that none of these assumptions are correct.

In the actual foam structure, there is conduction heat transfer interaction between the solid and gas. The temperature profile is complex in detail, especially since the bubble geometry is complex. The approach taken in succeeding sections is to provide upper and lower bounds to the conduction in foam by examining idealized geometries which would have higher or lower conductivities than the actual foam structure. Questions concerning the effects of assumed bubble shape, of struts, and of variable gas conductivity are addressed. We have not assumed in our analyses that the overall conductivity may be expressed

as the sum of gas, solid, plus radiation contributions. However we will show in later chapters that the magnitude of the effects of heat transfer interaction by these three mechanisms is small for typical foam insulations. We will speak of "solid contribution" as the effective conductivity without radiation, minus the gas conductivity.

2.1.2 Basis for Limit Models

The temperature field in real foam is a complex three dimensional function. There is no "exact" solution to conduction heat transfer in foamed materials since the bubble geometry cannot be described by any one repeating elemental cell. In real foam, cells of different sizes, shapes, and with different numbers of faces are packed together. A finite difference solution could be performed for some "representative" element, but even then a certain amount of judgement is required in order to determine what is "representative". The approach taken in this work has been to idealize the geometry to make it analytically manageable, and relate the idealized results to conduction heat transfer in real foam. In order to estimate the error in these idealizations, upper and lower bounds have been placed on the actual heat transfer. The closer together these bounds, the less uncertainty in the final result.

In order to understand the limit analyses which follow, one must understand what makes one model an "upper limit" and another model a "lower limit". Although the real conduction problem is formidable, it is possible to make idealizations defining new problems which can be

solved exactly. In order to determine whether the solution to the new problem represents an upper or lower limit to the original (real) problem, one must determine whether the idealizations will enhance or reduce heat transfer compared to the original case.

For example, one idealized way to enhance heat transfer in foam would be to take all of the solid polymer and place it in a single column stretching from one side of the sample to the other. This new problem can then be solved exactly and the solution will be an upper limit for heat transfer in foam. Unfortunately this idealization will so drastically increase the conduction that the model's usefulness is quite limited. Fortunately, other less drastic idealizations can be shown to increase the heat transfer and thus provide better (more accurate) upper limit models.

The above example points out that changes in geometry provide one way to idealize a problem. If the high conductivity material is reoriented parallel to the heat flow direction, the conduction will be increased. Conversely, if the high conductivity material is reoriented perpendicular to the heat flow direction, the conduction will be decreased.

Another class of idealizations which are important in this work are idealizations involving properties of materials. For example, the conductivity of a material could be assumed to be zero or infinity in one coordinate direction, and be the real value in an orthogonal direction. For any given problem geometry, if the conductivity of a

material is assumed infinite in any direction, the calculated conduction heat flux will always be equal to or greater than the actual. Conversely, if the conductivity of a material is assumed to be zero in any direction, then the calculated conduction heat flux will always be equal to or less than the actual. The reason is that paths of infinite conductivity provide local short circuits, thus reducing the overall effective resistance. Points of zero conductivity are local open circuits (infinite resistance), thus increasing the overall resistance.

One other technique for lower limit analysis depends on the physical fact that in conduction heat transfer the heat will always flow via the path of least resistance. This is analogous to an electrical resistor network where electric current will find the path of least resistance. If one arbitrarily assumes the heat flow path through a given geometry, the calculated effective resistance will always be greater than or equal to the actual resistance. In other words, for a given overall temperature difference, the calculated conduction heat flux will always be less than or equal to the actual heat flux. Therefore, another technique for lower limit analysis is to specify lines of flux through the geometry and calculate the effective resistance to heat flow.

Many idealizations could be made simultaneously for a given coduction problem. If all idealizations increase heat transfer, then the resulting solution still represents an upper limit. If all idealizations reduce heat transfer, then the solution is a lower limit.

However, if some increase and others decrease heat transfer, then we have neither an upper nor a lower limit to the original problem.

2.1.3 Analytical Approach

From the previous discussion it is clear that approximate models are used for estimation of conduction in foam. In following sections, the actual foam geometry is idealized as stacked cubes, arranged in-line or staggered. It is also idealized as a large number of sticks with equal probability for any stick to be oriented in any direction. Finally it is idealized as a large number of small planes with equal probability of any plane being oriented in any direction. Upper and lower limits are placed on these idealized geometries and the relationship of these models to the conduction heat transfer in real foam is detailed. From the upper and lower limit analyses of these idealized geometries, an approximation is assembled for upper and lower limits to the conduction heat transfer in real foam.

Section 2.2 presents conduction analyses in two dimensions for the purpose of developing the analytical concepts used in the three-dimensional cases, presented in section 2.3. A conduction model for foam is presented, followed by some typical results, interpretation of these results, and a summary of conduction conclusions.

2.2 Two Dimensional Limit Models

While the two dimensional limit models are not useful for predicting foam thermal conductivity, they are instructive because of their simplicity. If the reader understands the two dimensional models, the three dimensional models will be extensions of the same basic concepts to more complex geometry, with only a few new concepts introduced.

This chapter begins with upper and lower limit conduction analysis for two-dimensional bubbles. The bubbles are square in cross section and may be arranged in-line with the heat flow direction, staggered in the heat flow direction, or arranged in-line with the heat flow at a 45 degree angle to the walls of the bubbles. Section 2.2.5 details an analysis for the in-line square bubble geometry where the heat flow is at an arbitrary angle to the sides of the squares. Finally, an upper limit analysis is presented for a large number of sticks where each stick has an equal probability of orientation in any direction.

2.2.1 Two Dimensional Geometries

Three of the two dimensional geometries are shown in Figure 2-1. In all three, the solid polymer is assumed to be uniformly distributed throughout. There are no large clumps nor nodules in the two dimensional cases. (These problems will be addressed in the three dimensional cases.) In all three cases, the cell "diameter" (d) is taken
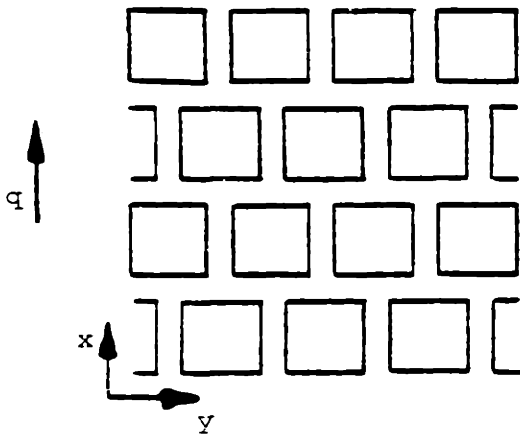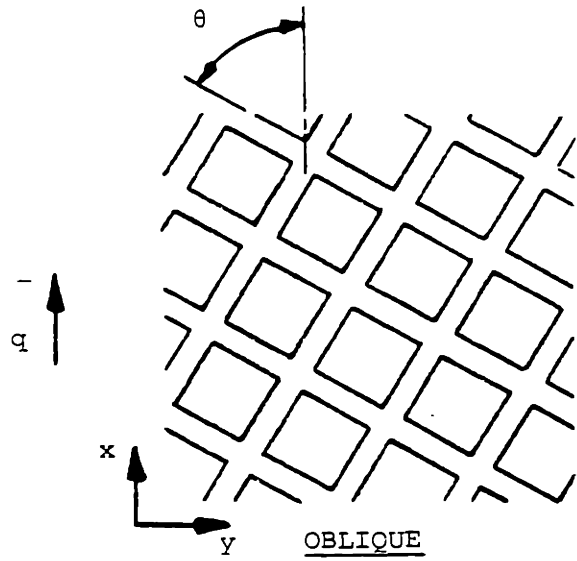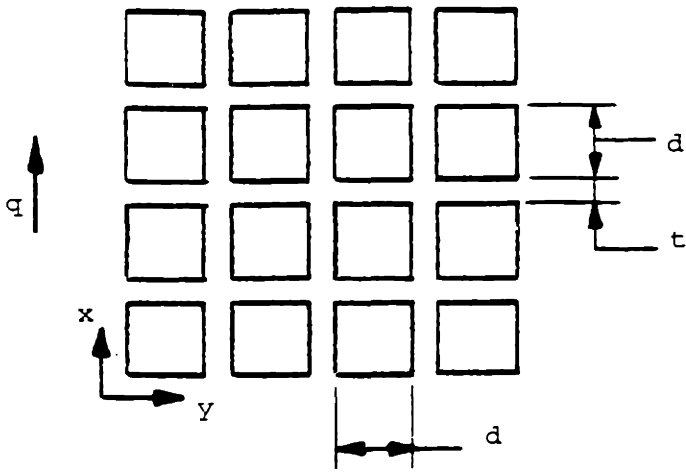
Figure 2-1 : Two Dimensional Square Bubble Geometries

to be the length of the gas space. The wall thickness (t) is shown in Figure 2-1.

For all three square bubble geometries, the porosity (δ), the volume of gas divided by the total volume, may be calculated from equation 2-1.

$$\delta = \frac{d^2}{(d+t)^2} \tag{2-1}$$

From a simple analysis of the force of gravity and the foam bouyancy in air, the porosity is expressed in equation 2-2 as a function of solid, gas, and air densities, ρ_s, ρ_g, ρ_a respectively, and "apparent" foam density (ρ_f).

$$\delta = \frac{\rho_s - \rho_a - \rho_f}{\rho_s - \rho_g} \tag{2-2}$$

The "apparent" foam density is the density calculated by dividing the weight of a foam sample by the volume of the sample. Given the densities and a representative cell diameter, d, it is easy to calculate the cell wall·thickness (t) from equations 2-1 and 2-2.

2.2.2 Limit Models for 2-D In-Line Geometry

For conduction analysis of the 2-D in-line geometry, it is helpful to make full use of symmetry. See the top drawing in Figure 2-1. In the heat flow direction, lines of symmetry may be drawn through the centerlines of walls as well as through the centerlines of cells. By

symmetry, these are adiabatic surfaces. Perpendicular to the heat flow direction, lines of symmetry may also be drawn through the centerlines of cells and through the centerlines of walls. In the case of steady state heat transfer with prescribed temperature at the edges of the foam, these lines are isotherms. The problem is therefore reduced to analysis of the repeating element shown in Figure 2-2.

The conduction upper limit is easily attained by changing the thermal conductivity of the solid and gas from ks and kg to infinity, for the y-direction only (perpendicular to the heat flow direction). If the y-direction conductivites are infinity, then all isotherms are horizontal lines and the resistor network shown in the left hand side of Figure 2-2 is exact. Since the lateral conductivites are actually finite, this resistor network represents an upper limit for the in-line geometry.

By reducing the y-direction thermal conductivity from ks and kg to zero, a lower limit is achieved. This lower limit is exactly modeled by the resistance network shown in the right hand side of Figure 2-2. This network can be understood once one recognizes that if the conductivity is zero in the y-direction, all lines in the x-direction are adiabatic.
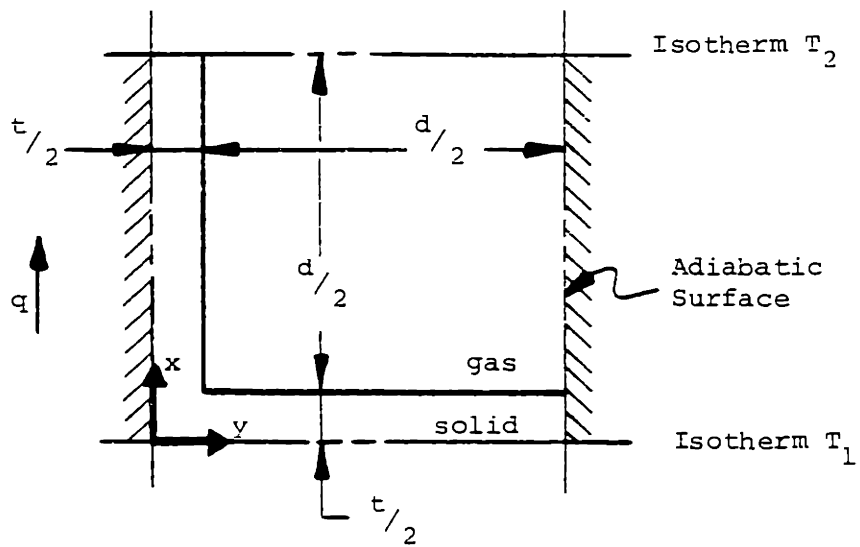
REPEATING ELEMENT

(Unit Depth into Paper)

UPPER LIMIT
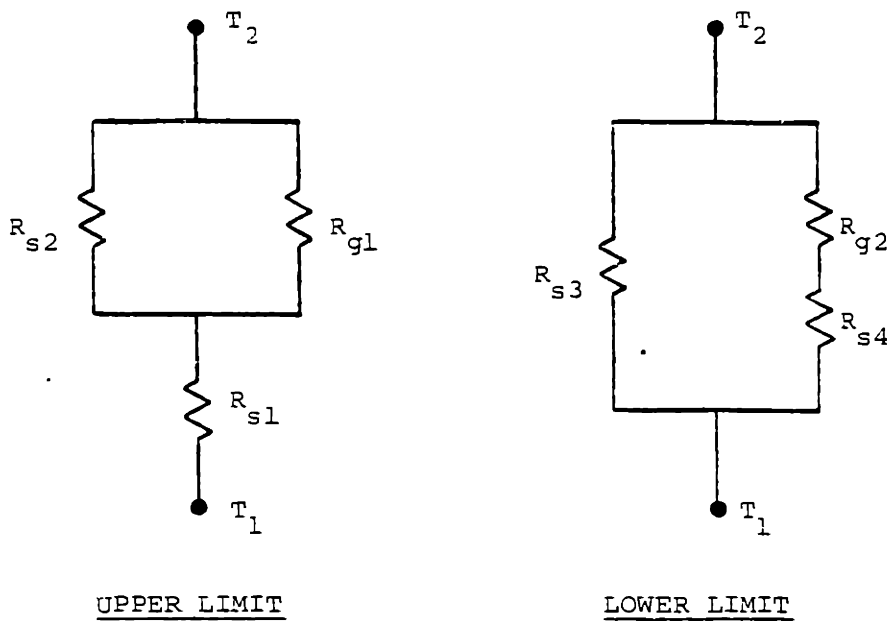
LOWER LIMIT

Figure 2-2 : Repeating Element and Circuit
Diagrams for 2-D In-Line Geometry

The resistances shown in Figure 2-2 may be calculated for the upper limit model from equation 2-3:

$$\text{upper limit} \begin{cases} R_{s1} & = & \dfrac{t}{k_s(d+t)} \\\\ R_{s2} & = & \dfrac{d}{k_s t} \\\\ R_{g1} & = & \dfrac{1}{k_g} \end{cases} \qquad (2\text{-}3)$$

and for the lower limit model from equation 2-4:

$$\text{lower limit} \begin{cases} R_{s3} & = & \dfrac{d+t}{k_s t} \\\\ R_{s4} & = & \dfrac{t}{k_s d} \\\\ R_{g2} & = & R_{g1} & = & R_g \end{cases} \qquad (2\text{-}4)$$

The overall resistances for the upper and lower limit models are given in equations 2-5 and 2-6 respectively.

$$R_{UL \atop s+g} = R_{s1} + \cfrac{1}{\cfrac{1}{R_{s2}} + \cfrac{1}{R_g}} \qquad (2\text{-}5)$$

$$R_{LL \atop s+g} = \left(\cfrac{1}{R_{s3}} + \cfrac{1}{R_{s4} + R_g} \right)^{-1} \qquad (2\text{-}6)$$

Given the overall resistances, upper and lower limits to conduction through the solid plus gas may be calculated from equation 2-7.

$$k_{s+g} = \cfrac{(d+t)/2}{R_{s+g} \; \cfrac{d+t}{2} \cdot 1} = \cfrac{1}{R_{s+g}} \qquad (2\text{-}7)$$

As might be expected for this geometry, the upper and lower limit results differ by only 1.5% for foam densities up to 5.0 pcf (80 kg/m^3).

2.2.3 Limit Models for 2-D Staggered Geometry

While the in-line square bubbles are convenient from the point of view of analysis, they are not representative of actual foam. In real foam, membranes are oriented at oblique angles and bubbles of different

sizes are packed together. By idealizing the foam as in-line squares we are overestimating the actual heat transfer. The reason is that the in-line geometry provides a direct solid conduction link from membranes in one level to membranes in the next level. In real foam the solid conduction path is far more tortuous. Membranes in real foam do join other membranes at a strut, however these membranes can be at any angle to the heat flow direction. This forces much of the heat to be conducted from solid to gas and back again. In the worst case all membranes oriented in the heat flow direction would terminate at membranes oriented perpendicular to the heat flow. This would force much of the heat to flow from the solid to the gas, rather than short-circuiting the gas as with the in-line model. This worst case is represented by the staggered bubble model.

In two dimensions this is represented by staggered squares. In three dimensions the cubes may be staggered in one or in two directions. For now we will concentrate on staggered squares. Later we will deal with cubical bubbles staggered in two dimensions.

It is apparent from the lower left drawing in Figure 2-1 that the same x-direction adiabatic lines of symmetry may be drawn for the staggered geometry as for the in-line. In this case, an adiabatic line of symmetry alternately passes through the centerline of a cell, then the centerline of a wall, etc. Y-direction lines of symmetry (isotherms) may be drawn through the centers of the cells, but not through the centers of the walls. The repeating element for the

staggered squares geometry is shown in Figure 2-3.

For the upper limit, we change the conductivity of the solid and gas from ks and kg to infinity in the y-direction. Once again all isotherms are horizontal lines and it becomes apparent that the upper limit staggered case is identical to the upper limit in-line case.

In order to understand the rationale behind a realistic lower limit for this geometry, it is important to recognize that if we use the same lower limit technique as we did for in-line squares (that is to make kg, ks equal to zero laterally) then the conduction heat flow would be so small as to be only a few percent greater than the heat flow through stagnant gas alone. For 5.0 pcf foam, this model would only be 6% higher than for pure gas. For comparison, the upper limit is 113% higher. This lower limit would indeed be valid, but unfortunately not close enough to the real case to be useful. A different approach is needed in order to find another lower limit, closer to the actual case. Note that our purpose in establishing lower and upper limits is to bracket the real situation. The closer the bracket, the more accurate the estimate of the real case.

In order to understand the lower limit staggered model, it is important to recall that the differential equation governing conduction heat transfer is linear. Therefore one may use superposition of solutions. The superposition technique is most familiar to readers who have had occasion to solve multi-dimensional heat transfer problems with heat generation. This is most easily done by superposition of a one
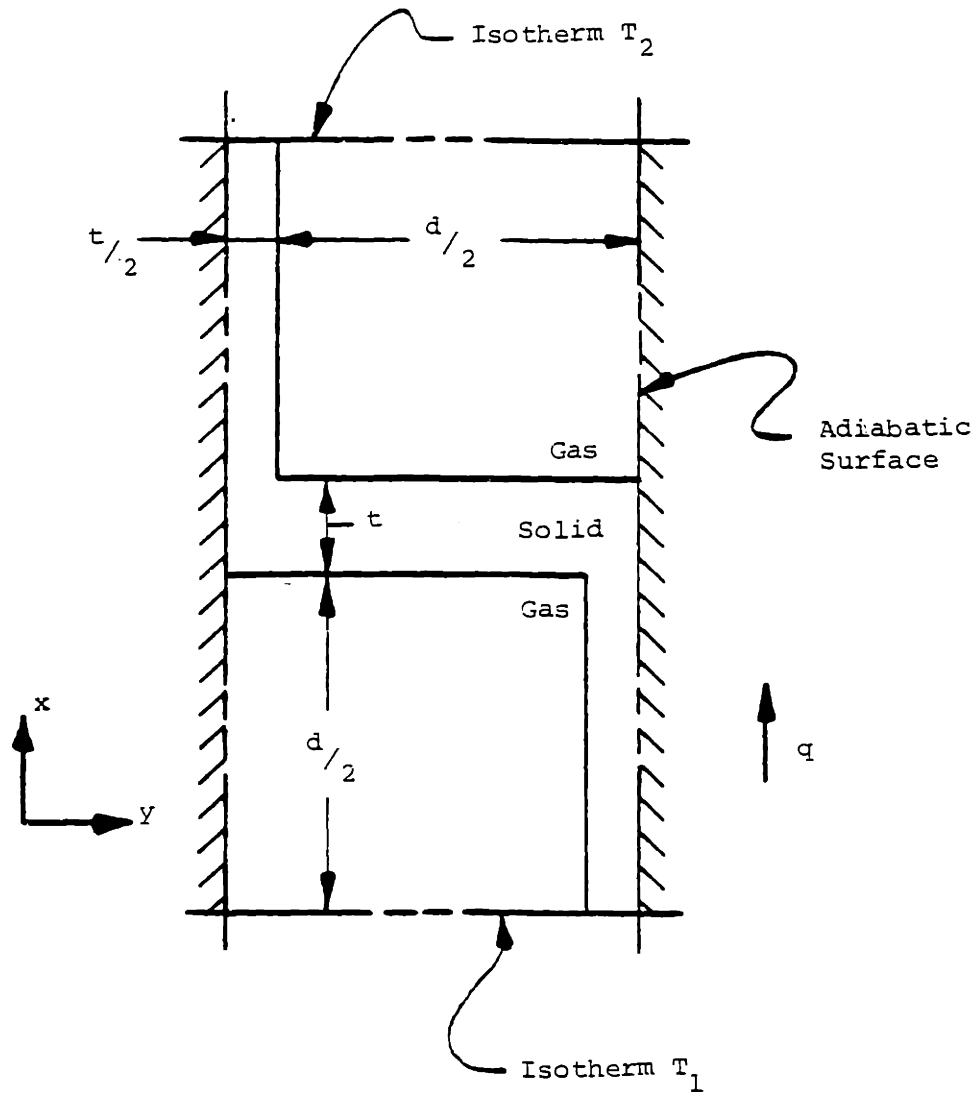
Figure 2-3 : Repeating Element for
the 2-D Staggered Squares Geometry

dimensional problem including heat generation with the multi-dimensional problem without heat generation. The temperature field T is expressed as the sum of two parts, A and B. The differential equation and boundary conditions are re-written in terms of these two components so that the sum A+B satisfies the differential equation and boundary conditions for T. A set of boundary conditions in A, with a differential equation in A, is thus derived. A set of boundary conditions for B with a differential equation in B are also thus derived. Problems A and B are solved independently, the solutions are added, and the sum is of course found to satisfy the differential equation and boundary conditions for T. The sum A plus B is thus an exact solution for T. Note that at any point, the gradient of T is the vector sum of the gradients of A and B. Thus, the flux at a boundary in T is just the flux at the boundary in A plus the flux at the boundary in B.

This is how the lower bound staggered model is derived, except with one twist. In this case problems A and B are not solved exactly. Instead, lower limit heat transfer solutions for A and B are derived, and their sum is therefore a lower limit solution for T.

The repeating element shown in Figure 2-3 is broken into two problems, A and B in Figure 2-4. The differential equation and boundary conditions for A and B add up to those for T in Figure 2-3, except for the addition of some adiabatic surfaces in A and B which result in the solution representing a lower limit. If the reader is uncomfortable
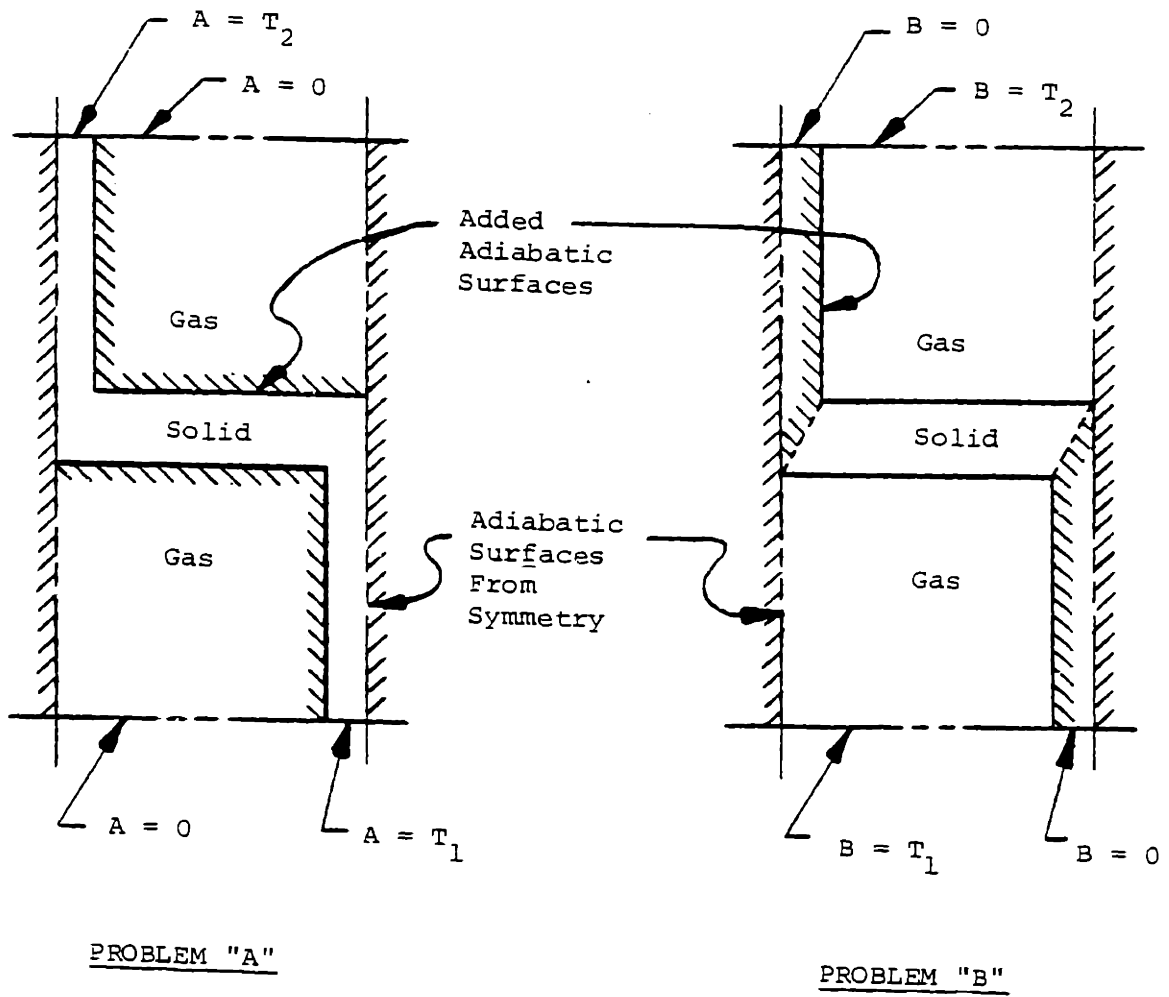
Figure 2-4 :   Superposition of Problems A and B
for the 2-D Staggered Squares Lower Limit

with adding adiabatic surfaces at will, simply think in terms of making the thermal conductivity zero along the interface.

From Figure 2-4, it is clear that each problem may now be solved with one-dimensional resistor networks. The heat flux in T (the sum A plus B) is just the sum of the heat flux in A with the heat flux in B. Equations 2-8 through 2-12 express this model mathematically.

$$R_A = 2\left(\frac{d+t}{k_s t}\right) + \frac{d/2}{k_s t} = \frac{2.5d + 2t}{k_s t} \tag{2-8}$$

$$R_B = 2\left(\frac{d}{k_g d}\right) + \frac{t}{k_s d} = \frac{2}{k_g} + \frac{t}{k_s d} \tag{2-9}$$

$$q_T = q_A + q_B = \frac{T_1 - T_2}{R_A} + \frac{T_1 - T_2}{R_B} = \frac{T_1 - T_2}{R_{s+g}} \tag{2-10}$$

$$R_{s+g} = \left(\frac{1}{R_A} + \frac{1}{R_B}\right)^{-1} \tag{2-11}$$

$$k_{s+g} = \frac{d+t}{R_{s+g}(\frac{d+t}{2})} = \frac{2}{R_{s+g}} = 2\left(\frac{1}{R_A} + \frac{1}{R_B}\right) \tag{2-12}$$

Figure 2-5 gives the results of this model as applied to new (unaged) polyurethane foam. As seen in the figure, the staggered lower limit model results are approximately 6% below the upper limit at 2.0 pcf (32 kg/m^3) density. A better way to express this difference is to subtract the gas conductivity from the conductivity of the medium and

Assumes k_s = 2.1 Btu-in/hr-ft^2-F

2-D Upper Limit

Lower Limit
2-D In-line

Lower Limit
2-D Staggered

Pure R-il

k_{s+g}

$\dfrac{Btu-in}{hr-ft^2-F}$

Figure 2-5 : Conduction Through Solid
Plus Gas for 2-D Limit Models

Density (pcf)
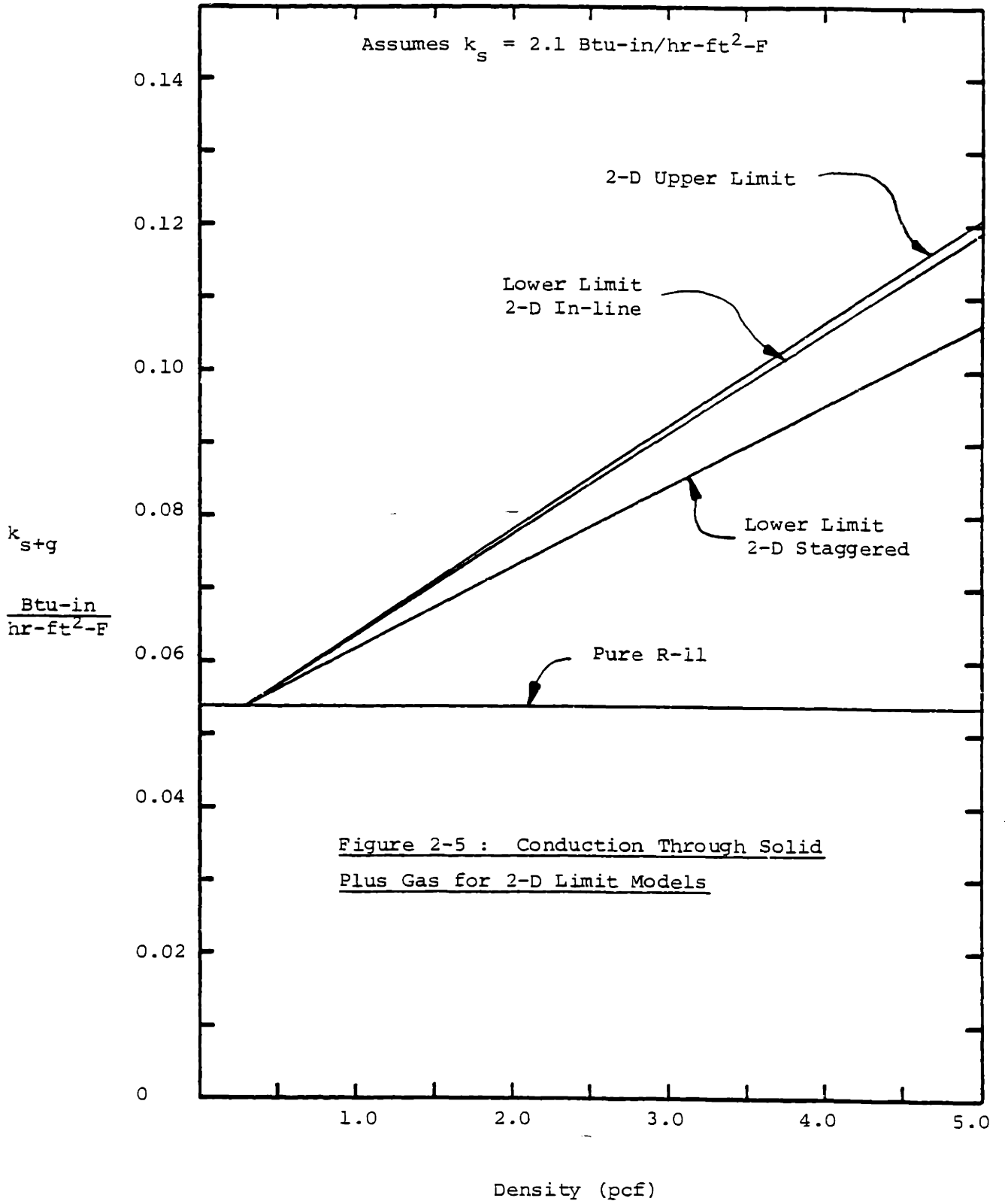
call this difference the "solid contribution". The calculated lower limit "solid contribution" is about 22% below the upper limit "solid contribution". This difference is due to the tortuosity of the staggered geometry conduction path.

2.2.4 Heat Flow Along 45 Degree Diagonal

While the cubical (square in 2-D) bubble analyses provide insight as to the magnitude of conduction. The membranes in real foam are oriented in every possible angular direction. In foams with elongated cells one would expect a greater proportion of the solid to be oriented in the direction of cell elongation, while in isotropic foams one would expect membranes would have equal probability of being oriented in any direction. The cubical cell models are representative of isotropic foams in the sense that equal numbers of membranes are oriented in the three coordinate axes. The question is: will placing membranes at angles oblique to the coordinate axes have an effect on the conduction? If yes, how much? If we can answer these questions then we can draw stronger conclusions about how the square bubble models relate to conduction in real foam.

In order to address this issue the diagonal geometry shown in Figure 2-1 was analysed, first for the case where equals 45 degrees. This is the same geometry as the in-line geometry except rotated 45 degrees to the heat flow direction. Lines of symmetry may be drawn through the corners of adjacent diamonds. These lines are adiabatic.

Lines of symmetry may be drawn perpendicular to the heat flow direction also through the corners of adjacent diamonds. These lines are isotherms.

The repeating element is thus a square with adiabatic sides, isothermal top and bottom, and with a solid membrane extending diagonally, as shown in Figure 2-6. The lower diagram in Figure 2-6, idealized repeating element, is the geometry we analyse. The difference is that two of the corners have been eliminated. An alternate perspective, totally equivalent, is to say the conductivity of the solid is infinite in the corner triangles. We are therefore ignoring a small resistance. This is negligible for low density foams where the wall thickness t is very small compared the the cell "diameter" d. For the two-dimensional square bubbles geometry, the ratio of d to t is approximately 88.0 at a foam density of 2.0 pcf (32 kg/m^3). We might expect the error due to this idealization to be less than but of the order of 1.0% of the "solid contribution".

2.2.4.1 Upper Limit-Diagonal

In order to establish an upper limit for this geometry we make the assumption that the conductivity of the solid is infinite in the y-direction. We also assume that the conductivity of the gas is infinite in the direction perpendicular to heat flow ($q_\perp$). Isotherms may then be drawn on either side of the volume element shown in the top drawing of Figure 2-7. An energy
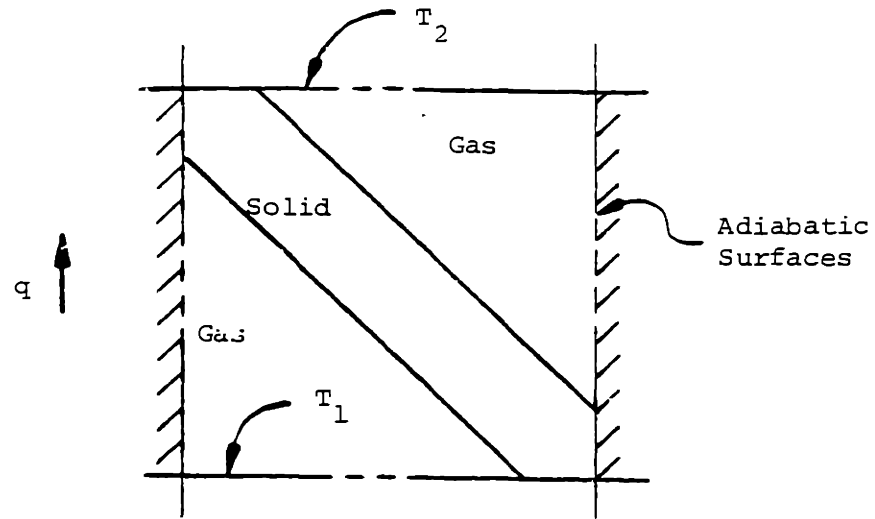
REPEATING ELEMENT
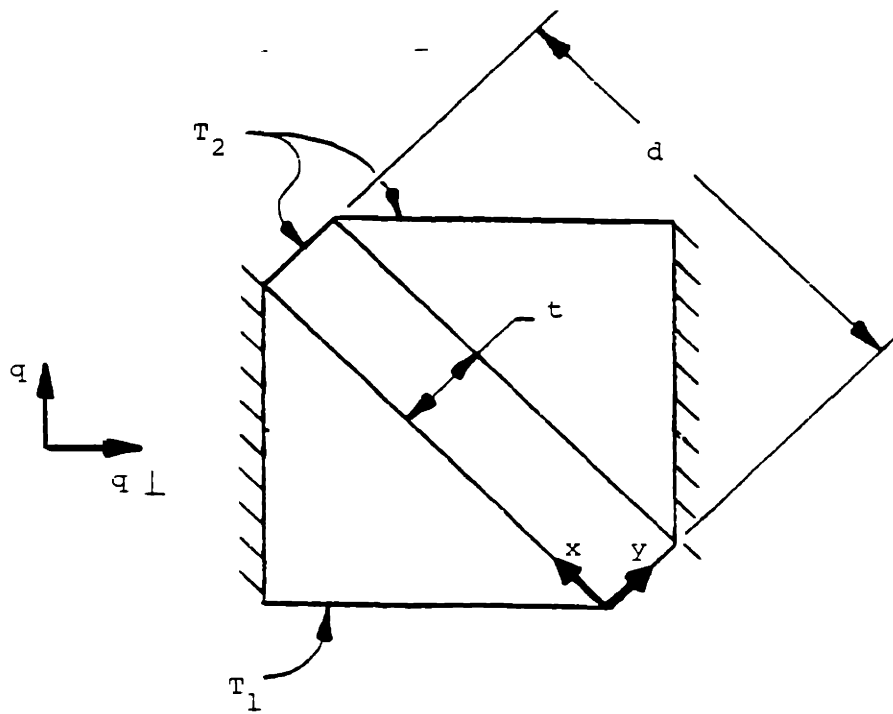
IDEALIZED REPEATING ELEMENT

Figure 2-6 : Repeating Element for Heat Flow Along Diagonals
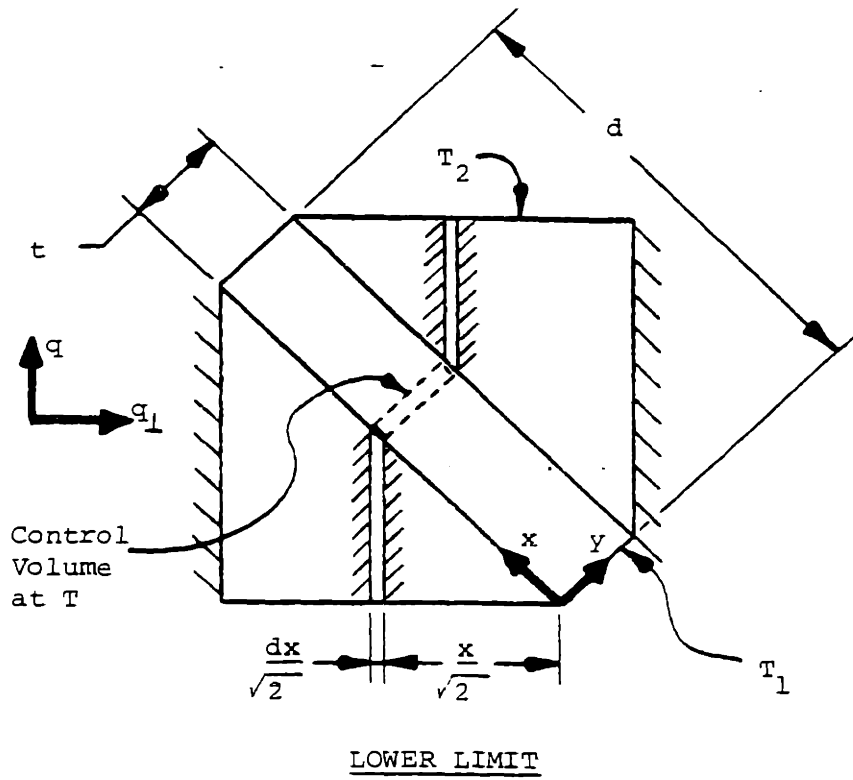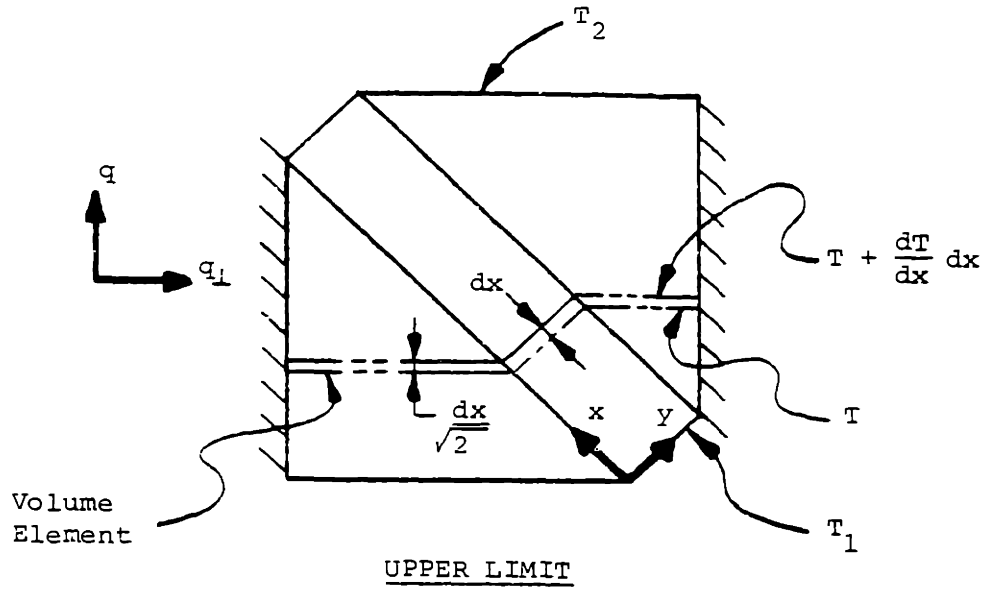
Figure 2-7 : Volume Elements for Heat Flow Along Diagonals

balance may be written for this element which equates the heat entering with the heat leaving. This balance is given in equations 2-13 through 2-15.

$$q_{in} = k_g \left(\frac{d-x}{\sqrt{2}}\right)\left(\sqrt{2}\ \frac{dT}{dx}\right) + k_s t\frac{dT}{dx} + k_g\left(\frac{x}{\sqrt{2}}\right)\left(\sqrt{2}\ \frac{dT}{dx}\right)$$

(2-13)

$$q_{out} = k_g\left(\frac{d-x-dx}{\sqrt{2}}\right)\left(\sqrt{2}\ \frac{dT}{dx}\right) + k_s t\left(\frac{dT}{dx} + \frac{d^2T}{dx^2}\ dx\right) + k_g\left(\frac{x+dx}{\sqrt{2}}\right)\left(\sqrt{2}\ \frac{dT}{dx}\right)$$

(2-14)

Equating heat entering with heat leaving and combining like terms we find that:

$$\frac{d^2T}{dx^2} = 0$$

(2-15)

integrating we get:

$$T = C_1 x + C_2$$

(2-16)

applying the boundary conditions:

$$\left.\begin{array}{l} x = 0\ ,\ T = T_1 \\ x = d\ ,\ T = T_2 \end{array}\right\}$$

(2-17)

we find:

$$\frac{T - T_1}{T_2 - T_1} = \frac{x}{d} \qquad (2\text{-}18)$$

Clearly the gradient is a constant and is given by:

$$\frac{dT}{dx} = \frac{(T_2 - T_1)}{d} \qquad (2\text{-}19)$$

The heat flow at any position x is given by equation 2-13, which may now be simplified to yield:

$$q = (k_g L + k_s t) \frac{T_2 - T_1}{d} \qquad (2\text{-}20)$$

If the effective conductivity of the medium is k_{s+g} and is defined by equation 2-21:

$$q = k_{s+g} \frac{(T_2 - T_1) \text{ Area}}{\text{Distance}} \qquad (2\text{-}21)$$

where:

$$\text{Area} = [(d+t)/\sqrt{2}] \cdot 1. \qquad (2\text{-}22)$$

$$\text{Distance} = (d+t)/\sqrt{2} \qquad (2\text{-}23)$$

then:

$$k_{s+g} = k_g + k_s \frac{t}{d} \qquad (2-24)$$

Note from equation 2-24, k_{s+g} approaches kg as the density approaches that of pure gas (t/d approaches zero). In the limit where the density approaches that of pure solid, equation 2-24 loses meaning because t/l becomes infinity. This is due to neglecting the resistance of the triangular corners. In the limit of pure solid, these corners become the entire volume. Thus the medium conductivity approaches infinity. As pointed out earlier, this is not a problem as long as the density is low. For 2.0 pcf foam, this error is estimated to be on the order of 1% of the "solid contribution", or approximately 0.33% of the total conduction heat flow. At higher densities the error is of course higher.

Table 2-1 gives the results of this model in comparison to the upper limit for staggered and in-line cubes. For a foam density of 5 pcf (80 kg/m^3), the difference between the diagonal upper limit and in-line upper limit is less than 0.2% overall or 0.3% of the "solid contribution". Such a small difference could be entirely due to neglecting the corner resistances in the diagonal model. The next question is: what effect does 45 degree orientation have on the lower limit model?

Table 2-1: Comparison of Heat Flow at 45 Degrees
to Upper Limit for 2-D Square Bubbles

Foam Density (pcf)	In-line Upper Limit	45 Degrees* Upper Limit	Difference (%)
1.0	0.0638	0.0638	——
2.0	0.0777	0.0777	——
3.0	0.0919	0.0920	0.1
4.0	0.1063	0.1065	0.2
5.0	0.1211	0.1213	0.2

Notes:

units - Btu-in/hr-ft^2-F

k_s = 2.1

k_g = 0.05388

ρ_s = 77.5 pcf

ρ_g = 0.351 pcf

* Based on equation 2-24

2.2.4.2 <u>Lower</u> <u>Limit</u> - <u>Diagonal</u>   The bottom picture in Figure 2-7 gives a clear indication of what follows. We now analyse the diagonal geometry with the gas conductivity equal to zero in the direction perpendicular to the heat flow ($q_\perp$). The corners will be neglected as will the y-direction heat flow resistance in the solid. Due to these two approximations the model which follows is not a true lower limit, but instead only serves to show the effect of lateral gas conductivity. We showed that neglecting the resistance in the corners might cost 0.33% accuracy. One would expect the error due to neglecting the y-direction resistance in the solid to be of the same order of magnitude or less. Any heat which flows through the solid in the y-direction must also pass through a long length of gas. This gas resistance will be large compared to the solid resistance, and therefore the solid resistance may be neglected. Note that the solid conductivity in the x-direction may not be treated similarly since such treatment would allow short circuiting of the gas conduction path.

Given these assumptions, Figure 2-8 shows the control volume for which an energy balance was written. The control volume consists of solid material, dx long by t wide at position x. The heat fluxes into and out of this control volume are noted in Figure 2-8 as q1,q2,q3, and q4.

The heat flows q1 and q2 may be found by recognizing that a simple resistance to heat flow exists between the control volume and the isothermal edges of the repeating element. This is due to the

$T(x) + \dfrac{dT}{dx} dx$

dx

q_2

t

q_4

$T(x)$

q_3

q_1

x y
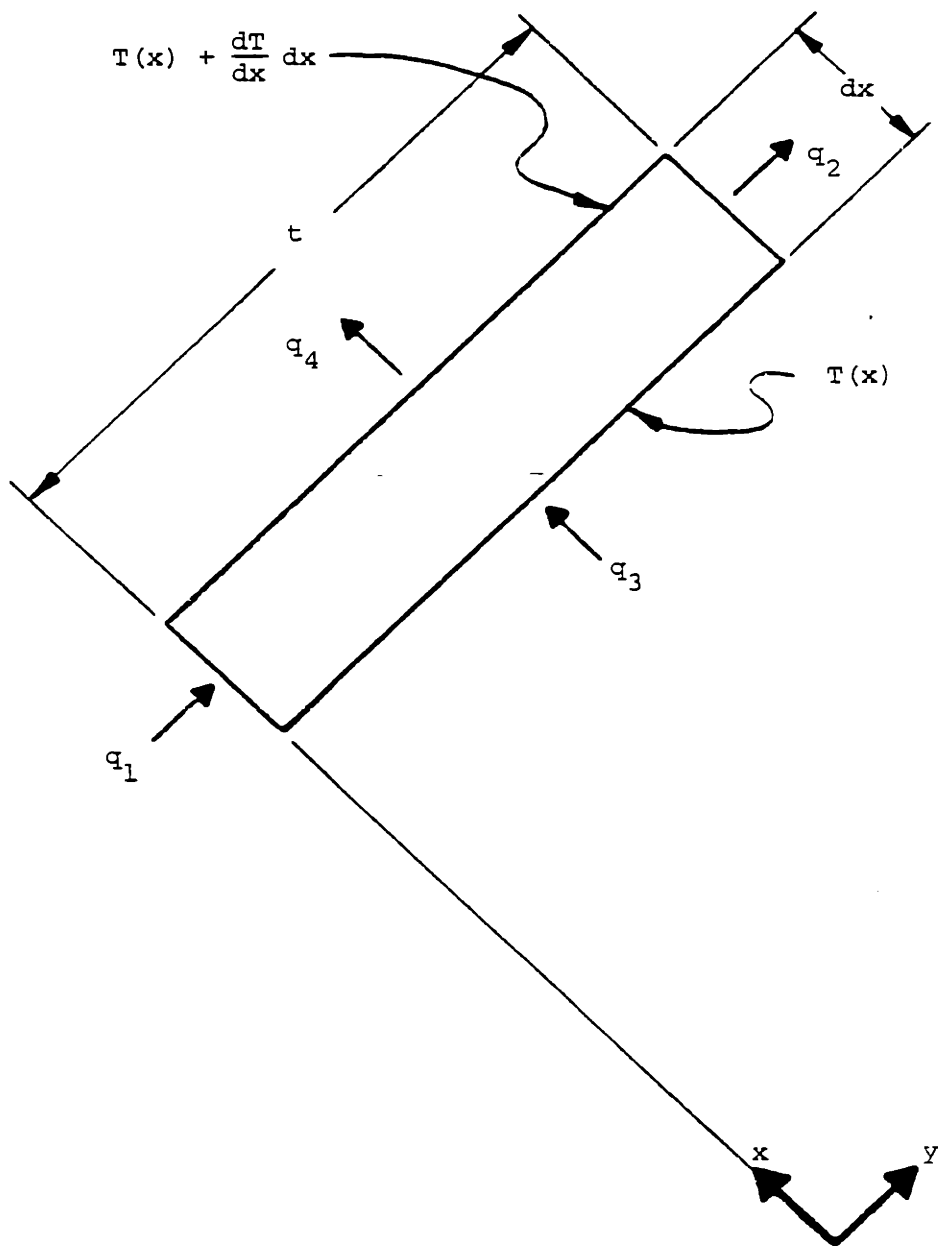
Figure 2-8 :   Control Volume at T for Lower Limit

assumption that k_g is zero in the direction perpendicular to heat flow. Equations 2-25 and 2-26 express this mathematically:

$$q_1(x) = \frac{T_1 - T(x)}{\left(\frac{x}{k_g dx}\right)} = \frac{k_g(T_1 - T) dx}{x} \qquad (2-25)$$

$$q_2(x) = \frac{T(x) - T_2}{\left(\frac{(d-x)}{k_g dx}\right)} = \frac{k_g(T - T_2) dx}{d-x} \qquad (2-26)$$

Note that the conductivity of the solid is infinite in the y-direction, hence the temperature in the solid is only a function of x. Therefore the heat flows q3 and q4 may be expressed as:

$$q_3 = -k_s t \frac{dT}{dx} \qquad (2-27)$$

$$q_4 = -k_s t \frac{d}{dx}(T + \frac{dT}{dx} dx) \qquad (2-28)$$

The energy balance for this control volume is given by:

$$q_1 + q_3 = q_2 + q_4 \qquad (2-29)$$

Substituting equations 2-25 through 2-28 into equation 2-29 and combining like terms:

$$\frac{d^2T}{dx^2} + \left(\frac{k_g}{k_s t}\right)\frac{T_1 - T}{x} + \left(\frac{k_g}{k_s t}\right)\frac{T_2 - T}{d-x} = 0 \qquad (2\text{-}30)$$

The boundary conditions for this equation are:

$$\left.\begin{array}{c} x = 0 , \quad T = T_1 \\[2ex] x = d , \quad T = T_2 \end{array}\right\} \qquad (2\text{-}31)$$

The solution to equation 2-30 is simply:

$$\frac{T - T_1}{T_2 - T_1} = \frac{x}{d} \qquad (2\text{-}32)$$

which may be verified by substitution into equation 2-30, and checked against the boundary conditions, equation 2-31. But this is the exact same solution (given in equation 2-18) as for the upper limit case. Therefore, except for the two simplifications noted earlier (ks in corners and ks in y-direction equal to infinity), the solution (equation 2-32 or equation 2-18) is an exact solution for this geometry.

We have proven that the lateral direction $(q_\perp)$ gas conductivity plays essentially no role for the case of two dimensional 45 degree diagonal heat flow. We have also shown that the two idealizations

represent an uncertainty of approximately 1% for low densities. Therefore the actual conductivity for this idealized geometry is less than, but within approximately 1% of the conductivity as calculated by equation 2-24.

2.2.5 Heat Flow at Arbitrary Angle to 2-D Squares

A more general upper limit analysis is presented here for the two dimensional in-line square bubble geometry. The heat flow direction is at an arbitrary angle θ to the sides of the square, as shown in Figure 2-9. As will shortly be seen, the solution is independent of θ.

For purposes of visualization, consider a foam sample of thickness L with isothermal surfaces at T1 and T2, as seen in Figure 2-9. The gas conductivity is assumed infinite in the y-coordinate direction. The solid conductivity is assumed infinite across the thickness of the membrane. These idealizations result in the isotherms shown in the bottom of Figure 2-9.

From the blow-up in Figure 2-9, it is clear that each isotherm passes through the same total cross section of solid and through the same total cross section of gas, per unit heat flow area. By conservation of energy under steady state conditions, the heat flow normal to each and every isotherm is constant from one side of the sample to the other. From these two statements it may be inferred that the magnitude of the temperature gradient is a constant throughout the foam.
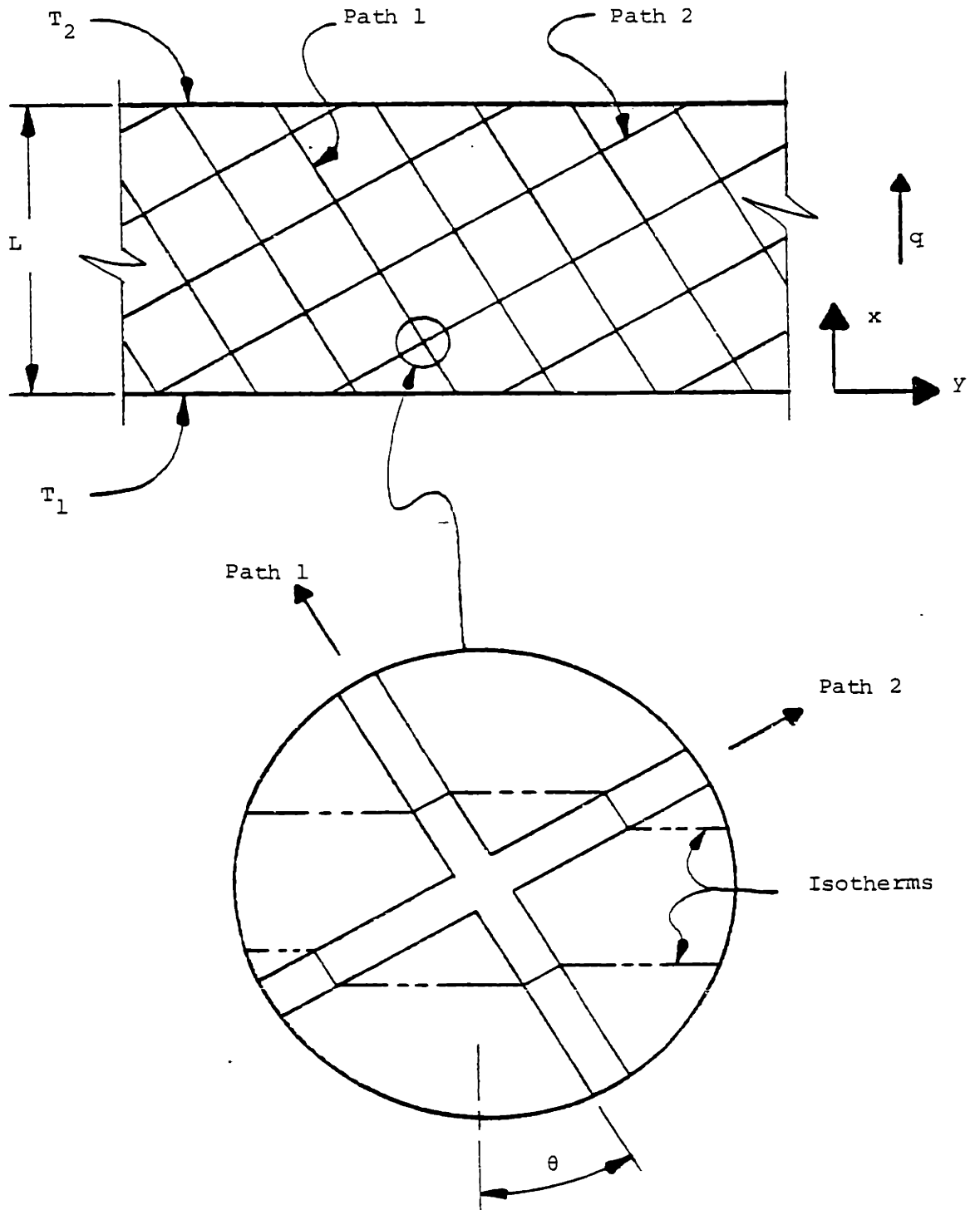
Figure 2-9 :   Heat Flow for In-line Squares at Arbitrary Angle

This inference may be more easily understood by applying the same argument to the geometry of Figure 2-10. Two geometries are shown, case 1 and case 2. If the y-direction conductivities are infinite, then cases 1 and 2 would have identical effective conductivities. Every isotherm passes through the same cross section of solid and gas. In steady state, the heat flow across each isotherm is a constant and the temperature gradient is constant throughout the material.

Going back to the geometry of Figure 2-9, the constant gradient (linear temperature profile) implies that the heat flow in the solid is constant and may be treated as a simple resistance. The total heat flow is also constant and thus the gas heat flow must also be constant. This allows us to treat the solid and gas conduction as two resistances in parallel. Equations 2-33 through 2-40 express this exactly.

$$R_{s+g} = \left(\frac{1}{R_g} + \frac{1}{R_s}\right)^{-1} = \left(\frac{L}{k_{s+g}A}\right)^{-1} \qquad (2-33)$$

For the gas resistance we neglect the fact that the solid occupies a small fraction of the volume. The gas resistance would therefore be slightly higher than that given by equation 2-34 below.

$$R_g = \frac{L}{k_g A} \qquad . \qquad (2-34)$$

$$R_s = \frac{T_1 - T_2}{q_{solid}} \qquad (2-35)$$
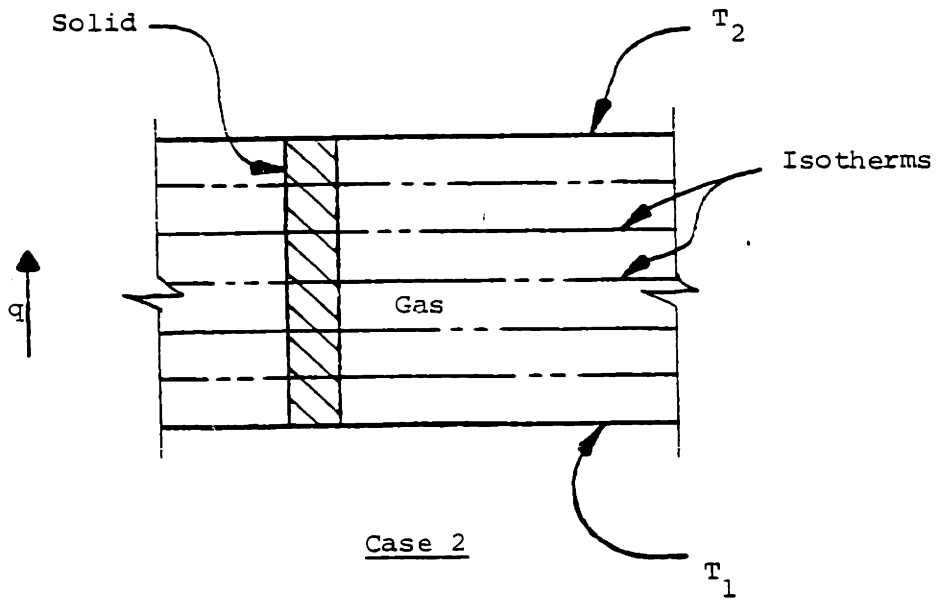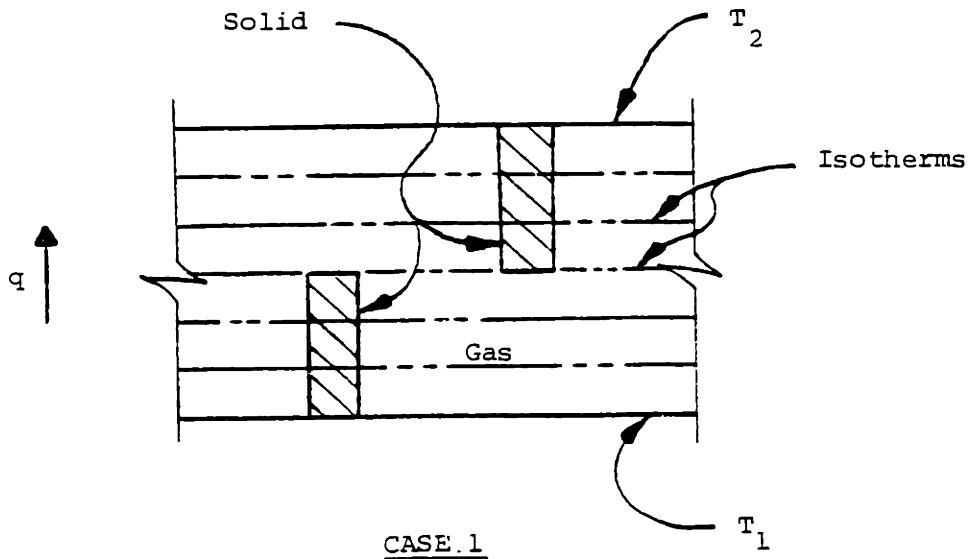
Figure 2-10 : Illustration of Effect
of Infinite Lateral Conductivity

The heat flow in a single path "1" is:

$$q_1 = \frac{k_s t (T_1 - T_2)}{\left(\dfrac{L}{\cos\theta}\right)} \qquad (2-36)$$

and for path "2":

$$q_2 = \frac{k_s t (T_1 - T_2)}{\left(\dfrac{L}{\sin\theta}\right)} \qquad (2-37)$$

If n_1 is the total number of paths "1" per unit area then:

$$n_1 = \frac{\cos\theta}{d} \qquad (2-38)$$

and n_2, the number of paths "2" is just:

$$n_2 = \frac{\sin\theta}{d} \qquad (2-39)$$

The total heat transfer in the solid is just the sum of the heat transfer in all paths "1" and "2":

$$q_{solid} = \frac{A}{L} (T_1 - T_2) \left(\frac{k_s t}{d}\right)(\cos^2\theta + \sin^2\theta) \tag{2-40}$$

Combining 2-33, 2-34, 2-35, and 2-40 results in:

$$k_{s+g} = k_g + k_s \frac{t}{d} \tag{2-41}$$

which is identical to equation 2-24, the solution for the 45 degree upper limit. Noting that for low densities:

$$1 - \delta = \frac{(t + d)^2 - d^2}{(t + d)^2} = \frac{t^2 + 2dt}{(t + d)^2} \simeq 2\frac{t}{d} \tag{2-42}$$

equation 2-41 may be approximated by:

$$k_{s+g} \simeq k_g + k_s \left(\frac{1 - \delta}{2}\right) \tag{2-43}$$

2.2.6 Random Sticks Upper Limit, 2-D

The previous analyses have shown that the square bubble assumption results in approximately the same upper limit solution regardless of the heat flow direction and regardless of stacking geometry. This section begins to explore what happens when the square bubble assumption is

relaxed. We will consider the case where the solid is in the form of sticks oriented at every angle. The total length of sticks oriented in any direction within a small angle $d\theta$ is constant; this is our definition of "random sticks".

In order to place an upper limit on this geometry, isotherms are assumed horizontal. That is, the conductivity of the solid and gas is assumed infinite in the direction perpendicular to heat flow. See Figure 2-11. Because the isotherms are horizontal lines, the temperature gradient must be constant under steady state conditions. All sticks at the same angle θ may be lined up end to end with no effect on the heat transfer so as to form continuous "bridges" crossing the thickness of the sample. Because there is an equal length of sticks at any θ, there are more bridges at small angles than at large angles. The heat flow across a single bridge at angle θ is given by:

$$q(\theta) = k_s \frac{t(T_1 - T_2)}{\left(\dfrac{L}{\cos \theta}\right)} \tag{2-44}$$

If $n(\theta)$ is the number of bridges at θ per unit angle per unit volume, and if $l(\theta)$ is the length of a bridge at θ, we may define a constant, λ, such that:

$$\lambda = n(\theta) \cdot l(\theta) = \text{constant} \tag{2-45}$$
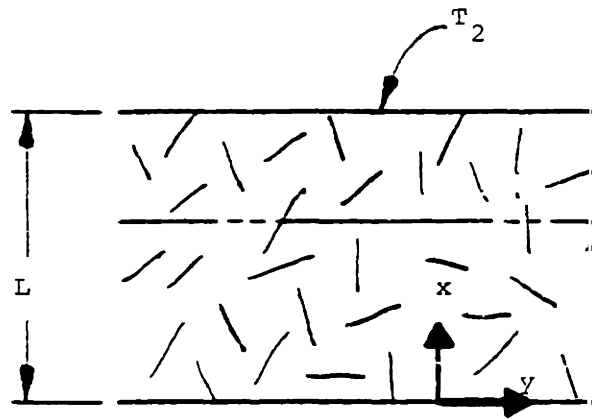
RANDOM STIC[
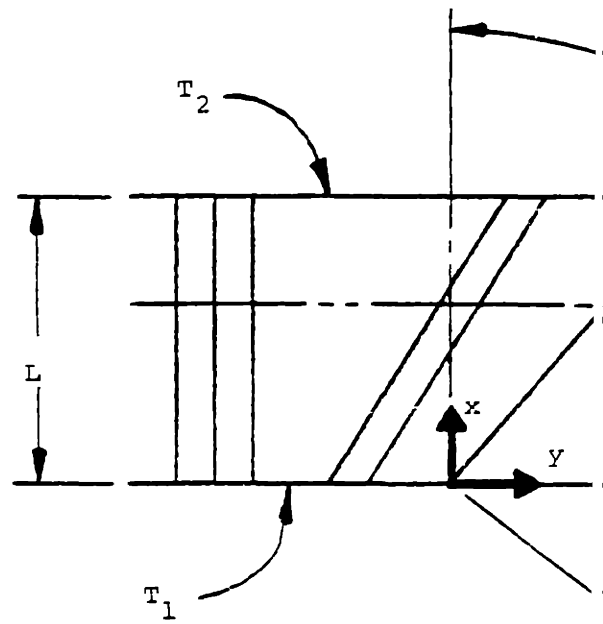
STICKS ALIGNED TO [

Figure 2-11 : Geometry for Upper

We also know from geometry:

$$l(\theta) = \cdot \frac{L}{\cos \theta} \tag{2-46}$$

thererore:

$$n(\theta) = \frac{\lambda \cos \theta}{L} \tag{2-47}$$

Physically, λ is the total length of all sticks at θ per unit volume, per unit angle, and is therefore a constant for random sticks, as defined here. The total solid conduction is the integral of the heat flow per bridge, times the number of bridges per unit volume per unit angle, times the volume, over all angles θ.

$$q_{solid} = \int_{\theta = 0}^{2\pi} (A \cdot L) \left(\frac{k_s t (T_1 - T_2) \cos \theta}{L} \right) \left(\lambda \frac{\cos \theta}{L} \right) d\theta \tag{2-48}$$

integrating we find:

$$q_{solid} = \frac{A(T_1 - T_2)}{L} \cdot \pi \cdot k_s t \lambda \tag{2-49}$$

But λ is related to the foam porosity.

$$1 - \delta = t \cdot \lambda \int_0^{2\pi} d\theta = t \cdot \lambda \cdot 2\pi \tag{2-50}$$

Solving for λ and substituting into equation 2-49:

$$q_{solid} = \frac{A(T_1 - T_2)}{L} \cdot k_s \left(\frac{1 - \delta}{2}\right) \qquad (2\text{-}51)$$

For the gas (ignoring the volume of the solid):

$$q_{gas} = \frac{A(T_1 - T_2)}{L} k_g \qquad (2\text{-}52)$$

From equations 2-51 and 2-52 we may find the effective conductivity of the medium, given by:

$$k_{s+g} = k_g + k_s \left(\frac{1 - \delta}{2}\right) \qquad (2\text{-}53)$$

which is identical to equation 2-43.

2.2.7 Conclusions for 2-D Analysis

The primary purpose of the two dimensional analyses was development of the analytical concepts and techniques which are used to solve the more difficult three dimensional problem. Superposition, symmetry, geometric modifications and material property modifications were all employed in this section, and will be further exploited in the next section. Nonetheless, the 2-D analyses also provide some insight into foam conduction.

The upper limit for diverse two dimensional geometric problems has been shown to be given by a simple expression, equation 2-53. Staggering the squares, tilting them at any angle, or having random sticks all give approximately the same result. The lower limit for the in-line geometry oriented normal to the heat flow is within 1.5% of the upper limit. The solution to the 45 degree bubble orientation case illustrates that the lower limit for the in-line squares geometry is quite close to the upper limit, even at orientations other than 90 degrees to the heat flow. This would lead one to suspect that equation 2-53 is not only an upper limit, but is also nearly exact for low densities for the in-line square bubble geometry at any orientation to the heat flow direction. At higher densities the resistance model expressed by equations 2-3 through 2-7 could be expected to be nearly exact for the square bubble geometry, even for oblique bubble orientation. The lower limit for the 2-D staggered square bubble geometry illustrates that the stacking arrangement could only effect a change in the "solid contribution" of about 22% for the most extreme cases. Finally, the random sticks result indicates that the choice of bubble shape is probably not important.

2.3 Three Dimensional Limit Models

This section presents the upper and lower limit models which are later used to predict thermal conductivity of foams. Upper and lower limit models for in-line and staggered cubical bubble geometry aligned normal to the heat flow direction are presented first. This is followed by upper limit analysis of the cubical bubble in-line geometry with the heat flow at an arbitrary (oblique) angle to the bubble walls. Random sticks and random planes are then analysed in three dimensions. We conclude with a model to calculate conduction in foams, along with some graphs presenting typical results.

2.3.1 Three Dimensional Geometries

Both the in-line and the staggered cubical bubble geometries are shown isometrically in Figure 2-12. For these geometries there are no struts, thus all solid material is assumed to be uniformly distributed in membranes. The cell "diameter" (d) is taken to be the length of the gas space. The "diameter" and the wall thickness (t) are shown in Figure 2-12.

For these two geometries the porosity (δ), the volume of gas divided by the total volume, may be calculated from Equation 2-54.

$$\delta = \frac{d^3}{(d+t)^3} \tag{2-54}$$

The porosity was also given as a function of foam, gas, air and solid densities (ρ_f, ρ_g, ρ_a and ρ_s respectively) under discussion of two
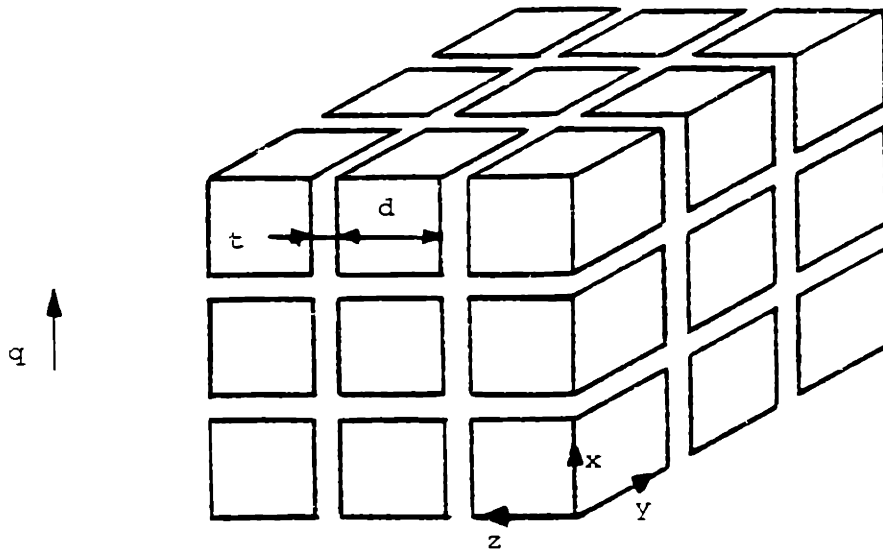
IN-LINE CUBES
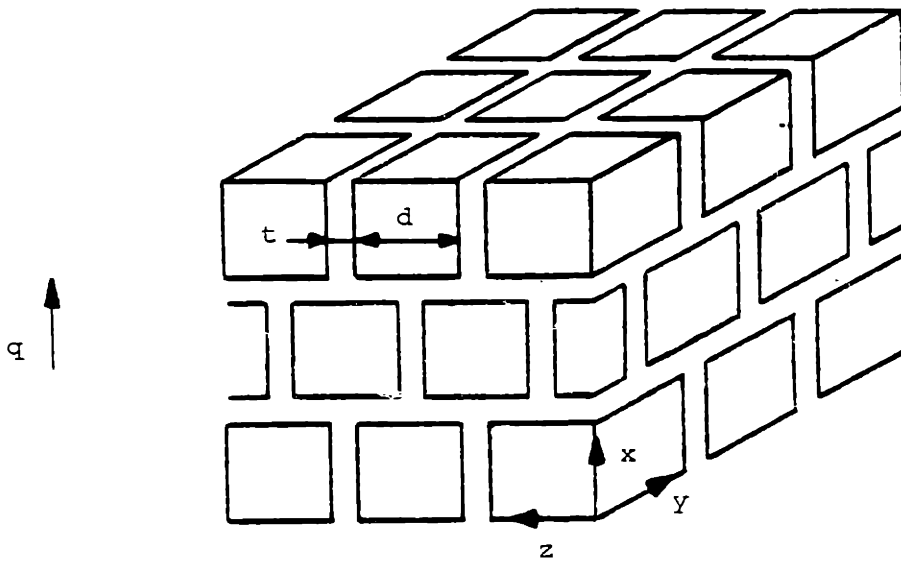
CUBES STAGGERED IN TWO DIMENSIONS

Figure 2-12 : In-Line and Staggered Cubical Bubble Geometry

dimensional bubble geometry. Equation 2-2 is repeated here for convenience:

$$\delta = \frac{\rho_s - \rho_a - \rho_f}{\rho_s - \rho_g} \qquad (2-2)$$

The exact same relation applies to 2-D and 3-D cells because it was derived by a force balance of gravity, bouyancy in air, and the measured weight of foam. Given the density information and a representative cell diameter, it is trivial to calculate the wall thickness (t) from equations 2-2 and 2-54.

As shown in Figure 2-13, the geometry is somewhat more complex with struts. Struts are stick-shaped elements which reside along the twelve edges of each cube where membranes intersect. To a good approximation for low foam densities, the overall heat transfer would not be affected by the shapes of the struts cross section. Struts with square cross-sections would give essentially the same heat transfer as would cylindrical struts, so long as the percentage of material in struts versus membranes was the same, and so long as the foam density was low. Microscopic examination of real foams indicate that a considerable portion of the solid (perhaps 85%) resides in the struts. Figure 2-14 gives some typical photographs of real foam under magnification. These particular samples contain a uniform dispersion of small coal particles in the solid. This helps provide better photographic contrast as well as qualitatively suggest a large concentration of solid in struts.
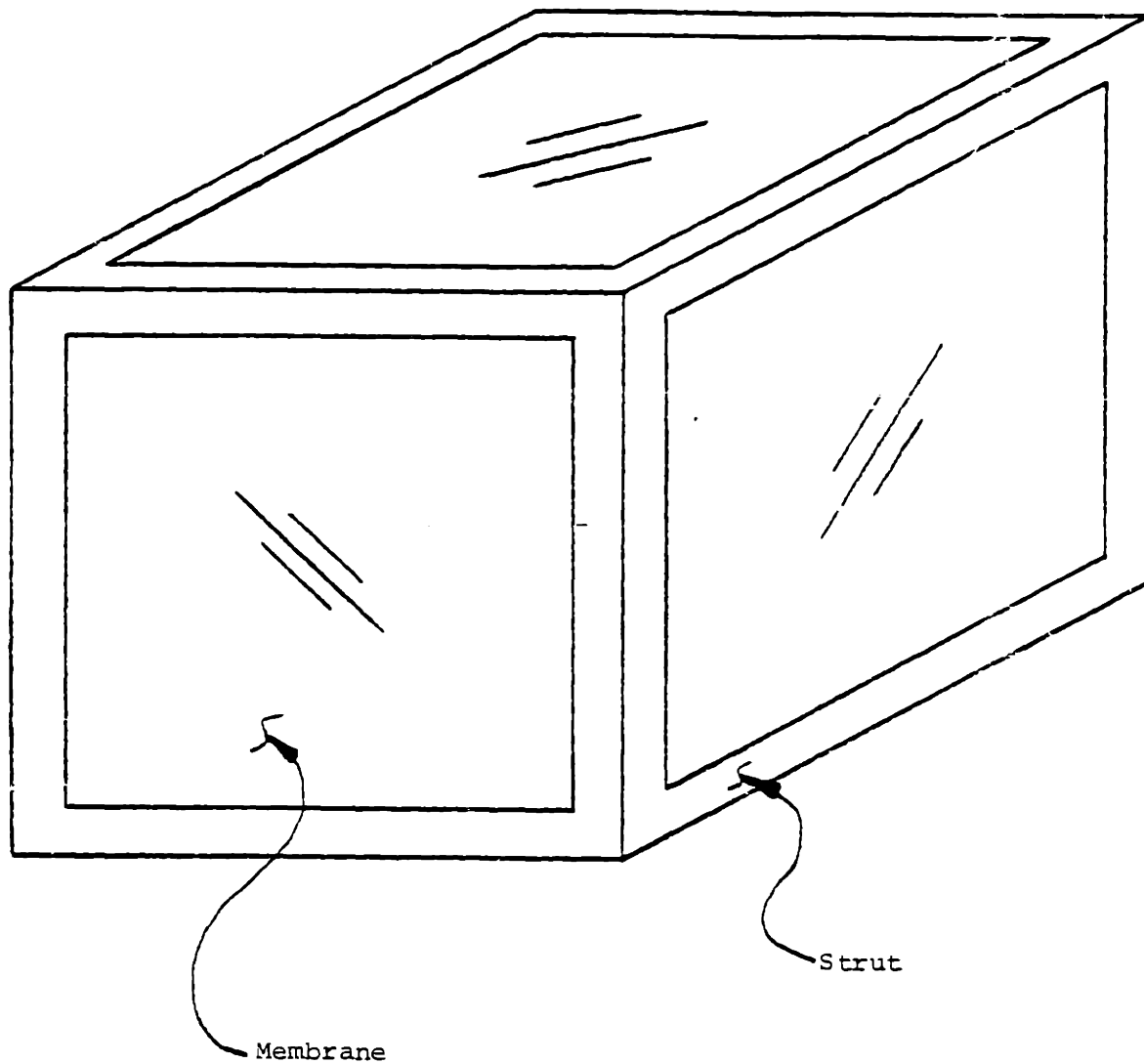
Figure 2-13 : Cubical Bubble Geometry with Struts
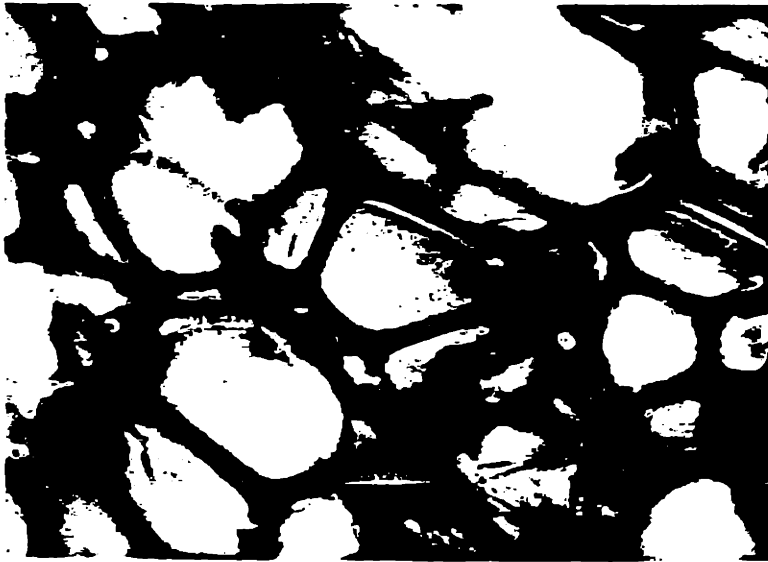
MAGNIFICATION - 80 X
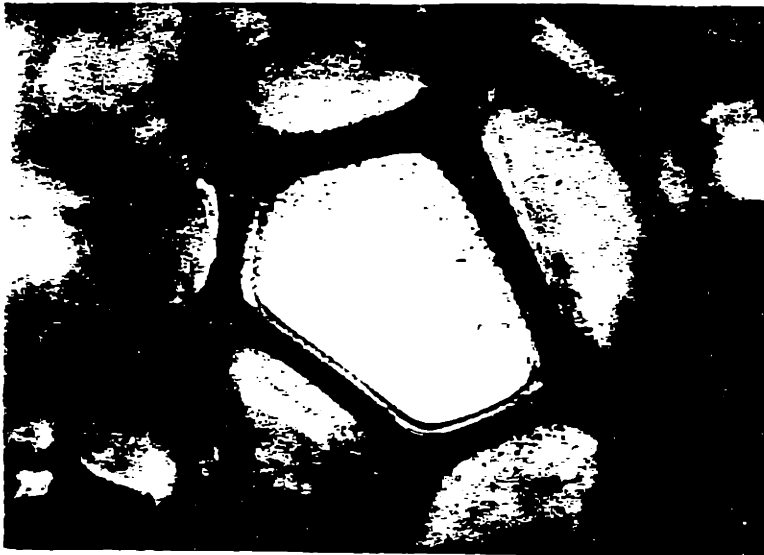
MAGNIFICATION - 160 X

FIGURE 2-14 : TYPICAL OPTICAL MICROSCOPE

PHOTOGRAPHS OF CLOSED CELL FOAM INSULATION

Choosing a Bubble Diameter

For the upper and lower limit cubical bubble conduction models, we will see that the choice of bubble diameter is totally arbitrary. Any choice of bubble diameter will give the same calculated conductivity as any other choice, so long as the percentage of solid in struts and the percentage in membranes remains constant. As the cell size changes in real foam, this mass distribution may well change. As will later be shown, this would strongly affect the solid conduction contribution. In radiation heat transfer, the material distribution may also be relevant since the size of the object relative to the wavelength of radiation affects its performance as an absorber/scatterer.

When estimating the percentage of total solid in struts versus membranes from microscope measurements of the sizes of the objects, one must recognize the differences between the cubical bubble geometry and the actual foam bubble geometry. The in-line cubical bubble geometry results in exactly three whole struts per bubble. (There are twelve forths of a strut per bubble.) In real foam, one would expect to have more struts per bubble since the real bubble geometry is similar to a pentagonal dodecahedron (twelve faced solid, each face is pentagonal). A dodecahedron has thirty edges. Since a regular dodecahedron does not fill space, the proportion of each strut or nodule occupied by one bubble cannot be calculated from the regular dodecahedron shape. Rather, one must rely on observations of foam which show that there are always three membranes intersecting at a strut. On average each bubble

would therefore contain one-third of each strut. This also gives rise to a concave sided triangular cross section in struts, as seen in Figure 2-15. This would be expected from the pentagonal dodecahedron geometry since the angles between faces are close to but not equal to 120 degrees. The dodecahedron geometry would also lead one to expect four struts intersecting at any corner. Observations on large celled foams confirm this suggestion. In summary for foam, one would expect each bubble to contain thirty thirds, or ten whole struts per bubble.

If one wished to estimate the mass distribution from microscopic measurements of strut cross section and/or membrane thickness, (also knowing foam density and bubble size), it is important to properly estimate the total membrane surface area per unit volume and the total length of struts per unit volume of foam. While a cubical bubble analysis provides one estimate, the dodecahedron model would suggest that the cubical bubble estimate would be inaccurate.

For purposes of estimating the fraction of solid in struts and membranes, Figure 2-15 could be used to estimate the cross sectional area of a "typical" strut. Using a cell geometry model such as the dodecahedron, it is possible to estimate the total length of struts per unit volume of foam. These two pieces of information allow estimation of the volume of solid in struts per unit volume of foam. This may be compared to $1 - \delta$, (volume of solid per unit volume of foam) in order to estimate the percentage of solid in struts. At the time of this writing Reitz (38) has begun to develop this technique. He uses a superior

0.0003 inch

7.6 microns

Magnification - 3000 X

Figure 2-15 :   Scanning Electron Microscope
Photograph of the Cross Section of a Strut

technique for obtaining strut cross section photographs than the technique used to obtain Figure 2-15. Reitz's preliminary estimates tend to fall close to 85% of the solid in struts for a typical polyurethane foam.

2.3.2 Limit Models for 3-D In-Line Geometry - 100% Membranes

Only the upper limit model was developed for the 3-D in-line cubical bubble geometry. There is no reason to calculate the lower limit for this geometry since the 2-D calculations proved our intuition correct: i.e., for the in-line geometry there is essentially no difference between the upper and lower limit results, and thus either model may be regarded as exact (within approximately 2%).

It is important to develop the upper limit for the 3-D in-line geometry and the lower limit for the staggered geometry. Recall that the in-line upper limit is also an upper limit for the staggered geometry. With the 3-D cubical bubble geometry and with 100% of the solid assumed to be in membranes, a greater percentage of the solid material is oriented in the direction of heat flow than in 2-D square bubbles. Thus one would expect the 3-D geometry to give higher conductivities. As will be seen later, this is in fact what happens.

Upper Limit

As in the two dimensional case it is helpful to make use of symmetry. Referring back to the upper half of Figure 2-12, planes of symmetry may be drawn through the centers of membranes in all three coordinate directions. Planes of symmetry may also be drawn through the centers of any cell, in all three coordinate directions. Planes of symmetry parallel to the heat flow (parallel to the xz and xy planes) are adiabatic. Planes of symmetry perpendicular to the heat flow (parallel to the yz plane) are isotherms.

The problem is reduced to analysis of the repeating element shown in Figure 2-16. Using the assumption that conductivity is infinite in the plane perpendicular to heat flow (yz plane), all yz planes become isotherms. This may now be modeled exactly with the resistance network shown in Figure 2-16. Since the conductivity was increased in order to arrive at this model, the model provides an upper limit to conduction for the in-line geometry.

Equations 2-55 through 2-57 mathematically express the resistances shown in Figure 2-16.

$$R_{s1} = \frac{2d}{k_s(2dt + t^2)} \tag{2-55}$$

$$R_{s2} = \frac{2t}{k_s(d+t)^2} \tag{2-56}$$

$$R_g = \frac{2}{k_g d} \tag{2-57}$$
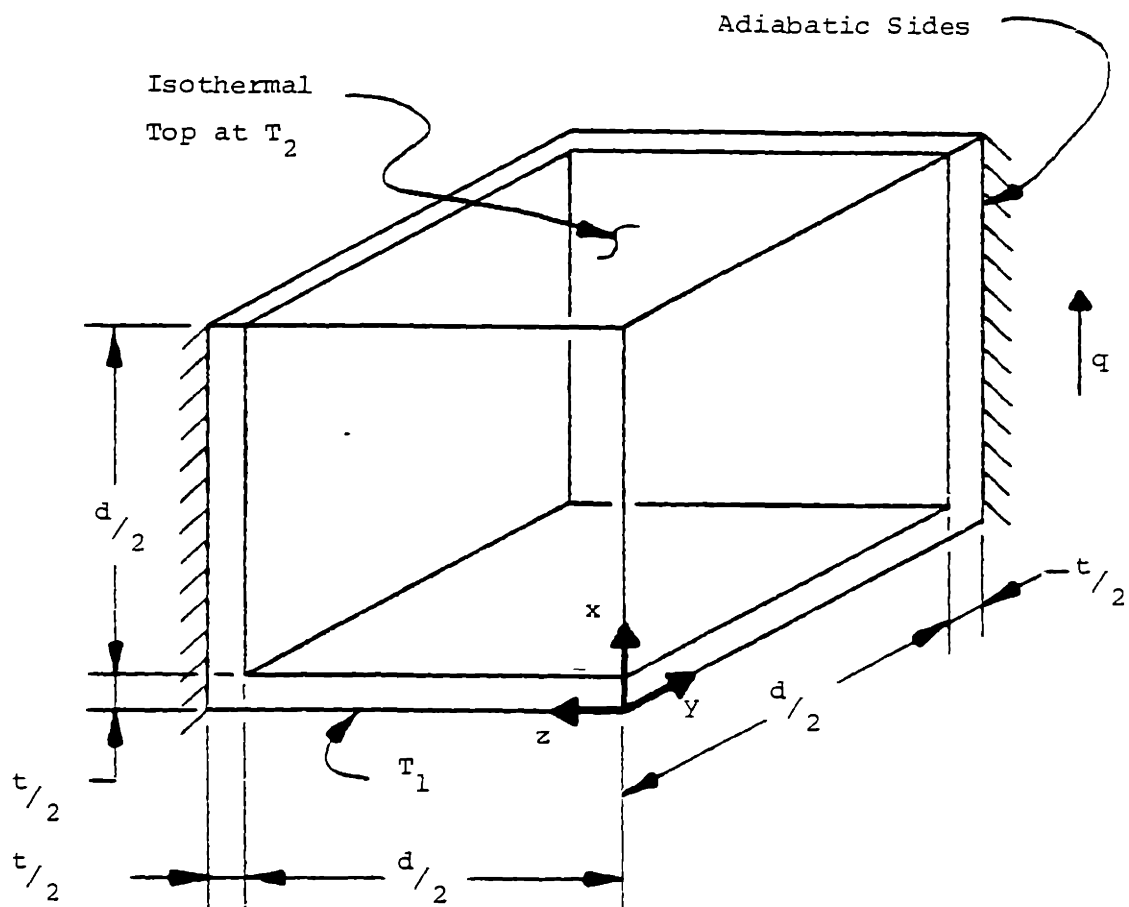
Figure 2-16 : Repeating Element and Circuit Diagram for 3-D In-line Upper Limit
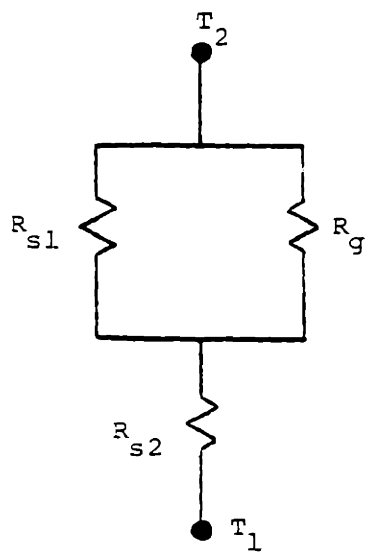
The effective resistance for this upper limit network is:

$$R_{UL \atop s+g} = R_{s2} + (\frac{1}{R_{s1}} + \frac{1}{R_g})^{-1} \qquad (2-58)$$

and the upper limit effective conductivity is then:

$$k_{s+g \atop UL} = \frac{2}{R_{UL \atop s+g} (d+t)} \qquad (2-59)$$

2.3.3 Limit Models for 3-D Staggered Geometry – 100% Membranes

By analogy to the two dimensional case, the upper limit for the staggered geometry is given by the same expression as the upper limit for the in-line geometry. By assuming the conductivity infinite in the yz plane, all yz planes become isotherms. Regardless of whether the cubes are staggered or not, the resistor network given in Figure 2-16 for the in-line geometry also applies to the staggered geometry. Thus, the upper limit conductivity for staggered cubes is given by equation 2-59.

Lower Limit

In order to develop an accurate lower limit model, an analysis was developed which is conceptually similar to the two dimensional lower limit staggered analysis. Referring to the lower drawing in Figure 2-12 for the staggered bubble geometry, planes of symmetry may be drawn parallel to the xy and xz planes through the centers of cells. The planes alternately cut through the centers of cells and the centers of membranes. These planes are adiabatic surfaces. Planes of symmetry parallel to the yz plane may be drawn through the centers of cells, but may not be drawn through the centers of membranes. These planes are isotherms. The resulting repeating element is shown in the top left corner of Figure 2-17.

Even with this idealized geometry, the temperature field is a complex three dimensional function. In order to place a lower limit on the conduction, the problem is broken into the sum of two parts, A and B. (See the two dimensional staggered lower limit analysis for justification.) By adding adiabatic surfaces appropriately, the split problem may become relatively simple to solve, yet without compromising too much accuracy.

If the reader will recall, in the two dimensional problem the temperature field was expressed as the sum A plus B. Problems A and B were solved separately, that is, lower limits were placed on A and B. The sum represents a heat transfer lower limit for T. In 3-D, problem A is (just as in the 2-D case) the conduction through the solid without

T₂

Adiabatic Sides

t/2   d/2   d/2

Solid Face, Half Thickness

T₁

T₁

Adiabatic Edges

Adiabatic
Line of
Symmetry

T₂

Half
Thickness

T₂

T₁

Isothermal
Line of
Symmetry

Full
Thickness

T₁

Half
Thickness

Full Thickness

45°

$\dfrac{(T_1 + T_2)}{2}$

$\dfrac{d}{2}$

dy   y

$\dfrac{d}{2}$

T₁

x

y
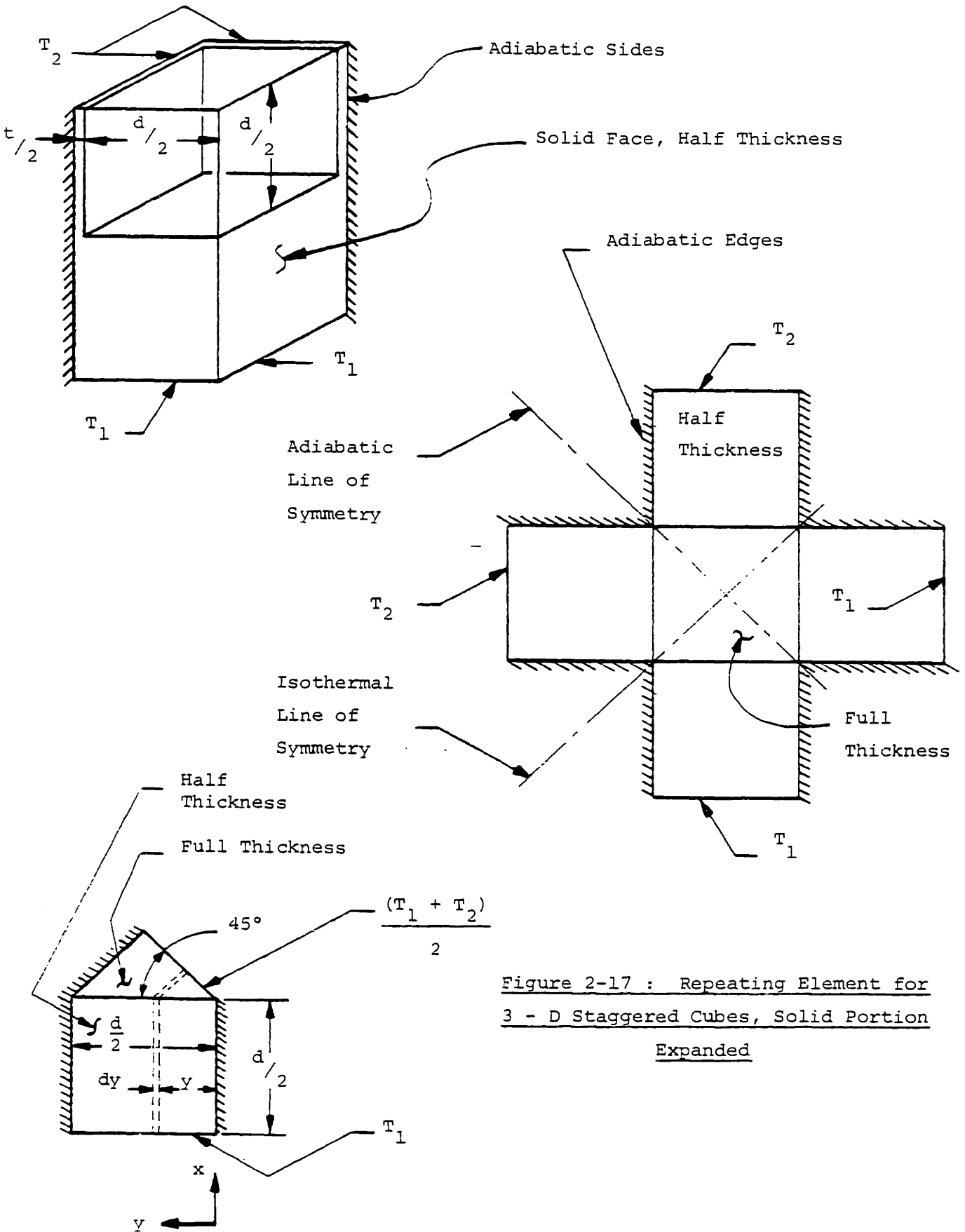
Figure 2-17 : Repeating Element for
3 - D Staggered Cubes, Solid Portion
Expanded

interaction with the gas. Problem B is (as in 2-D) the conduction through the gas, across the midsection membrane, and through the lower volume of gas. Were it not for some adiabatic surfaces (see Figure 2-4 for the 2-D case) which must be added to keep the analysis simple, the differential equation and boundary conditions for A and B would add up to those for T, and thus the solution (A+B) would be exact.

Solution of Problem B

The only conceptual difference between the 3-D and the 2-D staggered models is that Problem A for 3-D cannot be solved with a simple resistance network. Problem B for 3-D can be solved with a simple resistance network consisting of two gas resistances plus one solid resistance in series. The effective resistance in problem B is just the sum of the three resistances. These relations are given in equations 2-60 through 2-62.

$$R_B = 2R_g + R_s \tag{2-60}$$

where:

$$R_g = \frac{2}{k_g d} \tag{2-61}$$

$$R_s = \frac{4t}{k_s d^2} \tag{2-62}$$

Since $R_s \ll R_g$, for low densities it is possible to neglect the solid resistance, thereby leaving Rb as just twice Rg. However, so as not to introduce small errors at higher densities, the solid resistance is included.

Solution of Problem A

In order to solve problem A, the solid portion of the repeating element is flattened from three to two dimensions as shown in the right hand side of Figure 2-17. Adiabatic and isothermal lines of symmetry become readily apparent, reducing the problem to the element shown in the lower left hand side of Figure 2-17. A lower limit for this element may be calculated by integration, as follows.

An arbitrary section is taken at y,dy wide, as shown dashed in Figure 2-17. The conductivity is assumed to be zero normal to the dashed lines. This allows calculation of the heat flow (dq) through the infinitesimal element using a simple resistance.

$$dq = \frac{T_1 - T_2}{2R_i} \qquad (2-63)$$

where:

$$R_i = \frac{d/2}{k_s(t/2)dy} + \frac{y\sqrt{2}}{k_s t(dy/\sqrt{2})} = \frac{d+y}{k_s t\, dy} \qquad (2-64)$$

The total heat flow is obtained from integration:

$$q = \int dq = \int_0^{d/2} \frac{T_1 - T_2}{2(d+y)} k_s t \, dy \qquad (2\text{-}65)$$

and·

$$q = \frac{T_1 - T_2}{2} k_s t \ln(1.5) \qquad (2\text{-}66)$$

Equation 2-66 gives the total heat flow through the element shown in the lower left hand side of Figure 2-17. In problem A there are two parallel paths (we ignored the other half by symmetry) , Therefore, for problem A:

$$q_A = (T_1 - T_2) k_s t \ln(1.5) \qquad (2\text{-}67)$$

but by definition:

$$R_A \equiv \frac{T_1 - T_2}{q_a} = \frac{2.4663}{k_s t} \qquad (2\text{-}68)$$

Combined Solution for Lower Limit

The reader may recall that in the two dimensional staggered lower limit problem, the heat flows in problems A and B were added, providing a lower limit conduction estimate in T. This is mathematically the same as two resistors in parallel, so that·

$$R_{LL} = \left(\frac{1}{R_A} + \frac{1}{R_B} \right)^{-1} \tag{2-69}$$

Finally:

$$k_{\substack{s+g \\ LL}} = \frac{4}{R_{LL} \ (d + t)} \tag{2-70}$$

Equation 2-70 gives the overall lower limit conductivity of the medium, including solid and gas contribution. The various terms in the equation may be calculated with equations 2-69, 2-68 and 2-60.

Results are presented in Figure 2-18 for the case of cubical bubbles, no struts, no radiation, and no cell elongation. It is somewhat surprising to see the 3-D lower limit model predicting higher conductivities than the 2-D upper limit model. Also note the difference between the 3-D upper and lower limits. At 2.0 pcf (32 kg/m^3) the difference is approximately 7% overall, or approximately 20% of the "solid contribution". At 5.0 pcf (80 kg/m^3) the difference is 12% overall, or 20% of the "solid contribution". These results use a value

Figure 2-18 : Effective Conductivity Using Upper and Lower Limit Models for Cubical Bubble Geometry - 100% Membranes
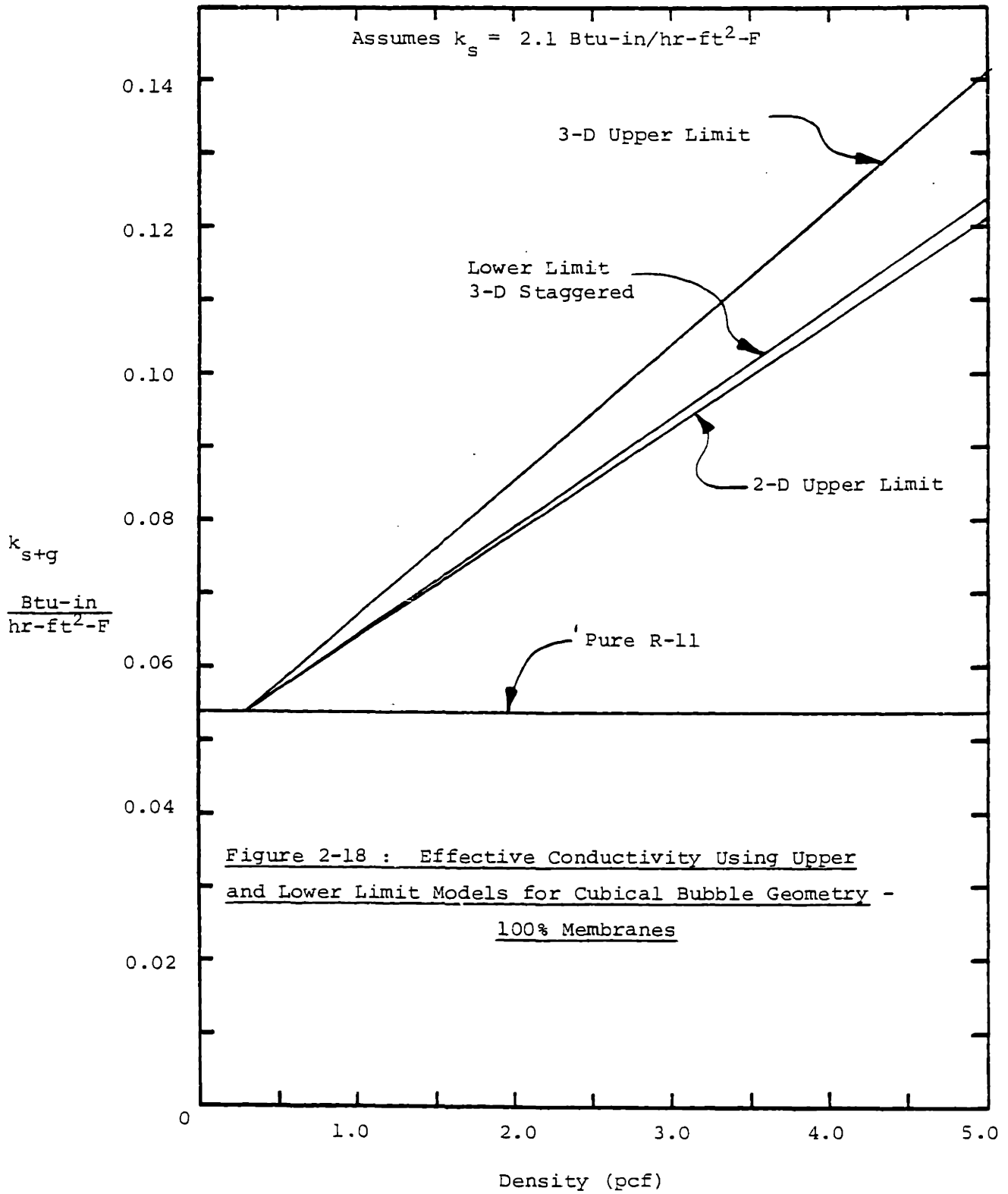
for solid conductivity of 2.1 Btu-in/hr-ft^2-F, and a value of 0.0539 Btu-in/hr-ft^2-F for gas conductivity. In section 2.3.8 we will see that the solid polymer conductivity may be disputed. Some references give values for solid polymer conductivity approximately one-half of the value used here. Lower solid conductivity also means less uncertainty in the overall conductivity due to the upper-lower limit differences.

<u>Comparison to Published Conduction Models</u>

The 3-D upper limit cubical bubble conduction model gives numerically identical results to the model proposed by Russell (2) for cubical bubbles in porous media. This indicates that Russell's model is an upper limit model. Therefore if one wishes to avoid calculating the resistances presented here, then Russell's equation may be used with equal accuracy. The equation proposed by Russell (2) is repeated here for convenience.

$$\frac{k_{s+g}}{k_s} = \frac{\delta^{2/3} + \frac{k_s}{k_g}(1 - \delta^{2/3})}{\delta^{2/3} - \delta + \frac{k_s}{k_g}(1 - \delta^{2/3} + \delta)} \qquad (2-71)$$

where:

k_{s+g} = effective conductivity in the absence of radiation

k_s = conductivity of solid material

k_g = conductivity of gas in pores

δ = porosity, volume of gas divided by total volume

If one is careful to correctly apply a formula proposed by Doherty (3), his equation will also give the same results. The only minor difficulty is that Doherty modeled foam with 2-D (square) bubbles, and so the terms in his equation must be modified to those for 3-D if the correct answers are to be obtained.

It is unfortunate that neither Russell nor Doherty identified their models as representing upper limits. To the best of this author's knowledge, no previous published references give a lower limit estimate for conduction in porous media, hence the error in these models has been heretofore unestimated.

The equation proposed by Russell is simple to apply and yet because of the form of the expression the physical significance is lost. For low density foams the porosity is close to 1.0, thus δ and $\delta^{2/3}$ are quite close. This, plus the fact that $k_g \ll k_s$ allows us to simplify the expression. If one multiplies the numerator and denominator of the right hand side of equation 2-71 by k_g, the denominator becomes the sum of two terms. The k_s term is much larger than the k_g term, which allows the simplification of dropping the gas conductivity term. The modified Russell equation which results is rewritten in equation 2-72.

$$k_{s+g} \simeq \left(\frac{\delta^{2/3}}{1 - \delta^{2/3} + \delta} \right) k_g + \left(\frac{1 - \delta^{2/3}}{1 - \delta^{2/3} + \delta} \right) k_s \qquad (2\text{-}72)$$

A simple numerical experiment shows that for porosities over 0.95 (corresponds to polyurethane foam density less than 4.1 pcf) the coefficient in front of k_g in equation 2-72 is within 2% of 1.0. The coefficient in front of the k_s term is within 2.5% of $0.667(1-\delta)$. Therefore, for purposes of physical intuition the Russell equation can be approximated by equation 2-73 for porosities greater than 0.95.

$$k_{s+g} \simeq k_g + \frac{2}{3}(1 - \delta) k_s \qquad (2-73)$$

The intuitive explanation is that for cubical bubbles oriented normal to heat flow. two-thirds of the solid material (four of six cube faces) is aligned in the direction of heat flow and thus contributes to the overall conductivity. The error associated with equation 2-73 is approximately 1.0% for 5.0 pcf foam density, and 0.1% for 2.0 pcf foam density. (The errors in the two terms partially cancel resulting in lower error in the sum than in each term.)

This intuitive reasoning can explain another facet of the cubical bubble geometry. If all of the solid material is placed in sticks along the edges of the cube so that the geometry resembles scaffolding, then equation 2-73 will be found to apply except the coefficient 2/3 is replaced by 1/3. This is because only four of the twelve edges of the cube are aligned in the heat flow direction. If the solution were indeed carried out, the error in this ultra-simplified approach would be comparable to the error in equation 2-73. For this reason, one might

suspect that struts in foam contribute to lower overall conductivity. In succeeding sections this will be shown to be a correct conclusion.

2.3.4 Upper Limit to Heat Flow in an Arbitrary Direction for In-Line Cubes

In this subsection we will examine the three dimensional analogy to the problem presented in section 2.2.5, Heat Flow at Arbitrary Angle to 2-D Squares. We examine the case where all of the solid material is in the membranes as well as the case when all of the solid material is in the struts.

2.3.4.1 Heat Flow at Arbitary Angle to Cubical Bubbles - 100% Membranes   The geometry for this analysis is the in-line cubical bubble geometry of Figure 2-12, except that the bubble walls are at an arbitrary angle to the direction of heat flow. Isotherms are assumed to be lateral planes parallel to the foam faces at T_1 and T_2. Hence the temperature gradient is everywhere normal to the faces. We define the angles between the temperature gradient vector and the x, y, z directions α, β, and γ respectively.

In order to understand the model, consider first the case of two isothermal planes at T_1 and T_2, separated by a distance L, with another plane at an angle α to the planes. See Figure 2-19 for this geometry. From geometry it is clear that the normal vector to the diagonal plane makes the same angle α to the temperature gradient vector. The heat
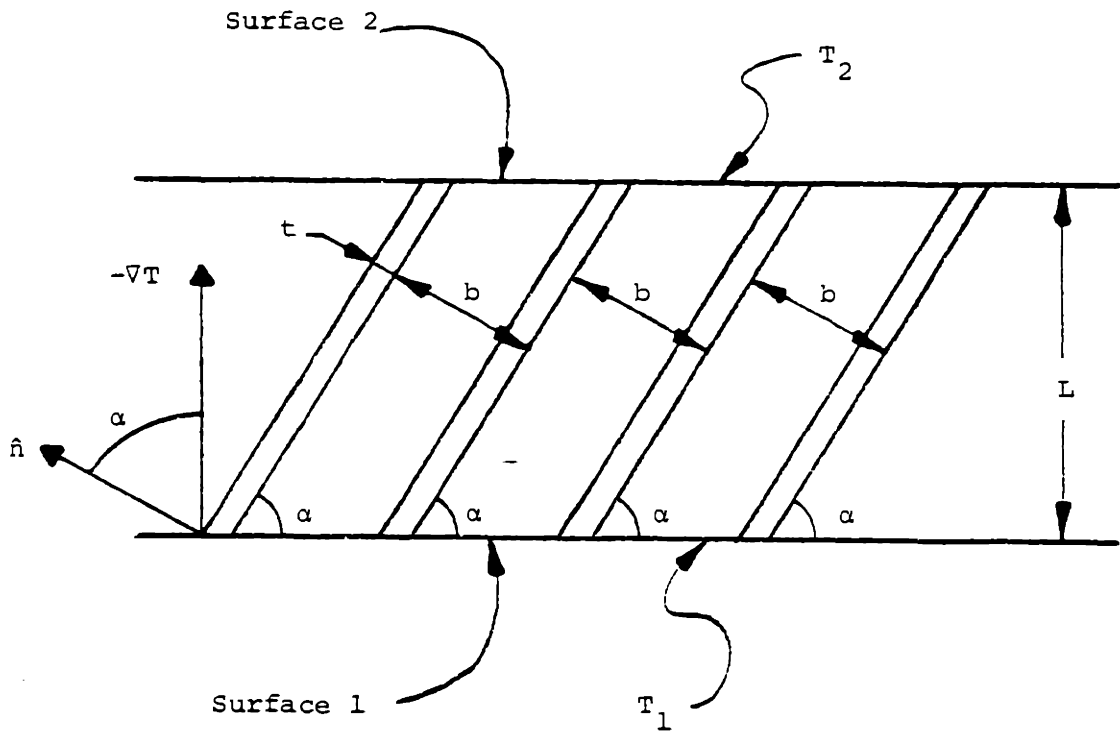
Figure 2-19 : Portion of Geometry for Heat Flow
at Arbitrary Angle to In-Line Cubes

flow through this plane is given by equation 2-74, where D is the depth of the plane into the paper and t is the plane thickness.

$$q(\alpha) \ = \ k_s \ D \cdot t \cdot \frac{\sin \alpha}{L} \ (T_1 - T_2) \qquad (2\text{-}74)$$

Many planes at the same angle α (parallel to the first diagonal plane) are spaced apart by a distance b. The number of planes at α per unit area of surface 1 is given by equation 2-75.

$$n(\alpha) \ = \ {}^{-}\frac{\sin \alpha}{D \cdot b} \qquad (2\text{-}75)$$

Consider two more sets of parallel planes, crossing from surface 1 to 2. Each set is normal to the other as well as normal to the original diagonal plane at α. Since all these planes are normal to each other, the in-line cubical bubble geometry has been assembled. If isotherms are once again assumed to be planes parallel to the surfaces of the foam at T_1 and T_2, then the normal vectors from the three coordinate planes make angles of α, β, and γ to the temperature gradient vector. The planes themselves thus make angles α, β and γ to the isotherms. Equation 2-74 and 2-75 may be re-written with β and γ for the other two planes. The total solid conduction is given by equation 2-76:

$$\frac{q_{solid}}{A} \ = \ q(\alpha) \cdot n(\alpha) + q(\beta) \cdot n(\beta) + q(\gamma) \cdot n(\gamma) \qquad (2\text{-}76)$$

This may be simplified to yield:

$$q_{solid} = \frac{A \cdot (T_1 - T_2)}{L} \, k_s \frac{t}{b} (\sin^2\alpha + \sin^2\beta + \sin^2\gamma) \qquad (2-77)$$

Schwartz (4) gives the following geometric theorem:

$$\cos^2\alpha + \cos^2\beta + \cos^2\gamma = 1 \qquad (2-78)$$

when α, β and γ are defined as they are in this case. But sine squared plus cosine squared equals one. so that:

$$\sin^2\alpha + \sin^2\beta + \sin^2\gamma = 2 \qquad (2-79)$$

Combining this result with a simple resistance for gas conduction gives:

$$k_{s+g} = k_g + k_s \frac{2t}{b} \qquad (2-80)$$

But:

$$\delta = \frac{(b - t)^3}{b^3} = \frac{b^3 - 3b^2t + 3bt^2 - t^3}{b^3} \simeq 1 - 3\frac{t}{b} \qquad (2-81)$$

which leads to:

$$k_{s+g} \simeq k_g + \frac{2}{3} (1 - \delta) k_s \qquad (2-82)$$

This of course agrees with equation 2-73, as it must since the solution is independent of angle.

2.3.4.2 <u>Heat</u> <u>Flow</u> <u>at</u> <u>Arbitrary</u> <u>Angle</u> <u>to</u> <u>Cubical</u> <u>Bubbles</u> <u>-</u> <u>100%</u> <u>Struts</u>   Consider a unit cube with 100% of the solid in the corners. The temperature gradient vector passes through one corner at an arbitrary angle. See Figure 2-20. In a similar fashion as the previous section, define α, β and γ as the angles between the gradient vector and the x, y, z axes, respectively. It the isotherms are planes normal to the gradient vector, then the solid conduction heat flow can be expressed as:

$$\frac{q_{solid}}{A} = q_x n_x + q_y n_y + q_z n_z \qquad (2-83)$$

where q_x, q_y and q_z are the heat flows through the x, y, and z directions, respectively. n_x, n_y, and n_z are the numbers of sticks in the x, y, and z directions per unit heat flow area. The q's and n's are given for any stick at arbitrary angle.

$$q(\xi) = k_s S^2 \frac{\cos \xi}{L} (T_1 - T_2) \qquad (2-84)$$

$$n(\xi) = \frac{\cos \xi}{b^2} \qquad (2-85)$$

where b, L, T_1 and T_2 are defined exactly as in the previous section. (See Figure 2-19).Equations 2-84 and 2-85 may be written for α, β and γ (x, y and z sticks), and substituted into equation 2-83. Using the identity given in equation 2-78, along with a simple resistance for gas conduction yields:

$$k_{s+g} = k_g + k_s \frac{S^2}{b^2} \qquad (2-86)$$
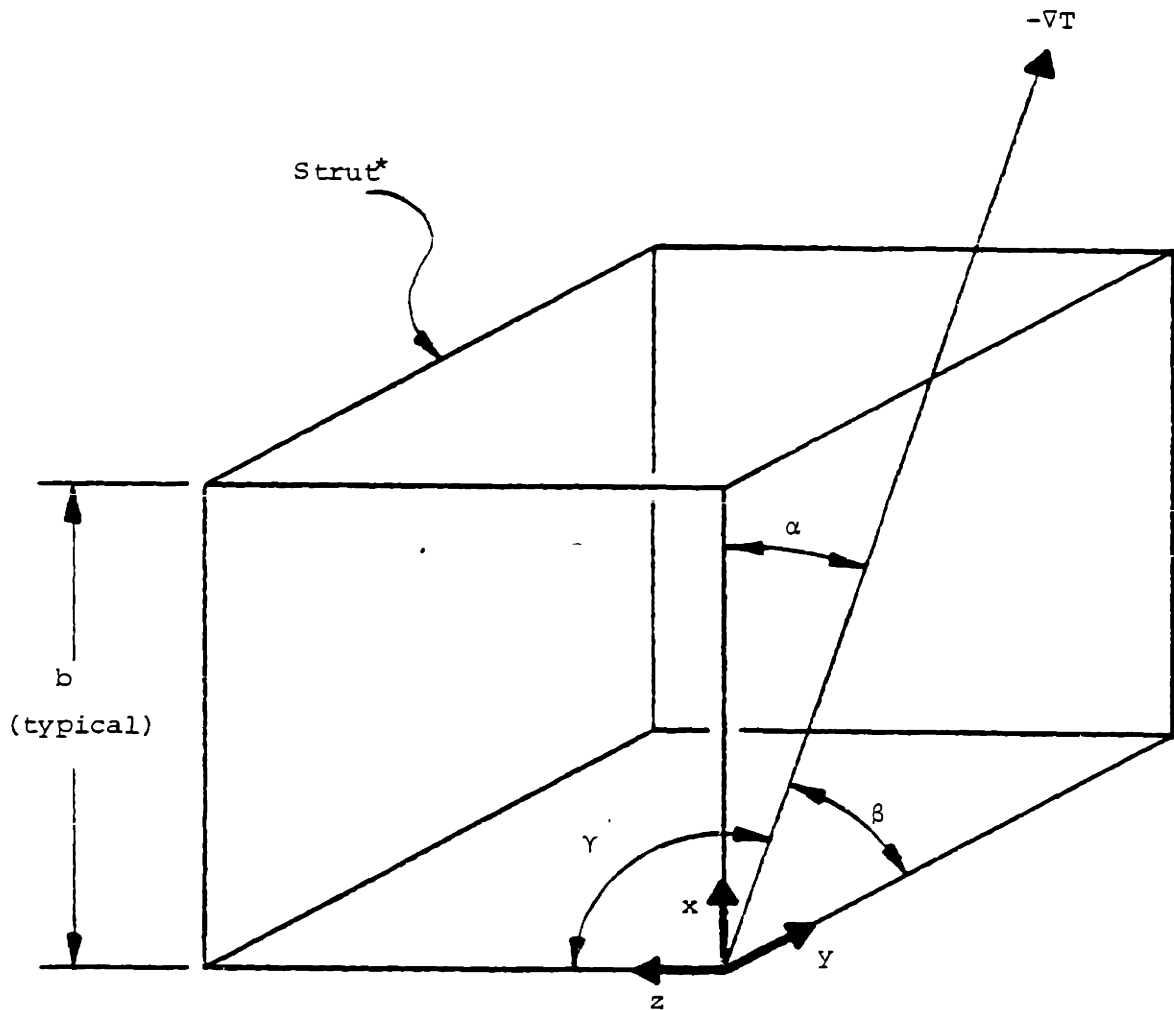
*Cross Sectional Area $= S^2$

Figure 2-20 : Geometry for Heat Flow at Arbitrary

Angle Through Cubical Bubbles - 100% Struts

which may be shown to be approximated by:

$$k_{s+g} \simeq k_g + \frac{1}{3} (1 - \delta) k_s \qquad (2\text{-}87)$$

Equation 2-87 agrees with the intuitive result discussed at the end of section 2.3.3, Limit Models for 3-D Staggered Geometry.

These results indicate that the upper limit for the cubical bubble geometry is independent of heat flow direction. For the in-line geometry, sections 2.2.2 and 2.2.4 suggest that the lower limit is within one or two percent of the upper limit even for heat flow in oblique directions. For the staggered geometry however, the difference may be as high as 20% of the solid contribution.

The cubical bubble geometry also suggests that the heat flow would be significantly different for foam with large struts. The next two sections show that this is indeed true.

2.3.5 Random Sticks Upper Limit, 3-D

All previous three dimensional analyses have used cubical bubbles in various orientations and packing arrangements. In order to determine what effect the cubical shape assumption has on the results, this section and the next section examine the heat flow through geometries which are more representative of real foam geometry. In this section we present an upper limit analysis of heat flow through a medium containing randomly oriented sticks. This would be representative of the geometry

for isotropic foam in the limit where 100% of the solid is in struts. The analysis is different from published analyses for glass fiber insulations. This is because the sticks would be joined end to end in foam. whereas in glass fiber insulation this is not the case.

This analysis is analogous to the one in section 2.2.6, Random Sticks Upper Limit , 2-D. The solid is assumed to be in the form of stick shaped elements which may be oriented in any direction relative to the heat flow. Since foams are often isotropic, the total length of all sticks per unit volume which are oriented in some direction (ϑ, ϕ) relative to the temperature gradient vector within an infinitesimal solid angle $d\omega$, is assumed a constant (λ). This is the definition of "random sticks". From this definition:

$$1 - \delta = S^2 \int_{4\pi} \lambda d\omega = 4\pi S^2 \lambda \qquad (2\text{-}88)$$

where S^2 is the cross sectional area of a stick.

Isotherms are again assumed to be planes parallel to the faces of the foam at T_1 and T_2. As in the 2-D analysis, all sticks in the (θ, ϕ) direction are lined up end to end forming bridges from one side of the foam to the other. The foam thickness is L. See Figure 2-11 for the 2-D picture. In 3-D, the angle ϕ has no effect on the heat transfer through any particular bridge. The heat flow across one bridge at (θ, ϕ) given by:

$$q(\theta, \phi) = k_s \frac{S^2 \cos \theta}{L} \Delta T \qquad (2\text{-}89)$$

if $n(\theta,\phi)$ is the number of bridges at θ,ϕ per unit volume per unit solid angle, and if $l(\theta,\phi)$ is the length of a bridge at θ,ϕ, then their product represents the total length of sticks at θ,ϕ per unit volume per unit solid angle. This product is constant by the definition of random sticks.

$$\lambda = n(\theta,\phi) \cdot l(\theta,\phi) = \text{constant} \qquad (2\text{-}90)$$

But from geometry:

$$l(\theta,\phi) = \frac{L}{\cos\theta} \qquad (2\text{-}91)$$

thus:

$$n(\theta,\phi) = \frac{\lambda\cos\theta}{L} \qquad (2\text{-}92)$$

The total heat conduction through all solid material is given by the integral over all solid angles of the product of the number of sticks at θ,ϕ per unit volume per unit solid angle, times the heat flow of a single stick at θ,ϕ times the volume. Mathematically this is given by:

$$q_{\text{solid}} = 2\pi \int_0^\pi \left(\frac{\lambda\cos\theta}{L}\right) \cdot \left(k_s \frac{S^2\cos\theta}{L} \cdot \Delta T\right)(L \cdot A) \cdot \sin\theta \ d\theta$$

$$(2\text{-}93)$$

which may be integrated to yield:

$$q_{solid} = \frac{A\Delta T}{L} \frac{4\pi}{3} k_s S^2 \lambda \qquad (2-94)$$

Including a simple resistance for the gas:

$$q_{gas} = \frac{A\Delta T}{L} k_g \qquad (2-95)$$

and substituting into equation 2-94 for λ from equation 2-88, the effective conductivity of the medium is given by:

$$k_{s+g} = k_g + \frac{1}{3}(1 - \delta) k_s \qquad (2-96)$$

which agrees with equation 2-87 for cubical bubbles, 100% struts, at arbitrary θ, ϕ.

This analysis could be modified to give an upper limit for the conduction in glass fiber insulation, or to give an upper limit when there is considerable cell elongation in foams. Instead of assuming that λ is constant (random sticks), one would use the actual material distribution as produced in the insulation. This information would then allow integration of equations 2-88 and 2-93. In insulation where there is preferential lateral orientation of the fibers, the conduction calculated by performing these integrations would be even lower than that given by equation 2-96. In foam insulation where there is elongation of cells in the heat flow direction, the conduction would be greater than that calculated by equation 2-96.

One must not forget that this is an upper limit based on infinite conductivity in the direction perpendicular to heat flow. This is an accurate limit model for foams, where struts join end to end. In glass fiber insulation the fibers are not joined at the ends. This limit model would be expected to overestimate the actual heat transfer in glass fiber insulation by a greater amount than it does in foams.

2.3.6 Random Planes - Upper Limit

The analysis for random planes is analogous to the previous analysis for random sticks. The random planes geometry is representative of the real geometry for isotropic foam in the limit where 100% of the solid is in the membranes. Consider the geometry of Figure 2-21. By similar reasoning as in the random stick analysis, all planes originally oriented at θ, ϕ are stacked end to end into bridges spanning L. The width of the plane, W, is assumed equal to the depth into the paper. The heat flow through any bridge at θ, ϕ is independent of θ, ϕ and is given by equation 2-97.

$$q(\theta,\phi) =. k_s \frac{t \cdot W}{W} \Delta T \qquad (2-97)$$

If $n(\theta, \phi)$ is defined as the number of bridges per unit volume per unit solid angle whose normal vector is at θ, ϕ and if $A(\theta,\phi)$ is the area of a bridge whose normal vector is at θ, ϕ, then their product represents the total area of all planes whose normal vectors pass through θ, ϕ per
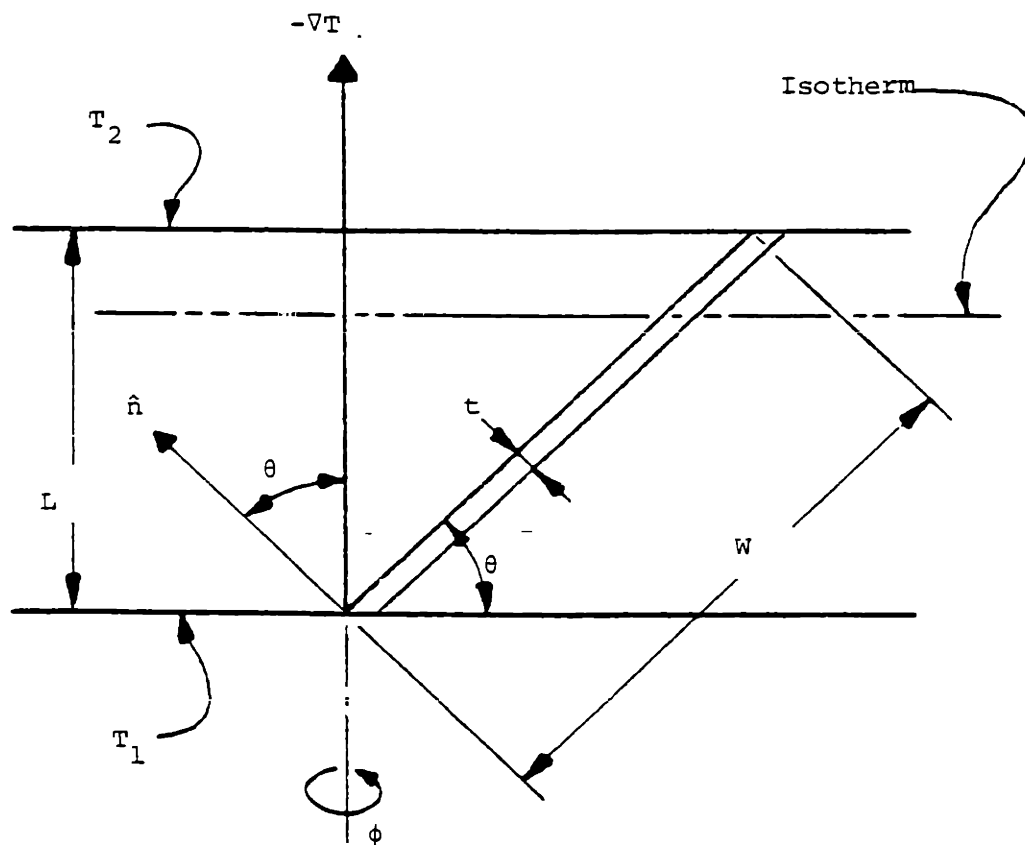
Figure 2-21 : Geometry for Analysis of Random Planes Upper Limit

unit volume per unit solid angle. This product is defined as λ, and is constant by the definition of random planes.

$$\lambda \equiv n(\theta,\phi) \cdot A(\theta,\phi) = \text{constant} \qquad (2\text{-}98)$$

By geometry:

$$A(\theta,\phi) = W^2 = \frac{L^2}{\sin^2\theta} \qquad (2\text{-}99)$$

hence:

$$n(\theta,\phi) = \frac{\lambda \sin^2\theta}{L^2} \qquad (2\text{-}100)$$

The total number of bridges times the heat flow per bridge gives the total solid conduction.

$$q_{solid} = (k_s t \Delta T) \cdot A \cdot L \, 2\pi \int_0^\pi \frac{\lambda \sin^2\theta}{L^2} \sin\theta \, d\theta \qquad (2\text{-}101)$$

which yields:

$$q_{solid} = \frac{A \cdot \Delta T}{L} k_s t \, \lambda \cdot \frac{8\pi}{3} \qquad (2\text{-}102)$$

We may determine λ from the foam density via the foam porosity:

$$1 - \delta = \int_{4\pi} \lambda \, t \, d\omega = 4\pi\lambda t \qquad (2\text{-}103)$$

Solving for λ, substituting into equation 2-102, and using a simple resistance for gas conduction yields:

$$k_{s+g} = k_g + \frac{2}{3}(1 - \delta)\,k_s \qquad (2\text{-}104)$$

which is identical to equation 2-82, the result for cubical bubbles with 100% of the solid in membranes and heat flow at arbitrary angle.

Note that by analogy to the random struts case, this model could be adapted to the case where there is considerable cell elongation. Instead of assuming constant λ, the actual distribution is used and equations 2-101 and 2-103 are integrated.

2.3.7. Conduction Model for Real Foam

We have shown that equation 2-59 gives the effective conductivity for in-line cubical bubbles with 100% of the solid in membranes. This result is independent of heat flow direction relative to the bubble walls. Russell's equation (2-71) gives numerically identical results and is more convenient to use than equation 2-59. Equation 2-73 is approximately correct for low foam densities.

When any of the solid material is in the form of struts, the effective conductivity is lower than that predicted by Russell's equation. For low densities with 100% of the solid in struts, equation 2-96 gives the effective conductivity of the medium. This result is also independent of the direction of heat flow relative to the cells.

Note that equation 2-96 predicts a "solid contribution" equal to one half of the solid contribution predicted by Russell's equation. (This is evident from the simplified Russell equation, equation 2-73.)

We have also shown that random sticks and random planes give approximately the same upper limit results as the cubical bubble geometry. This indicates that there is no effect due to the assumed cubical cell shape on the conduction heat transfer, within the uncertainty of the limit models. The cubical bubble limit models give "solid contribution" results within a 20% spread between the extreme cases where the bubbles were arranged in-line and staggered.

The random sticks and planes analyses can be modified to account for non-isotropic shapes, such as would be found in foams with cell elongation or in glass fiber insulation. A less accurate modification would be to use rectangular prisms rather than cubes, and use the resistance network solution of sections 2.3.2 and 2.3.3.

In summary, we have solved cases where all of the material is in the struts, or all of the material is in the membranes. Real foam has signficant amounts of solid in both areas. Considering the accuracy of the horizontal isotherm approximation, (2% error in solid contribution at best, 20% error in solid contribution at worst) it is reasonable for the combined struts and membranes case to simply use a weighted average of the solution for struts with the solution for membranes. If the isotherms were actually planes perpendicular to the gradient vector, then this weighted average would be exact. One can either weight the

average by volume, or, since the solid density is constant, one can weight the average by mass.

For the upper limit model for real foam, one should use a weighted average of the results of equation 2-104 and 2-96, where the weighting is determined by the amount of solid in membranes versus struts. This is expressed in equation 2-105, where P_s is the percentage of the total solid in struts.

$$k_{s+g} = k_g + \left(\frac{2}{3} - \frac{P_s}{300}\right) (1 - \delta) \, k_s \qquad (2-105)$$

A slightly more accurate formulation would use a weighted average of the result from Russell's equation (eq. 2-71) with equation 2-96. This would include the gas-solid conduction interaction, whereas equation 2-105 clearly does not.

Unfortunately it is not as simple to devise a realistic lower limit for real foam geometry. Based on the fact that the solid contribution for the staggered cube geometry is 20% below the solid contribution for the in-line geometry, it is reasonable to expect that the actual foam "solid contribution" would be less than but within 20% of the solid contribution calculated via the upper limit model. Equation 2-106 expresses this "lower limit".

$$k_{s+g_{LL}} \simeq k_g + 0.8 \left(\frac{2}{3} - \frac{P_s}{300}\right) (1 - \delta) \, k_s \qquad (2-106)$$

Using equations 2-105 and 2-106 the conduction heat transfer was calculated for fresh foam (assuming a constant gas conductivity equal to the conductivity of pure R-11). The results are presented in Figure 2-22 and 2-23. The solid conductivity was taken to be 2.1 Btu-in/hr-ft^2-F for Figure 2-22 and 1.0 Btu-in/hr-ft^2-F for Figure 2-23. The uncertainty band ranges from zero to 12% of the overall conductivity depending on the foam density, solid polymer conductivity, and percentage of solid in struts.

Using the most accurate upper limit conduction model (weighted average of equations 2-71 and 2-96) we will now show that the change in conduction heat transfer during aging is due entirely (within 1%) to the change in gas conductivity. (Assuming the polymer conductivity k_s does not change.) Table 2-2 gives the effective conductivity as calculated for a fixed polymer conductivity, fixed foam porosity, and with different gas conductivities. Clearly, the "solid contribution" is approximately constant, and is therefore independent of aging. The variation is approximately 2.5% of the solid contribution, or 0.6% of the effective conductivity in the absence of radiation. This result could have been anticipated given the separation of solid and gas contributions in equation 2-105, which is within 1% of the weighted average of equations 2-71 and 2-96 for all cases.

Assumes k_s = 2.1 Btu-in/hr-ft^2-F

P_s = 0

P_s = 50

P_s = 100

Pure R-11

k_{s+g}

$\dfrac{\text{Btu-in}}{\text{hr-ft}^2\text{-F}}$

Figure 2-22 : Calculated Conduction with
Varying Percentage of Solid in Struts

Density (pcf)

Figure 2-23 : Calculated Conduction with Varying Percentage of Solid in Struts
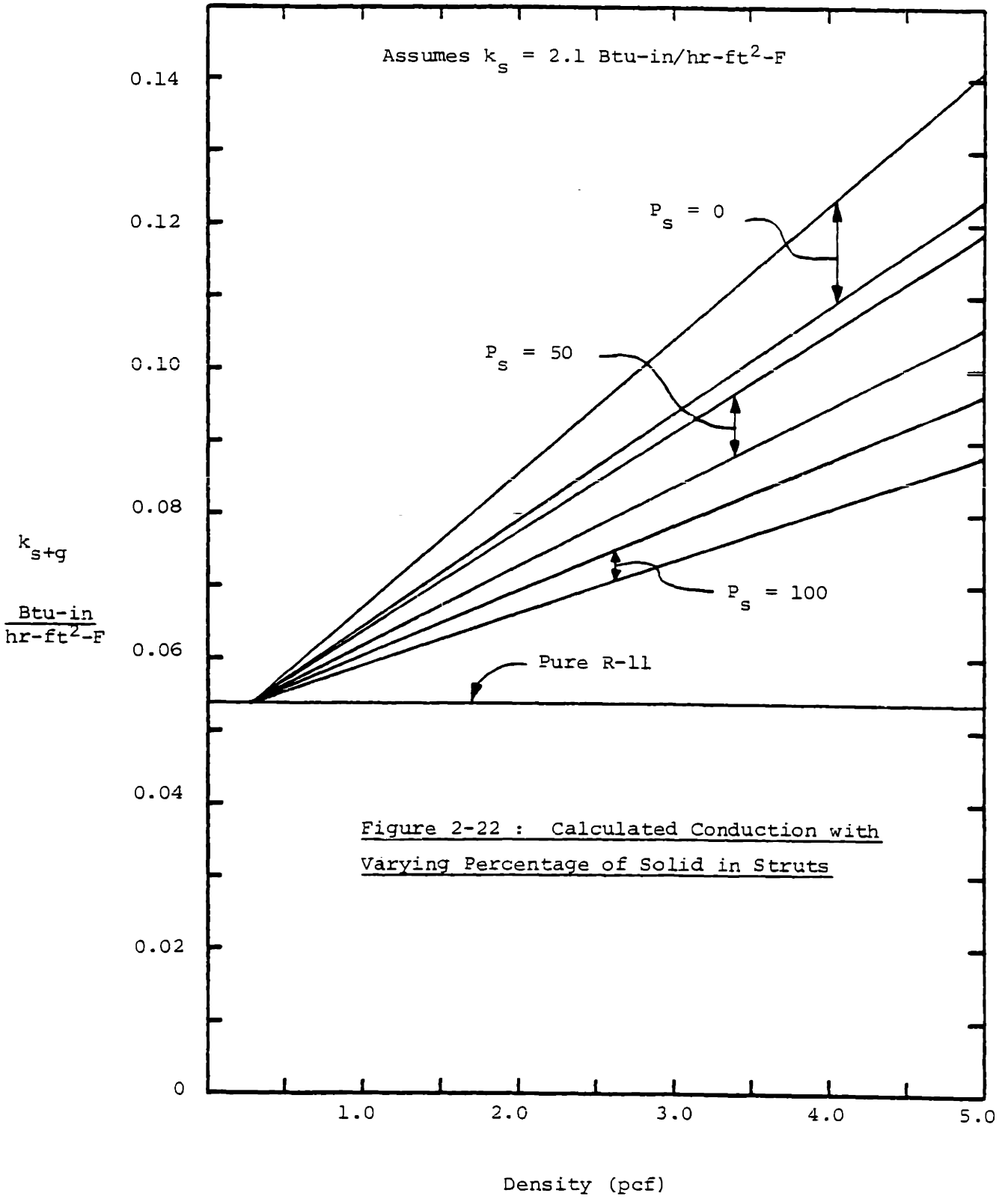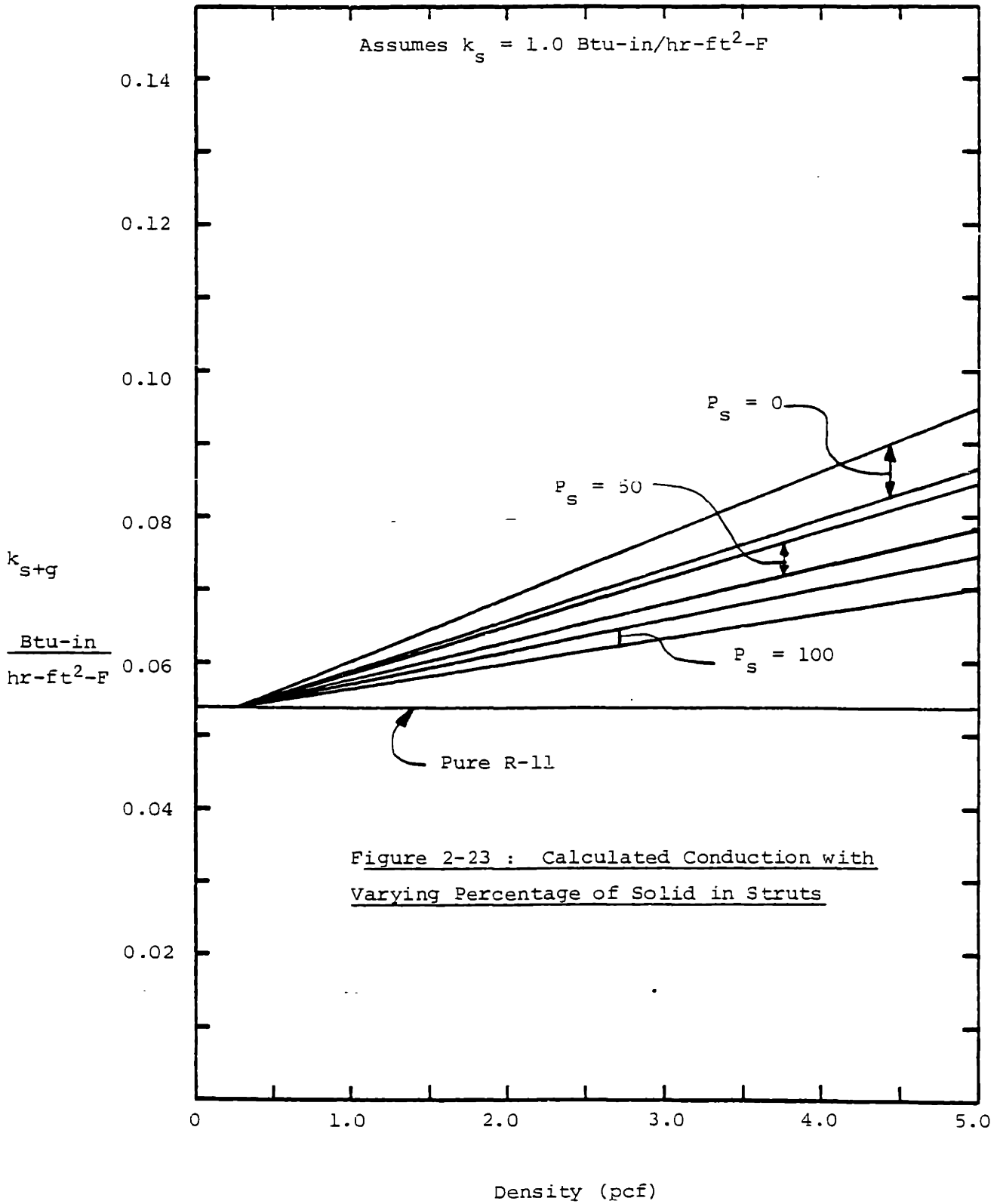
Table 2-2 :   The Change in Solid Contribution During Aging

Cell Gas	Initial Foam Density	k_{gas}*	k_{s+g}**	Solid Contribution
R-11	1.5	.0539	.0705	.0166
	5.0	.0539	.1189	.0650
50% R-11 50% N_2	1.5	.0900	.1065	.0165
	5.0	.0900	.1546	.0646
100% N_2	1.5	.1762	.1924	.0162
	5.0	.1762	.2397	.0635

Units : Btu-in / hr-ft^2-F

*Uses Lindsay - Bromley model for mixtures (6)

**Assumptions :

    1) 50% solid in struts, 50% in membranes

    2) Constant foam porosity during aging

    3) Constant polymer conductivity during aging

    4) k_s = 2.1

2.3.8 Published Values of Polymer Conductivity

The uncertainty band of the conduction model is rather small compared to the uncertainty in the properties of the materials involved. The gases involved are oxygen, nitrogen, water, carbon dioxide, and freon. Their individual conductivities are well documented and reliable. Data for thermal conductivity of mixtures of these gases is far less readily available, yet some data exists (5) and there is theoretical reason to believe that it is accurate and reliable. The solid polymer conductivity however, is an entirely different matter.

Data extracted from the literature and from some industrial sources is listed in Table 2-3 for polyurethane, phenolic and polystyrene. With such a large spread of data there is no possibility of concensus. From Deanin (9) the thermal conductivity is proportional to the square root of the weight average molecular weight for molecular weights below 100,000. Over 100,000 Deanin claims that this effect diminishes. From Miller (10) , crystalline polymers can have twice the thermal conductivity of their non-crystalline counterparts. Furthermore, Miller states that the conductivity of a polymer can increase in the direction of orientation if there is a great deal of molecular orientation. One might expect the membranes to have some degree of molecular orientation, while this might not be the case in the struts. All this leads the author to conclude that the question of polymer conductivity requires further in-depth study.

Table 2-3 : Reported Values of Polymer Conductivity

Polymer	Temperature		Conductivity		Reference	
	°F	(°C)	$\dfrac{Btu\text{-}in}{hr\text{-}ft^2\text{-}F}$	$\dfrac{W}{mK}$		
Polyurethane	—		1.16	0.167	Norton	(17)
Polyurethane	64.	(18)	1.27	0.183	Vdovin	(28)
Polyurethane	64.	(18)	1.27	0.183	Vdovin	(28)
Polyurethane	64.	(18)	1.19	0.172	Vdovin	(28)
Polyurethane	—		2.10	0.302	Sommerfeld	(29)
Polyurethane	68.	(20)	2.42	0.349	Schmidt	(30) (32)
Phenolic	98.7	(37.1)	2.04	0.294	TPRC	(31)
Phenolic	99.	(37.2)	2.24	0.323	TPRC	(31)
Phenolic	68.6	(20.3)	2.27	0.328	TPRC	(31)
Phenolic	74.2	(23.4)	3.16	0.455	TPRC	(31)
Polystyrene	100	(37.8)	*0.67	0.097	TPRC	(31)
Polystyrene	100	(37.8)	*0.73	0.105	TPRC	(31)
Polystyrene	100	(37.8)	*0.85	0.123	TPRC	(31)
Polystyrene	100	(37.8)	*0.88	0.127	TPRC	(31)
Polystyrene	100	(37.8)	*1.03	0.148	TPRC	(31)
Polystyrene	100	(37.8)	*1.09	0.157	TPRC	(31)

* interpolated for value at 100°F

2.4 Conduction Conclusions

A conduction model has been developed for foam insulation. With accurate knowledge of foam density, percentage of solid in struts versus membranes, and solid polymer conductivity this model allows estimation of solid conduction. An upper limit is calculated and the actual solid contribution to heat transfer is within 20% of this upper limit. For fresh low density foam this results in 0% - 12% uncertainty in the overall conductivity, depending on the foam density, polymer conductivity, and percentage of solid in struts. For aged foams, the uncertainty is even less.

Unfortunately the solid polymer conductivity is extremely variable and therefore might have to be measured for each foam formulation. Furthermore, no published method exists for measuring the percentage of solid in struts, other than microscopic examination. It is anticipated that the ongoing work of Reitz at M.I.T. will result in an accurate method For these reasons the uncertainty in the theoretical model is sufficiently small.

The model has been used to show that the change in solid contribution during aging is less than 2.5% assuming that the polymer conductivity remains constant with age.

Finally, conduction models widely used throughout the foam literature give essentially the same results as Russell's equation and therefore do not take into account the effect of struts. This factor causes the published models to seriously overestimate the solid conduction contribution to overall heat transfer.

3. RADIATION THEORY

This chapter develops the theory which is shown to be valid by the experiments in the next chapter. Accordingly, this is not intended to be an exhaustive review of published radiation literature. Rather, this focuses on the approximate technique which the author advocates, as well as on the exact, general theory which forms a part of the justification for the approximate technique.

3.1 Introduction

The theory of radiation heat transfer can be approached on two distinct planes. On a macroscopic level the insulation may be treated as an isotropic continuum which attenuates radiation both by absorption and nonisotropic scattering. The direction of scattering relative to an incident beam is characterized by a normalized function called the phase function. The radiation properties are considered constant throughout the foam. On a microscopic level the insulation is geometrically irregular and has discontinously changing optical properties. The characteristic dimensions of objects such as the thickness of membranes and the cross section of struts are comparable to the wavelength of the radiation. Neither the small object nor the large object limiting case simplifications to the general scattering theory are applicable.

Houston (14) and Koram (33) have addressed the radiation problem for glass fiber insulation on both planes. They each used the general scattering theory on a microscopic level to predict the macroscopic

radiation properties. These properties are used in an exact numerical solution to the general conduction-radiation transport problem. While this is an admirable feat for any insulation, the glass fiber geometry is well characterized in comparison to the foam cell geometry. This approach would therefore be even more difficult for foams. This approach also requires measurement of the complex index of refraction for all wavelengths, a property which changes for different materials.

The approach of this work has been to develop an easy to use approximate model for the macroscopic radiation problem in foams, and to develop a simple experimental technique for measurement of the required radiation parameter. Therefore, we do not address the theoretical problem on the microscopic level but instead perform relatively simple experiments to determine the macroscopic radiation properties. We also devised a scattering experiment, which, in conjunction with the exact macroscopic theory of Koram (33) may be used to estimate the error in the simple model and the simple experimental technique. These experimental results are also suitable for comparison to the theoretical scattering results of Houston or Koram, but this is not the main purpose.

In summary, our goal is to develop a simple experimental technique and a corresponding model which may be used to predict radiation in foams. The exact theory and the experimental scattering results are used to estimate the error in the simple technique. As will be noted

throughout the text, the radiation theories which are applied have all been developed by authors from other fields of application.

Terminology

Before proceeding into the theory it is necessary to establish the terminology which will be used throughout this work. For the reader totally unfamiliar with the terms which follow, it may be wise to read a more general text on the subject matter. (Hottel (20) pp. 199-202, pp. 378-380, pp. 408-413). The reader already familiar with scattering coefficients, absorption coefficients, phase functions, isotropic scattering and the meaning of gray may skip directly to section 3.2.

The most important radiation properties for our purposes are the absorption coefficient (a), scattering coefficient (σ_s) and phase function (Φ). In order to understand these terms, consider a beam of radiation of intensity I_o (energy per unit time per unit area per unit solid angle) within a small cone of solid angle $\Delta\omega_o$, incident on an infinitesimal thickness (dx) of material with properties a, σ_s, Φ. Some of the energy will be absorbed, some will be directly transmitted, and some will be scattered in all directions, including backwards. If we define the extinction coefficient (K) as the sum a + σ_s, then the transmitted intensity will be less than the incident intensity, (I_o), by an infinitesimal amount, ΔI_o, given by:

$$\Delta I_o = I_o K dx \qquad (3-1)$$

which for a finite specimen thickness (t) could be integrated to yield:

$$\frac{I(t)}{I_o} = e^{-Kt} \qquad (3-2)$$

Note that K has units of inverse length. The dimensionless product Kt is called the "optical thickness", and is denoted by τ.

The "albedo" is defined as the ratio of the scattering coefficient to the extinction coefficient. It is denoted by ω_s, and represents the relative importance of scattering to total extinction. It assumes values from 0. (corresponds to pure absorption) to 1.0 (pure scattering).

The infinitesimal decrease ΔI_o in equation 3-1 is due to both absorption and scattering. The total scattered intensity is given by $I_o \sigma_s dx$ while the remainder of energy which was not transmitted (ΔI_o - $I_o \sigma_s dx$) is given by $I_o a dx$. The total scattered intensity is also given by equation 3-3:

$$I_o \sigma_s dx = \int_{4\pi} \frac{\Delta I(\theta, \Psi)}{\Delta \omega_o} \, d\Omega \qquad (3-3)$$

where·

Ω = solid angle

θ = polar angle

Ψ = azimuth

$\Delta I(\theta, \Psi)$ = intensity scattered into (θ, Ψ) direction by element dx thick

$\Delta\omega_o$ = solid angle of incident beam

If the scattering is "isotropic", then $\Delta I(\theta, \Psi)$ will have a constant value for all angles θ, Ψ. If the scattering is "nonisotropic" then $\Delta I(\theta, \Psi)$ will not be a constant. In most materials (including foam and glass fiber insulation) the scattering is nonisotropic, but the value of $\Delta I(\theta, \Psi)$ is independent of Ψ.

For a nonisotropically scattering medium which has the same scattering coefficient as an isotropically scattering medium, the total scattered intensity (equation 3-3) will be the same. The difference between these cases is in the directional distribution of scattered energy. This will have an effect on the radiant heat transfer. We define the phase function, $\Phi(\theta)$, to be the ratio of the scattered intensity at θ to the scattered intensity if the medium were isotropically scattering. For isotropic scattering the scattered intensity at all angles θ is just:

$$\Delta I_{ISO} = \frac{I_o \sigma_s dx \Delta\omega_o}{4\pi} \qquad (3-4)$$

Hence·

$$\Phi(\theta) \equiv \frac{\Delta I(\theta)}{\Delta I_{ISO}} = \frac{4\pi \Delta I(\theta)}{I_o \sigma_s dx \Delta\omega_o} \qquad (3-5)$$

and from equation 3-3 we find:

$$\phi(\theta) \quad = \quad \frac{4\pi \; \Delta I(\theta)}{\displaystyle\int_{4\pi} \Delta I(\theta) \; d\Omega} \tag{3-6}$$

Hence for isotropic scattering the phase function has a value of 1.0 for all θ. For nonisotropic scattering the phase function can assume any positive finite value at an angle θ. Note that the denominator of equation 3-6 is not a function of θ or Ψ. If both sides of equation 3-6 are integrated over all solid angles (4π), then the integral of the phase function is found to be 4π, regardless of how nonisotropic the scattering might be. Therefore, the phase function is a normalized function describing the directionality of scattering.

In equation 3-6 we may express $d\Omega$ as simply $2\pi \sin \theta \; d\theta$ or $2\pi \; d(-\cos \theta)$ or even $2\pi \; d(1 - \cos \theta)$. Hottel (20) shows that:

$$\phi(\theta) \quad = \quad \frac{\Delta I(\theta)}{\displaystyle\int_{0}^{1} \Delta I(\theta) \; d\left(\frac{1 - \cos \theta}{2}\right)} \tag{3-7}$$

Figure 3-1 gives an isotropic and a typical nonisotropic scattering phase function taken from experimental results reported in chapter 4. It is apparent from equation 3-7 that the area under the curve over some range of θ, divided by the total area under the curve, is the fraction of total scattered energy within that range of θ. Figure 3-1 therefore
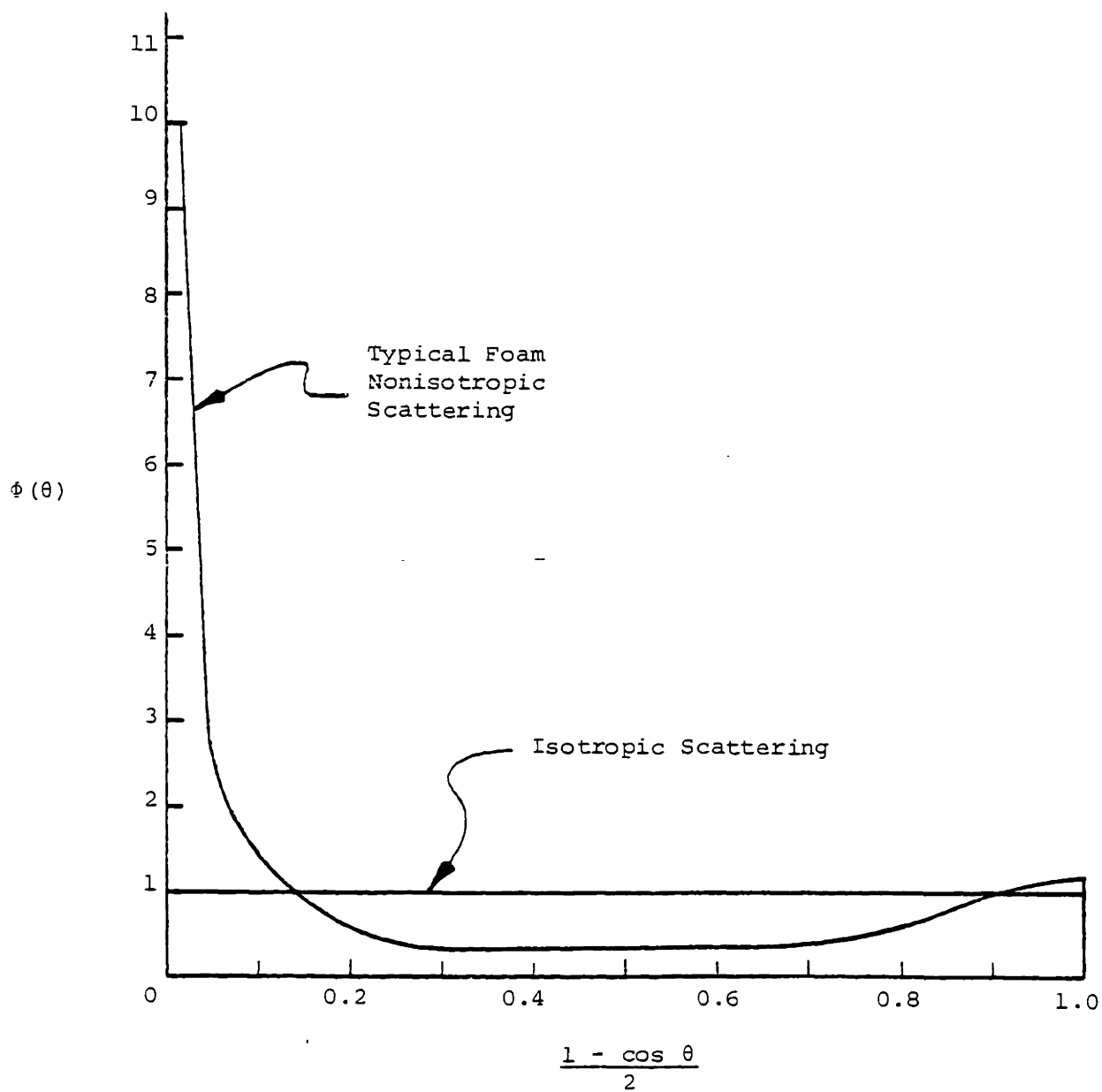
Figure 3-1 : Illustration of Isotropic
versus Nonisotropic Phase Functions

shows graphically for a typical insulation phase function that much of the total scattered energy is strongly forward scattered.

One other term used throughout this work is "gray". We define gray to mean that the material's radiation properties (a, σ_s, ϕ) do not change with wavelength. When we use the terms "non-gray", we mean that the properties do change with wavelength. Often a nongray problem may be approximated through solution of a gray problem where appropriate mean values are chosen for the radiation properties. We use "spectral" values of properties with regard to the value of the property at a particular wavelength. We use "mean" values of properties with regard to approximating nongray behavior with an equivalent gray problem solution.

3.2 Exact Solution Theory for the Combined Conduction-
Radiation Problem

This section provides a short summary of the macroscopic radiation problem which was solved by Houston (14) and by Koram (33) for glass fiber insulation. Accordingly, the reader is referred to reference 14 for more details.

The problem involves simultaneous conduction and radiation in a nongray medium which emits, absorbs, and anisotropically scatters. The medium is planar and is bounded by two gray isothermal walls. These conditions are representative of the conditions during insulation thermal conductivity measurement.

Heat transfer by radiation in this type of medium is described by the general equation of radiative transport, given by Siegel and Howell (13) as:

$$\frac{dI_\lambda(s)}{ds} = -(a_\lambda + \sigma_{s\lambda})\, I_\lambda(s) + a_\lambda I_{\lambda b}(s) \qquad (3\text{-}8)$$

$$+ \frac{\sigma_{s\lambda}}{4\pi} \int\limits_{\omega'=4\pi} I_\lambda(s,\omega')\; \Phi_\lambda(\omega,\omega')\, d\omega'$$

where·

I_λ = spectral radiative intensity

$I_{\lambda b}$ = spectral black body intensity

s = distance in the (θ, Ψ) direction

  (specified by the solid angle ω)

ω = solid angle

ω' = solid angle of incident intensity

a_λ = spectral absorption coefficient

$\sigma_{s\lambda}$ = spectral scattering coefficient

Φ_λ = spectral phase function

λ = wavelength

While equation 3-8 appears formidable, taken term by term it is readily understandable. The left hand side is the rate of change of the intensity of radiation at wavelength λ along s, which means in the (θ, Ψ)

direction. This change is given by the sum of the three right hand side terms. The first term is the decrease in intensity along the s direction due to absorption (a_λ) or scattering ($\sigma_{s\lambda}$). The second term is the increase due to emission. Any medium which absorbs energy must also emit radiant energy. The absorption coefficient is used instead of an "emissivity" because of Kirchoff's Law. The last term (the integral) represents the increase due to energy scattered into the s direction from other directions. One must integrate the contribution from each direction ($\sigma_{s\lambda}\ \phi_\lambda\ I_\lambda$) over all incident solid angles ($\omega' = 4$).

Equation 3-8 is for monochromatic radiation at wavelength λ. In order to solve for the total radiant flux at a point, one must integrate the monochromatic intensity over all wavelengths and solid angles. The radiative flux is given by:

$$q_r = \int_{\lambda=0}^{\infty} \int_{\omega=4\pi} I_\lambda \cos\theta \, d\lambda \, d\omega \tag{3-9}$$

where θ is the polar angle.

The conduction heat flux is characterized by an effective thermal conductivity for the medium in the absence of radiation (k_{s+g}). k_{s+g} is given for foam by the conduction model of chapter 2.

$$q_c = -k_{s+g} \frac{dT}{dx} \tag{3-10}$$

In the most general case k_{s+g} could be a function of both position and temperature. For example the material properties could be a function of temperature and the gas conductivity could vary across the thickness of the test specimen.

By conservation of energy in steady state, the total heat flow must be constant from one side of the insulation to the other. Therefore:

$$\frac{d}{dx} (q_r + q_c) = 0 \tag{3-11}$$

The problem is now fully stated and may be solved numerically. Koram (33) and Houston (14) each developed a computer program to do that. Dr. Koram has run his program using the experimental data presented in the next chapter. The results of these computations confirm the approximate theory presented later in this chapter and are presented after the data in Chapter 4.

Viskanta (11) solved a special case of this general problem. That is, for a gray medium which conducts, absorbs, emits and isotropically scatters. The medium has a constant effective conductivity in the absence of radiation. His results are presented in dimensionless form and will be useful for the validation of the approximate model solution.

It should be noted that there is one assumption implicit in this mathematical formulation which neither Viskanta nor Houston mention. That is, k_{s+g} is locally uncoupled from the radiation. If the medium

were truly a homogeneous continuum, then there would be no doubt. However, since both foam and fibrous glass insulation are actually nonhomogeneous, k_{s+g} may be affected slightly.

In both insulation systems the solid material accounts for all of the radiant absorption and only a small fraction of the volume. The solid has a much higher thermal conductivity than the surrounding gas. From a conduction point of view, radiation absorption is equivalent to heat generation in the solid while radiant emission is equivalent to negative heat generation. If these two terms are not equal and opposite at every point, the conduction model developed in Chapter 2 is, strictly speaking, not valid.

The total heat flux is constant from one side of the sample to the other. Due to the temperature difference, the radiant flux varies with position. The conduction flux therefore varies in an equal but opposite way so as to keep the total flux constant. This may only be achieved by having the absorption and the emission not locally equal. Hence, the conduction model is not valid in the strictest sense. Nevertheless, these local effects should be negligible in the macroscopic model of the process.

3.3 Simplified Radiation Models

In the previous section we presented the equation of transfer for the nongray, anisotropic scattering, combined conduction-radiaion problem. In this section we present a method whereby the general

nonisotropic scattering problem may be approximated by an equivalent isotropic scattering problem. Using this approximation along with the experimental knowledge (presented in Chapter 4) that the medium is optically thick, we present the method whereby the integro-differential equation may be reduced to a simple differential equation. The nongray behavior is approximated with an equivalent gray medium case. Finally, the simple differential equation is integrated and an approximate model is used to account for the effects near solid boundaries where the simple differential equation is not valid. The problem reduces to three simultaneous algebraic equations in three unknowns.

3.3.1 Approximation of Nonisotropic Scattering

As mentioned in Chapter 1, various approximations to the anisotropic scattering problem may be found in the literature. It was determined that neither the two flux approximation nor the linear anisotropic scattering models were useful for our purposes. The reason is not that these models are faulty, but rather that two better approximations are available. One is the P-1 approximation presented clearly by Lee and Buckius (23). This approximation is very accurate but requires experimental or theoretical knowledge of the phase function (presented in Chapter 4). The second is the Rosseland diffusion approximation for isotropic scattering. It will be shown that this is very simple to use and predicts radiation heat transfer within approximately 10% for low density foam when the extinction coefficient is measured by a simple technique described in section 4-2. Since this

corresponds to an error in the overall conductivity prediction of approximately 2.5%, it will probably be sufficiently accurate for most purposes. An improvement to this simple technique described in section 4.3.6., or sophisticated experiments (or analysis) are required for improvements over this accuracy.

The two-flux approximation requires an experimental apparatus comparable in complexity to the apparatus required for the direct measurement of the phase function, but does not provide the accuracy of the P-1 approximation. The linear anisotropic scattering approximation is only slightly more accurate than the isotropic scattering approximation, but requires knowledge of the relative importance of scattering and absorption. Thus, more complex experiments are required relative to the simple isotropic scattering model, and only a marginal increase in accuracy is obtained. For these reasons, only the isotropic scattering case and the P-1 approximation will be used in this work.

3.3.1.1 <u>Isotropic</u> <u>Scattering</u> <u>Approximation</u>: In section 3.1 we defined the absorption coefficient, scattering coefficient, and phase function. The reader unfamiliar with these terms is referred to any general radiation text for further explanation. Siegel and Howell (13) or Hottel and Sarofim (20) would be suitable.

For the isotropic scattering case, one simply assumes that the phase function has a value of 1.0 over the entire sphere, and thus all scattering is isotropic. Given this assumption, we will show in later sections how the general problem may be accurately solved. For now we

note that the problem will eventually be reduced to a simple algebraic system of three equations in three unknowns.

It is important to understand the cause and magnitude of the error in the isotropic scattering approximation. It will be shown in Chapter 4 that scattering in real foam is strongly forward oriented. This means that for an incident beam, of the energy which is scattered a large portion continues to propagate in a direction only slightly altered from the incident direction. This was previously illustrated in Figure 3-1 for an experimentally determined phase function. If more of the energy were scattered at large angles, the radiant flux would be decreased. By assuming that the scattering is isotropic we are overestimating the attenuation, and are therefore underestimating the radiation heat transfer. Since we know experimentally that the scattering is forward oriented, we may assume that the isotropic scattering model will always underestimate the actual radiation heat transfer.

The magnitude of the error in this approximation depends on both the degree to which the scattering is forward oriented, and on the relative importance of scattering compared to absorption (i.e. on the albedo). In other words, if the scattering coefficient were small in comparison to the absorption coefficient, ($\omega_s=0$) then the error in the calculated radiation heat transfer due to the isotropic scattering assumption would be small. Of course, if the scattering were nearly isotropic, then the error would be small even if the process were not absorption dominated. As will be seen in Chapter 4, the attenuation of

radiation in foams is dominated by absorption but the scattering is highly forward oriented. For low density foams, the error in the calculated radiation heat transfer will be approximately 10%. For low density foams where radiation accounts for approximately 25% of the total heat transfer (this will be shown in succeeding chapters), the isotropic scattering approximation will result in an overall heat transfer underestimate of approximately 2.5%. This of course is sufficiently accurate for most purposes.

3.3.1.2 P-1 Approximation When experimental or theoretical knowledge of the phase function is available, greater accuracy may be achieved through the P-1 approximation than is obtainable with the isotropic scattering assumption. This approximation is derived in Siegel and Howell (13), but is more clearly applied by Lee and Buckius (23). An earlier reference (Hottel, 20) makes note of the exact same approximation found in the paper by Lee, but no mention is made of the magnitude of the error. Hottel (20) credits Chu (40) with this development for the optically thick case. The approximation will be found to be quite accurate, but unfortunately the apparatus required to measure the phase function is quite expensive and requires specialized expertise. Nonetheless, some experimental phase functions are presented in Chapter 4, and this approximation may be used to determine the radiation heat transfer given the measured phase function.

The technique presented by Lee and Buckius (23) involves using the phase function to determine a correction factor which is then applied to the isotropic scattering approximation. They do not state the exact magnitude of the error in this approach, however from the graphs presented one may estimate that the error in predicted heat flux is less than 1.0% for most cases. In the worst case presented, the error is approximately 3% of the radiative heat flux. The phase function used in this worst case is comparable to the measured phase functions presented in chapter 4. Therefore, we may expect approximately 3% error for real foams. In chapter 4 we will show that the error is in fact even less than 3%.

To apply the approximation, one simply integrates the phase function times the cosine of the polar angle over the sphere. This integral divided by 4π is called the asymmetry factor, $<\cos\theta>$. For the case of azimuthally independent phase function, this factor is given by equation 3-12.

$$<\cos\ \theta>\ \equiv\ \frac{1}{2}\ \int_{-1}^{+1}\ \Phi(\theta)\ \cdot\ \cos\ \theta\ \cdot\ d(\cos\ \theta) \qquad (3-12)$$

Lee and Buckius (23) show how to modify the extinction coefficient and albedo using this asymmetry factor. It is more intuitively meaningful and completely equivalent to define a new, modified scattering coefficient σ_s^* as:

$$\sigma_{s\lambda}^*\ \equiv\ \sigma_{s\lambda}\ (1\ -\ <\cos\ \theta>) \qquad (3-13)$$

The absorption coefficient is of course unaffected. The new

function is simply 1.0 everywhere; that is we assume isot

scattering. Using the modified scattering coefficient in any sol

for isotropic scattering now yields the same radiation heat fl

would the nonisotropic scattering case with the original scatt

coefficient and phase function. The intuitive explanation as

this works so well is that the scattering coefficient is modifi

accordance with the extent that the phase function differs

isotropic scattering. The more strongly forward scattering the

function, the more the scattering coefficient is decreased.

3.3.2 Rosseland Diffusion Approximation

Regardless of whether the isotropic scattering or the

approximation is used, we are given an absorption coefficient

scattering coefficient (their sum is the extinction coefficient) a

need to solve the nongray combined conduction-radiation proble

absorption, emission and isotropic scattering. This problem c

handled with the Rosseland diffusion approximation.

The Rosseland diffusion approximation is essentially a soluti

the equation of transfer (eq. 3-8) when the optical mean fre

(mean free path of a photon, inverse of extinction coefficient) i

compared to the distance over which significant temperature diffe

occur. Hottel (20) gives probably the most clear mathen

derivation of this approximation. One of the more intuitive deri

he presents uses analogy to the diffusion process in a gas. The

are analogous to gas molecules, the average velocity of the photons being c/n (speed of light divided by refractive index). The mean free path of the photons is just the inverse of the extinction coefficient. From this he derives equation 3-14, which by analogy to the kinetic theory of gases is only applicable when the physical size of the medium is several mean free paths or larger.

$$q_r = - \frac{4}{3K} \frac{de_b}{dx}$$ (3-14)

where:

    K = extinction coefficient

    e_b = blackbody emissive power

But:

$$e_b = n^2 \sigma T^4$$ (3-15)

where:

    σ = Stefan-Boltzmann constant = 0.1713 x 10^{-8} Btu/ft^2-hr-R^4

    T = temperature

    n = refractive index $\simeq$ 1.0 for insulations

therefore:

$$q_r = - \frac{16\sigma}{3K} T^3 \frac{dT}{dx}$$ (3-16)

We will refer to equation 3-16 as the Rosseland equation. The analogy to the Fourier conduction equation is evident, i.e. $16\sigma T^3/3K$ may be

thought of as the "radiation conductivity". For large enough optical thicknesses we will show that this "radiation conductivity" could simply be added to the solid plus gas conductivity to obtain the overall insulation conductivity. The Rosseland equation will be applied to the combined conduction-radiation problem in the next section. Note that the Rosseland equation is not valid for nonisotropic scattering and is not valid near solid boundaries.

Accuracy of Diffusion Approximation

Viskanta (11) numerically solved the gray, combined conduction-radiation problem with isotropic scattering from the equation of transfer and the conduction equation. Fine, et al. (12) repeated the solution and showed that the same results (within 2.0%) could be obtained with the Rosseland diffusion approximation for the pure absorption case ($\omega_s = 0$) so long as the medium has an optical thickness greater that 2, an extinction coefficient greater that 25 ft^{-1} (0.82 cm^{-1}), and so long as a different model is used to describe the radiation within an optical thickness of approximately 0.7 from the wall. For optical thicknesses greater than 10, the error is less than 0.1% in the pure absorption case ($\omega_s = 0$) if the approximate model described by Fine, et al. is used.

From the results of Fine for isotropically scattering media, the effect of the albedo may be seen to diminish rapidly with optical thickness. At low optical thickness (1.) and low surface emissivity (0.1), the radiant flux varies by a factor of four between the pure

scattering and the pure absorption case. At an optical thickness of 2, and a surface emissivity of 1.0, the variation is reduced to 12% of the radiant flux. At an optical thickness of 17, the difference between the pure scattering and the pure absorption case is reduced to 3.5% of the radiant flux. At an optical thickness of 50, the difference may not be read off the graph. In chapter 4 it will be shown that one inch thick foam specimens typically range in optical thickness from 40 to 100. Hence for all cases of practical importance to foams, absorption and isotropic scatter may be considered to have an equal effect on heat transfer (i.e. the albedo has no effect).

Approximation of Nongray Behavior

The nongray case may be handled with the Rosseland diffusion approximation through proper definition of the mean extinction coefficient. Ozisik (36) shows that the proper mean extinction coefficient is given by:

$$(\overline{K})^{-1} = \int_0^\infty \frac{1}{K_\lambda} \frac{\partial I_{\lambda b}(T)}{\partial I_b(T)} d\lambda \qquad (3-17)$$

where:

$\overline{K}$ = Rosseland mean extinction coefficient

K_λ = spectral extinction coefficient

T = temperature

λ = wavelength

$I_{\lambda b}$ = intensity at λ emitted by blackbody

I_b = total black body radiation intensity

In order to evaluate this integral, the spectrum is broken into bands over which K_{λ} is constant. Ozisik shows how tabulated fractional functions of the second kind may be used to perform the integration. He also provides the table which is required for this averaging technique.

3.3.3 Combined Conduction-Radiation Models

Because the Rosseland equation is not valid near solid boundaries, it becomes necessary to model the radiation process near the insulation boundaries. However, let us temporarily ignore the inaccuracy of the Rosseland equation near the boundaries. Consider one dimensional heat flow at steady state through an infinite slab of finite thickness, L. The conduction heat flux is given by equation 3-10, repeated here:

$$q_c = -k_{s+g} \frac{dT}{dx} \qquad (3-10)$$

therefore:

$$q_T = q_c + q_r = -(k_{s+g} + \frac{16\sigma T^3}{3K}) \frac{dT}{dx} \qquad (3-18)$$

From the energy equation (3-11) we know that q_T does not vary with x. Therefore equation 3-18 may be integrated; x goes from zero to L (insulation thickness) and T goes from T_2 to T_1.

$$q_T L = k_{s+g}(T_1 - T_2) + \frac{4\sigma}{3K}(T_1^4 - T_2^4) \qquad (3-19)$$

But:

$$T_1^4 - T_2^4 \simeq 4T_m^3(T_1 - T_2) \qquad (3-20)$$

where:

$$T_m \equiv \frac{T_1 + T_2}{2} \qquad (3-21)$$

therefore:

$$k_f \equiv \frac{q_T L}{T_1 - T_2} \simeq k_{s+g} + \frac{16\sigma T_m^3}{3K} \qquad (3-22)$$

where k_F is the overall thermal conductivity of the foam. Equation 3-22 is only strictly valid for an infinitely thick medium, however for optical thicknesses over 100 the error is negligible. An optical thickness of 100 corresponds to a 3 inch (7.6 cm) thick slab if the extinction coefficient is 400 ft^{-1}. For optically thinner samples one must either resort to modeling the radiation heat transfer near the

boundary, or accept the small error in equation 3-22. The error in equation 3-22 is approximately 5% of radiation contribution at an optical thickness of 8.3 with bounding surface emissivities of 1.0 and an albedo of 0.0.

Note that equation 3-22 predicts the foam thermal conductivity to be independent of thickness. Hence, the "thickness effect" referred to in the heat transfer literature is completely due to altered radiation heat transfer near solid boundaries. The conductivity calculated by equation 3-22 would thus be the "full thickness conductivity" if the "full thickness" has an optical thickness greater than 100.

Three boundary models are discussed below. While these all give results close to the exact solution of Viskanta (11) the author advocates the first model because it is the most accurate and yet is simple to use. However, one must not expect that these models will completely model the surface effects in real foam. In real foam, there may be changes in density, cell size, etc near the surface of the foam which will affect the radiation and conduction in ways not accounted for here. Also, in new fresh cut foams the surface bubbles are often broken, resulting in large differences in gas conductivity between the first few layers of bubbles. This too will affect the radiation near the boundaries, but is not included in the models.

3.3.3.1 <u>Optically</u> <u>Thin</u> <u>Limit</u> <u>Boundary</u> <u>Radiation</u> <u>Model</u> : In reference
12, Fine, et al. propose an approximate model for intermediate optical
thicknesses based on the use of an optically thin region near each
boundary with the Rosseland diffusion equation applying to the much
larger central region. The optically thin limit means that the radiant
interchange between the solid surface and the outer bound of the central
region is undiminished by the material in between. Using the
nomenclature defined in Figure 3-2, the rate equation for boundary A is:

$$q = k_{s+g} \frac{T_1 - T_a}{L_a} + \varepsilon_1 \sigma (T_1^4 - T_a^4) \tag{3-23}$$

and the rate equation for boundary B is:

$$q = k_{s+g} \frac{T_b - T_2}{L_b} + \varepsilon_2 \sigma (T_b^4 - T_2^4) \tag{3-24}$$

while the rate equation for the center region is given by:

$$q = k_{s+g} \frac{T_a - T_b}{L_c} + \frac{4\sigma}{3KL_c} (T_a^4 - T_b^4) \tag{3-25}$$

We have three equations (3-23, 3-24, 3-25) and three unknowns (T_a,
T_b, q) which must be solved simultaneously. The only problem is that we
have not specified L_a, L_b and L_c beyond the obvious fact that they must
add up to the sample thickness. Fine, et al. (12) show that if a
boundary optical thickness of 0.69315 is chosen (which in reality
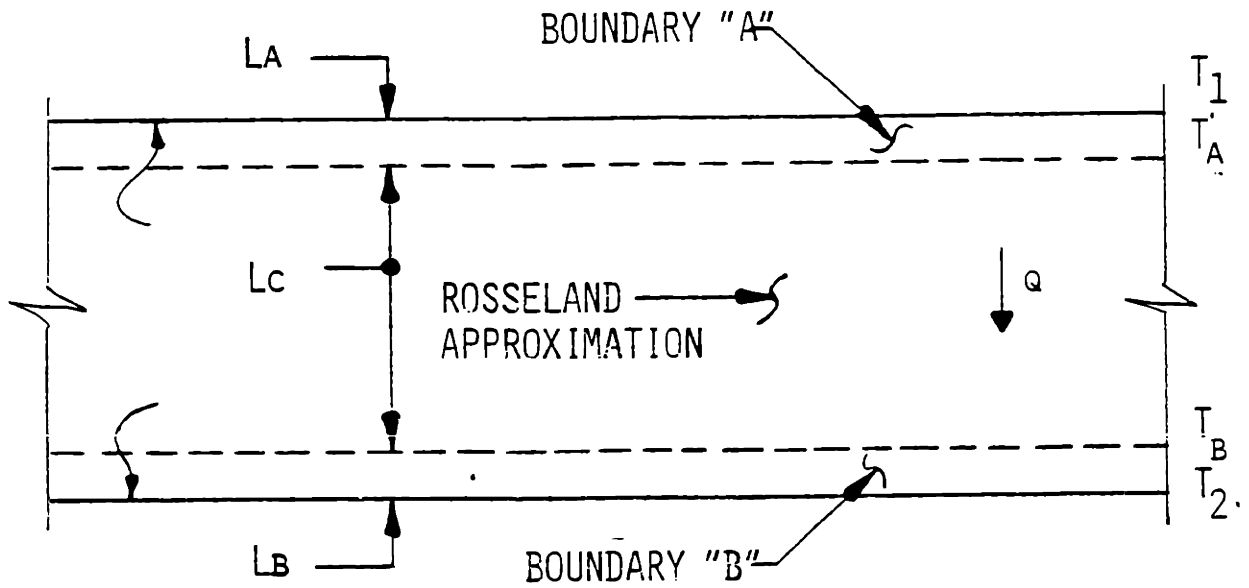
$$Q = F_N (T_1, T_A) \qquad - 1^{ST} \text{ BOUNDARY}$$

$$Q = F_N (T_A, T_B) \qquad - \text{ROSSELAND}$$

$$Q = F_N (T_B, T_2) \qquad - 2^{ND} \text{ BOUNDARY}$$

THREE EQUATIONS, THREE UNKNOWNS (Q, T_A, T_B)

FIGURE 3-2 : NOTATION FOR THREE-ZONE MODELS

results in approximately 67% of the flux leaving the boundary to be attenuated before reaching the central region), then the predicted effective thermal conductivity agrees closely with the values obtained in the exact numerical analysis reported in the same reference, for the case of surface emissivities of 1.0 and albedo of 0.0. Under these conditions the error is only 2.% at an optical thickness of 2, and negligible at optical thickness greater than 10.

Unfortunately it is pure coincidence that the errors in this model cancel for a boundary optical thickness of 0.69315. If some other optical thickness is chosen, then the agreement with the exact case is not as close. The errors which cancel are: 1) That radiation between the surface and core is not attenuated, and 2) The core acts as a blackbody radiator at the surface temperature. While Fine, et al. do not include the emissivities, ε_1 and ε_2 in equations 3-23 and 3-24, the author has inserted them. This is because the model agrees well with the results of Viskanta and Grosh (35) for large optical thickness and for conduction-radiation numbers of 1.0 and 10. The conduction-radiation number (N_{cr}) is defined by:

$$N_{cr} \equiv \frac{k_{s+g}\, K}{4\sigma T_*^3} \tag{3-26}$$

where T_* is an arbitrary temperature. A comparison of the results of Viskanta and Grosh (35) with the results from this model is given in Table 3-1. In practice the optical thickness will be greater than 10

Table 3-1 <u>Comparison of Results of Boundary Emissivity Effects</u>

Note: $T_1/T_* = 1.0$ OPTICAL THICKNESS = 10

$T_2/T_* = 0.5$ $\omega_s = 0$ (PURE ABSORPTION)

Surface Emissivity $\varepsilon_1 = \varepsilon_4$	N_{cr}	$\dfrac{q_T}{\sigma T_*^4}$		$\dfrac{q_c}{q_T} = \dfrac{k_{eff}}{k_f}$	
		Viskanta (35)	Optically Thin Limit	Viskanta (35)	Optically Thin Limit
1.	1	0.315	.315	0.635	.635
1.	10	2.114	2.115	0.9461	.9454
0.9	1	0.314	.314	0.637	.638
0.9	10	2.113	2.114	0.9465	.9460
0.5	1	0.307	.307	0.651	.651
0.5	10	2.110	2.110	0.9479	.9480
0.1	1	0.297	.298	0.673	.670
0.1	10	2.107	2.105	0.9492	.9500

and the conduction-radiation number between 1 and 10, thus the emissivity effect error in the approximate model will be minimal.

3.3.3.2 Emissive Power Jump Model :

Siegel and Howell (13) develop an equation for energy transfer which uses a discontinuous emissive power jump in passing from the medium to the solid boundary. Applying this boundary condition to the case of infinite gray parallel plates separated by a non-conducting, gray, absorbing, emitting, isotropically scattering medium, they obtain the following rate equation:

$$q_r = \frac{\sigma(T_1 - T_2)}{\frac{3KL}{4} + \frac{1-\varepsilon_1}{\varepsilon_1} + \frac{1-\varepsilon_2}{\varepsilon_2} + 1} \qquad (3-27)$$

where T_1 and T_2 are the wall temperatures, ε_1 and ε_2 are the wall emissivities, and L is the thickness of the sample. Note the similarity to the radiation term in equation 3-12.

Siegel and Howell (13) also give a similar analysis with a suitable correction factor to be applied when the medium is simultaneously conducting.

3.3.3.3 Integral Solution to Boundary Problem :

It is possible to solve the radiation problem near the wall using an integral technique. This technique is analogous to the one used to solve heat or mass or momentum boundary layer equations in fluid flow. Basically one uses a three zone approach, in exactly the same way as for the optically thin limit model. See Figure 3-2. In order to solve for the heat transfer across the

boundaries, a temperature profile from T_1 to T_a and T_b to T_2 is assumed. An arbitrary point is chosen at which one totals the various contributions to heat transfer. Figure 3-3 shows five contributions to the radiation heat flow at the imaginary plane which divides the core from the boundary region. In the figure, Q_E is obtained from the Rosseland one way flux (see Siegel and Howell (13)), while the other contributions are obtained from integration, using the assumed temperature profile. The conduction is obtained from the temperature gradient at the point.

This analysis was performed for the most convenient, but still somewhat realistic temperature profile, linear in the fourth power of temperature. The process is lengthy and will not be reported in detail here. The key equations required for this analysis are given in Appendix B. If one wished to assume a more realistic profile then the analysis could be repeated with the improved profile.

The accuracy achieved with this technique was not as good as the accuracy of the optically thin limit model. However, this model is not as sensitive to the choice of boundary optical thickness as is the optically thin limit model. This fact may make the integral solution more accurate than the optically thin limit model for highly nongray materials. This technique is also cumbersome to use, requiring computations of exponential integrals and lengthy algebra. Therefore, it is not recommended.
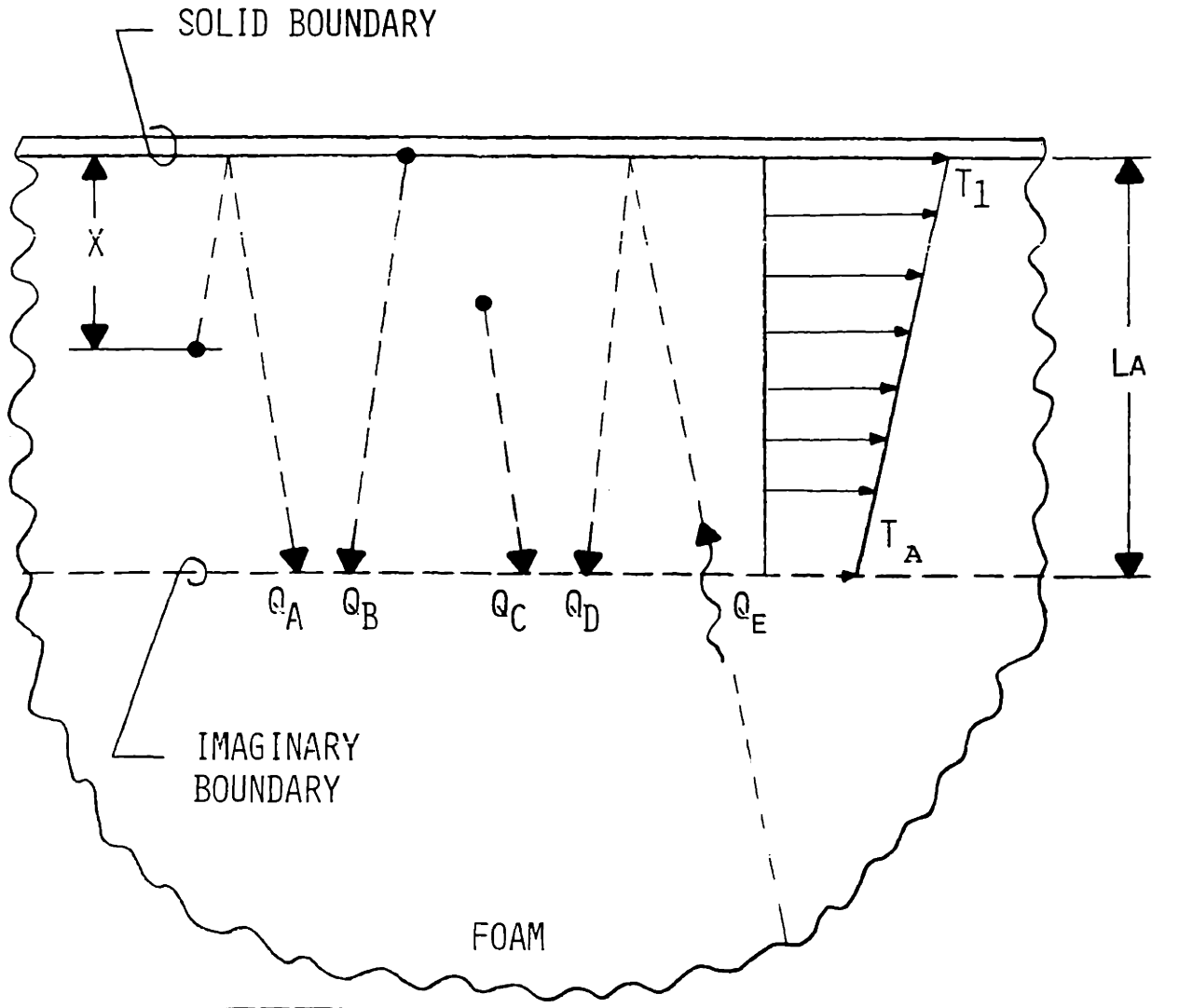
FIGURE 3-3 : INTEGRAL SOLUTION TECHNIQUE FOR
BOUNDARY RADIATION PROBLEM

3.4 Summary - Radiation Theory

The general equation of radiative transfer was presented for a nongray, absorbing, emitting, nonisotropically scattering medium. The simultaneous conduction-radiation problem may be accurately solved using the P-1 approximation of Lee and Buckius (23) in conjunction with the Rosseland diffusion approximation in a three zone model proposed by Fine, et al. (12). In chapter 4 we will present the error of this approximation when applied to experimentally determined radiation properties. For foams, the isotropic scattering approximation requires much less experimental information than the other models, and underestimates radiation by approximately 10%, as will also be shown in chapter 4. For a sufficiently large optical thickness ($\tau > 50.$) the albedo has essentially no effect on the conductivity for the gray, combined conduction-radiation, absorbing, emitting, isotropically scattering case. The effect of surface emissivity may be handled with the three zone model for sufficiently optically thick media ($\tau > 10.$). In the next chapter it will be shown that typical foam optical thicknesses range from 40 to 100 for one inch thick samples. Hence, the three zone model will be found to be sufficiently accurate for most practical purposes.

4. RADIATION EXPERIMENTS

This chapter presents the experimental basis for the radiation model. Spectral transmissivity measurements for polyurethane films are presented first, proving that opaque wall radiation models have no physical basis. The simple technique for extinction coefficient measurement is presented next along with typical results showing that foams are optically thick. Finally, results of the scattering experiment are presented to provide a more complete physical understanding of the radiation transfer process in insulation. These results enable quantification of the error in the simple extinction coefficient measurement technique. Recommendations are provided for an improved experimental technique if one wishes to achieve greater accuracy than obtainable with the simple technique.

4.1 Transmission Through Cell Walls

The transmissivity of cell walls were measured to determine if the opaque cell wall radiation models are valid. Polyurethane films were obtained from two sources. Large surface bubbles (up to 2 cm diameter) form on the tops of foam buns if the bun is allowed to rise unconstrained on the top surface. Cell walls extracted from these "free rise bun" surface bubbles were nearly as thin as membranes in the bulk foam. Because they are a byproduct of the foaming process, their chemical composition was the same as the composition of typical foam. Although the precise chemical structure may differ from the bulk foam due to differences in thermal history, the infrared absorption behavior

of these films should be qualitatively similar to that of cell membranes in the bulk foam.

The second source of films was foam designed to have large cells. By creating foams with a mean cell size of approximately 0.5 cm, it was possible to locate and remove films up to 1.0 cm in diameter. These foams were produced by using essentially no surfactant in the mix. Therefore the chemical composition is not identical to that of typical foams. These films were also found to be much thicker than the films obtained from free rise buns.

Figures 4-1 and 4-2 present typical spectrographs of films obtained from free rise buns and from large celled foam, respectively. The measurements were taken on a Perkin-Elmer 283B Infrared Spectrophotometer. Note that a black body radiating at 75 F (24 C) emits 89% of its energy between 5 and 30 microns wavelength. This is therefore the wavelength range of concern for radiation heat transfer purposes. The free rise bun films (Figure 4-1) are typically much thinner and have much higher transmissivities than the films from large cell foam (Figure 4-2). The sample in Figure 4-1 has an average thickness of approximately 6×10^{-5} inches (1.5 microns) while the sample in Figure 4-2 is 1.4×10^{-3} inches (36 microns) thick. Note that if one assumes dodecahedron shaped bubbles with 85% struts and 0.010 inch (.25 mm) cell diameter, the calculated wall thickness is approximately 1.2×10^{-5} inches (0.3 micron). Therefore, cell membranes would have even higher transmissivities than the sample in Figure 4-1.
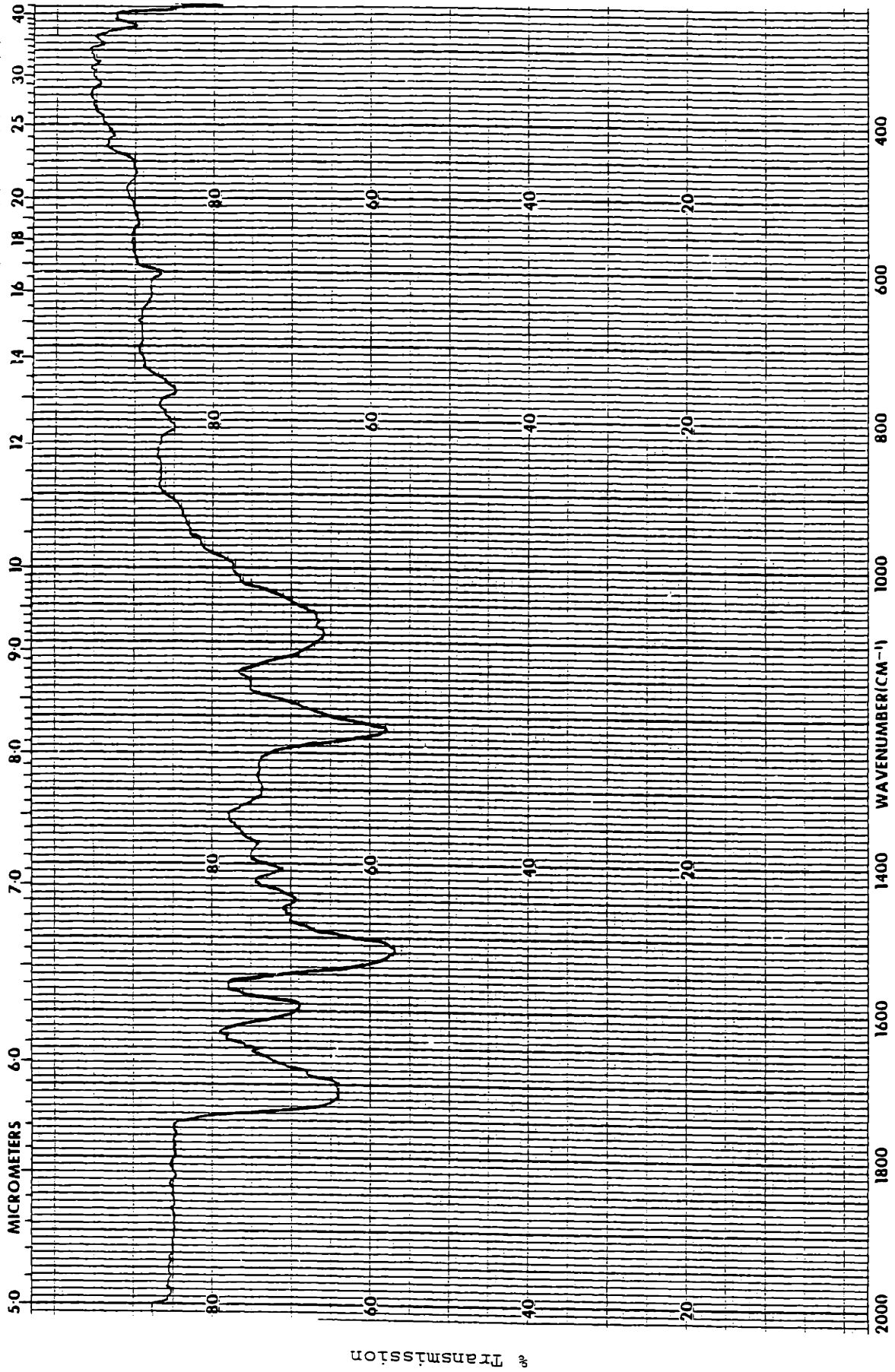
Figure 4-1 : Transmission Through Free Rise Bun Film
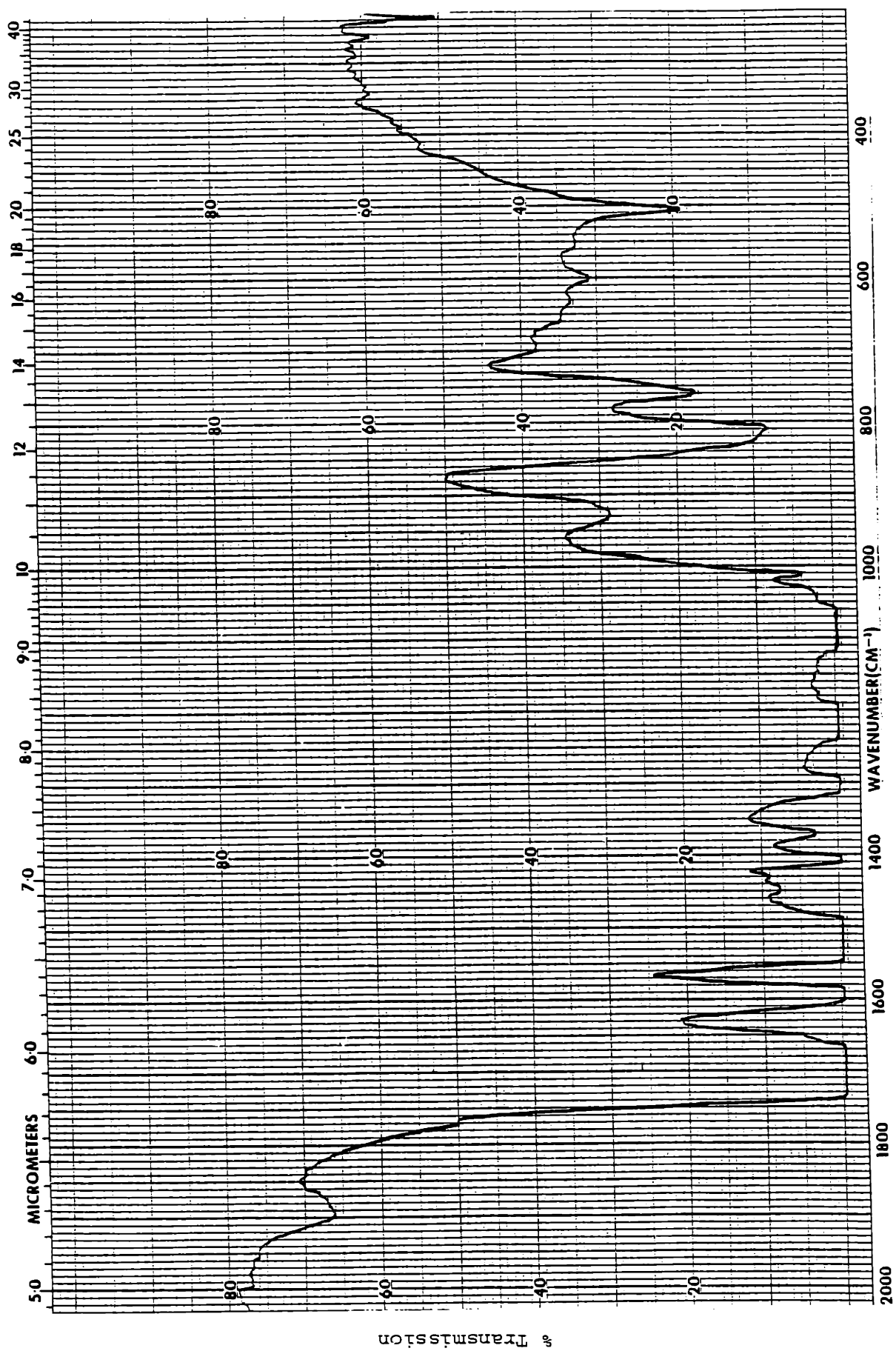
Figure 4-2 : Transmission Through Film From Large Cell Foam

On this basis, the opaque cell wall radiation model may be dismissed.

4.2 Simple Technique for Extinction Coefficient Measurement

The approximate radiation model developed in Chapter 3 requires only one radiation parameter - the extinction coefficient. The model contains the assumption that scattering is isotropic, and that scattering and absorption contribute in a similar fashion to the extinction coefficient. In this section a straightforward technique to measure the extinction coefficient is presented.

The test foam is sliced into approximately 6 to 8 slices, ranging from a maximum thickness of 0.100 inches (2.54 mm) to the thinnest slice which will not crumble. Foam slices as thin as 0.025 inch (0.64 mm) thick were easily obtained using only a Hobart meat slicer. Thinner slices were obtained using a surgeon's scalpal. The scalpal technique is more time consuming than using a meat slicer and is unneccessary for most foams. It has been found that foams slice cleanly when the blade slices rather than chops. The rotating blade of the Hobart meat slicer is adequate for most purposes.

Once the foam has been sliced, single samples are placed into a conventional infrared spectrometer. A Perkin-Elmer 283B Infrared Spectrophotometer was used for all measurements reported in this work. A standard cell mount is slid into place, allowing the beam to pass through the hole onto the detector. The gain and baseline settings on the spectrometer are adjusted at this time. A foam slice is taped flat

to the standard cell mount. The spectrometer records the percentage of energy transmitted at each wavelength from 2.5 microns to 40 microns. To save time one can skip from 2.5 to 5 microns and scan from 5 to 40 microns. This produces a spectrograph, generally similar to the one shown in Figure 4-3. A spectrograph is taken for each of the foam slices.

Finally, the thickness of each foam slice is measured. The thickness is measured after the infrared transmission measurements since the thickness measurement could affect the transmission by disturbing some of the partially broken surface bubbles. Two different techniques were used to measure the thickness; good agreement between the two techniques was found.

The fastest and easiest technique to measure the thickness was to use a Lufkin Rule Company Model Number 3610 paper micrometer. The advantage of the paper micrometer is that two flat measuring surfaces are attached to the ends of the spindle and caliper. See Figure 4-4. These surfaces are much larger in diameter than the spindle on a conventional micrometer. The edges are also rounded and smooth so that the micrometer does not snag or grab the material being measured as the spindle rotates. The measuring surfaces are positioned directly on the spot where the transmission measurement was taken and the micrometer is closed until the sample offers resistance to side to side motion. This is called the "touch" measurement. The side to side motion is stopped and the micrometer is closed further until a small but unmistakeable
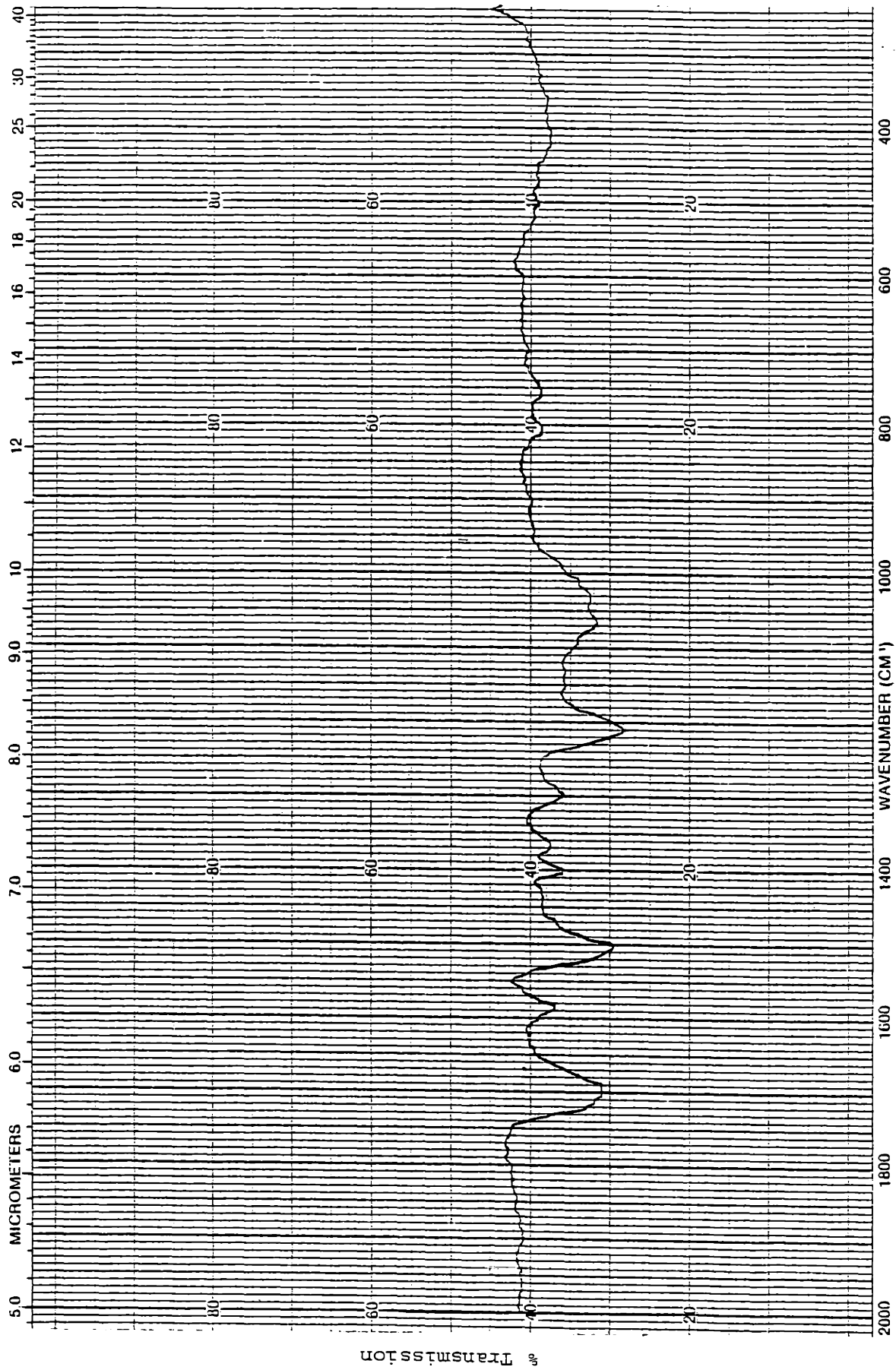
Figure 4-3 : Transmission Through 0.0215 in Thick Polyurethane Foam Sample
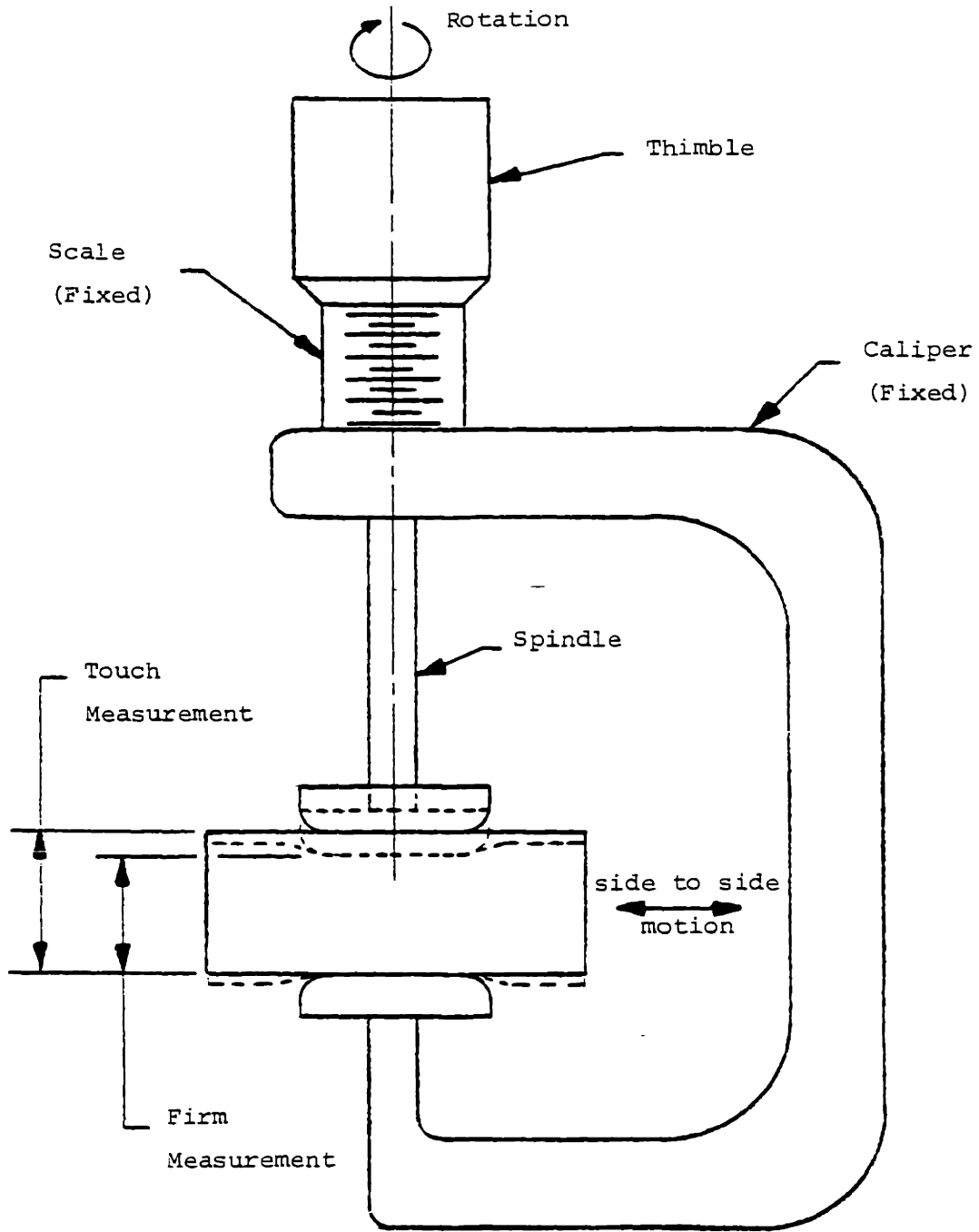
Figure 4-4 : Illustration of the Use of
the Lufkin Paper Micrometer

resistance is felt which opposes further turning of the thimble. This is the "firm" measurement. The difference between the touch and firm measurements was usually approximately one half of a foam bubble diameter. The average of the two measurements is taken as the sample thickness. This process is illustrated in Figure 4-4. This averaging technique accounts for surface irregularity.

The other technique used for determination of the thickness was to weigh a known area of the sample on an analytical balance. The sample thickness can be calculated from the area, weight and density of the sample. This process has the disadvantage of being more time consuming, requiring two measurements, and requiring knowledge of density, which may vary somewhat throughout the foam. This technique was used as a check against the micrometer measurement. It was also used to measure the thickness of thin glass fiber insulation samples which were not amenable to the micrometer technique.

The extinction coefficient may be calculated from the measurements described above. The most accurate method of determining the extinction coefficient is to break the spectrum into wavelength bands over which the transmission is approximately constant. The bands are selected from observations of the spectrographs. For each band, the average transmission is plotted against the measured sample thickness on semi-log paper. The slope of the resulting straight line is the spectral extinction coefficient for that band. If there is little spectral variation in the spectrographs, as in Figure 4-3, then the

average transmission from 5 to 30 microns wavelength can be used to represent the whole spectrum. Figure 4-5 was prepared for a 2.0 pcf polyurethane foam using the single band approximation.

Figure 4-6 shows a typical spectrograph for glass fiber insulation. The large "window" at 8 microns wavelength should not be lumped into a single band approximation, but rather should be divided into several bands.

Once the spectral extinction coefficient has been determined for the infrared wavelengths, the Rosseland mean extinction coefficient must be calculated. The calculation procedure is discussed in section 3.3.2 and in reference 36.

The line drawn in Figure 4-5 has the following equation:

$$\frac{\%T}{100} = e^{-Kt} \qquad (4-1)$$

where K equals 483 ft^{-1} and t is the thickness in feet. Therefore the extinction coefficient for the 2.0 pcf polyurethane foam was found to be 483 ft^{-1} (15.8 cm^{-1}).

Stern (37) measured the extinction coefficients of four foam samples; two polyurethanes, one polyisocyanurate, and one polystyrene foam. The results ranged from 623 ft^{-1} (20.4 cm^{-1}) for a 1.77 pcf polyurethane foam to 1294 ft^{-1} (42.5 cm^{-1}) for a 2.68 pcf polyurethane foam. Clearly for all foams tested to date, the extinction coefficient

Figure 4-5 : Data for 2.0 pcf
Polyurethane Foam Extinction
Coefficient Measurement
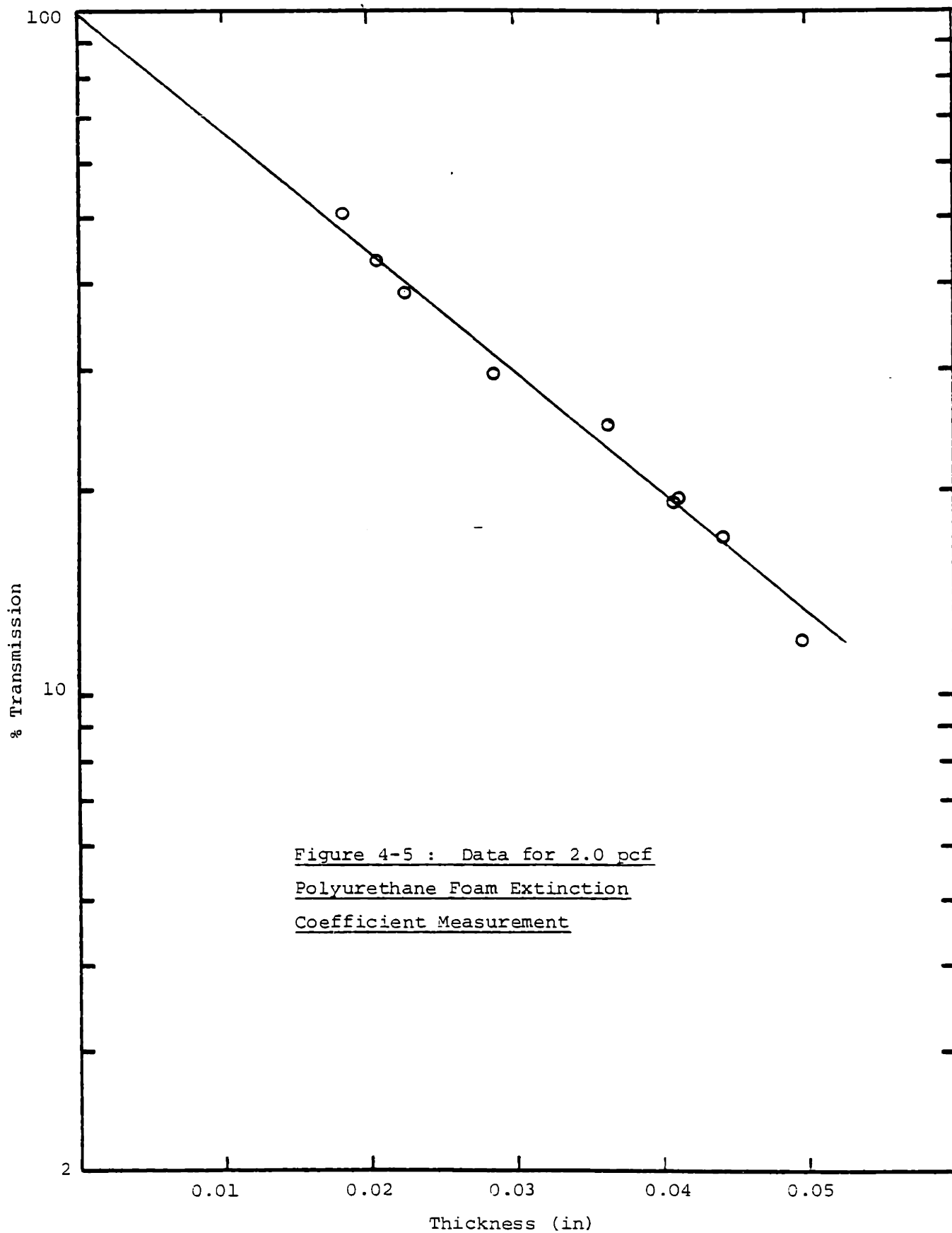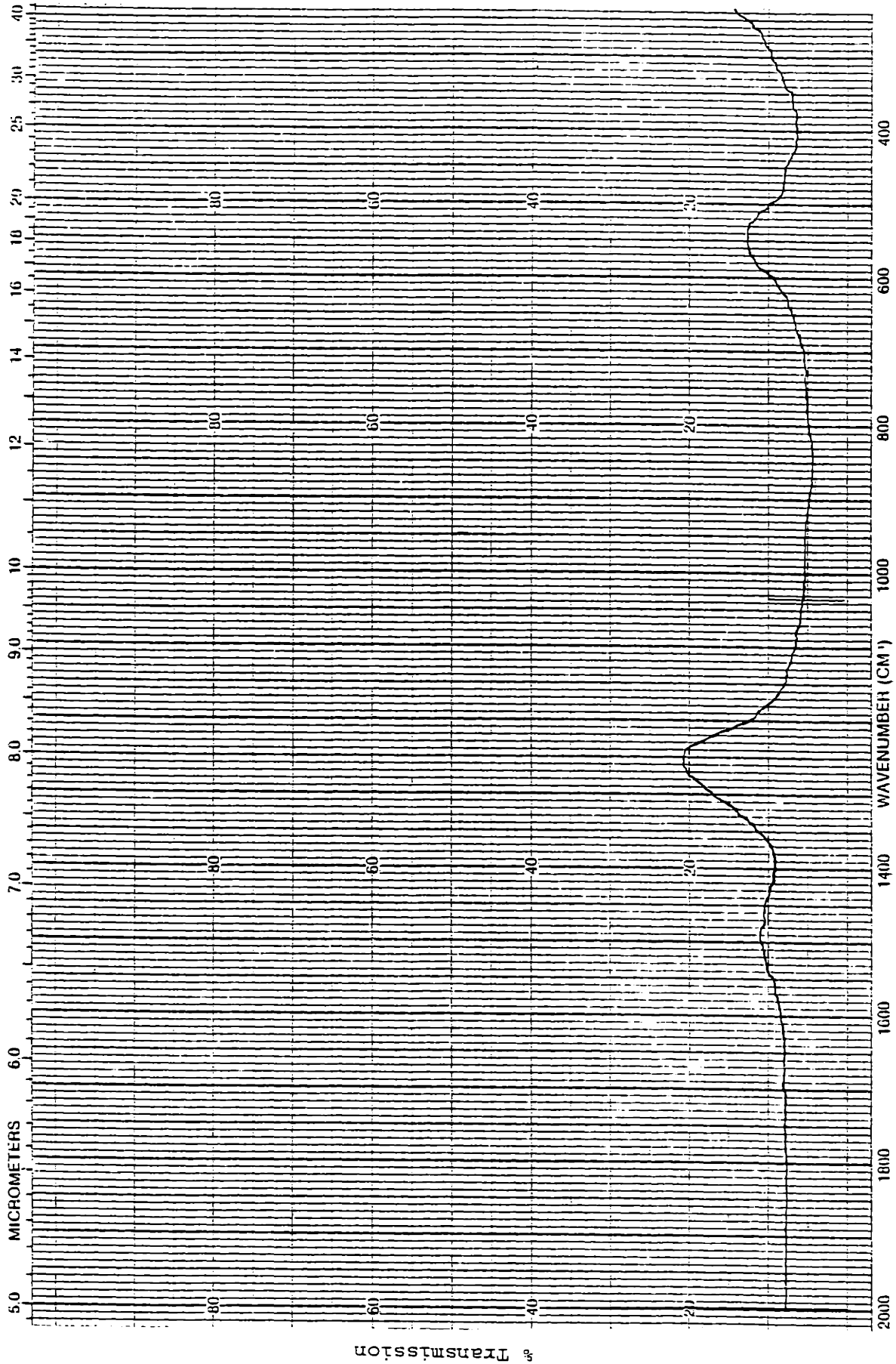
Figure 4-6 : Transmission Through 0.126 in Thick Glass Fiber Insulation Sample

is much larger than the value of 25 ft^{-1} (0.82 cm^{-1}) required for the three zone model of section 3.3.3.1. An optical thickness of 10 is achieved in the foam of Figure 4-5 at a sample thickness of only 0.25 inch (6.4 mm). Therefore, in the pure absorption case ($\omega_s=0$), the theoretical error due to the optically thin assumption and the three zone model is less than 0.1% for foam samples greater than 0.25 inch (6.4 mm). At 0.25 inch, the error in using the Rosseland equation with no boundary correction (equation 3-22) will be approximately 5% of the radiation contribution for surface emissivities of 1.0 and for an albedo of 0.0.

The error involved in this simple technique for extinction coefficient determination is primarily dependent on the scattering nature of the insulation. Where there is considerable nonisotropic scattering, this technique will be in error. For low density foams, we will show in the next section that the error in this simple technique is approximately 10.7% of the measured extinction coefficient. For glass fiber insulation the error will be approximately 60%. In both cases, the extinction coefficient is overestimated.

Note that this technique has been found to work consistently well when the foam is homogeneous. However, if the cell size distribution is wide or if filler materials are added to the foam and are not uniformly dispersed, then there will be scatter in the results of percent transmission versus thickness. This is of course because each data point represents the local conditions in the foam. If the local

conditions vary widely, then the data will vary widely. In such a case a larger number of data points (40-50) are required to achieve an accurate average value.

Figure 4-7 gives some of the spectral results for a 1.97 pcf phenolic foam. The manufacturer (39) stated that the foam has a bimodal cell size distribution. The probable cause of the scatter in the data is the nonuniform distribution of different sized cells. Nonetheless it is interesting to note that the phenolic appears to have a much higher mean extinction coefficient than the polyurethane foams of equal density. Using the calculation technique described in section 3.3.2 the Rosseland mean extinction coefficient was estimated at 1700 ft^{-1} (56. cm^{-1}) for this phenolic sample.

Figure 4-7 : Transmission Versus
Thickness for 1.80 pcf Phenolic Foam
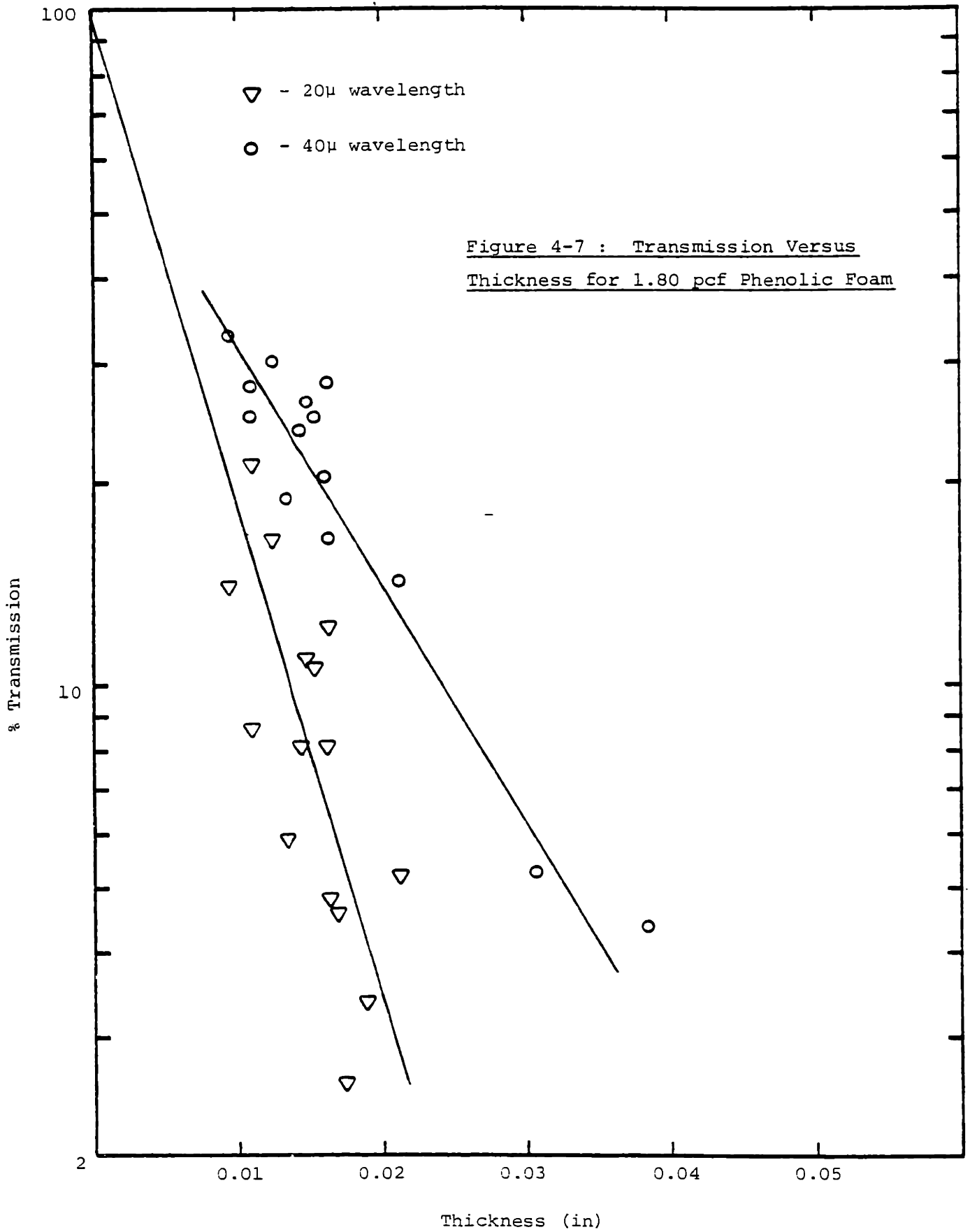
4.3 Scattering Experiment

A technique is presented for direct measurement of the insulation's spectral radiation properties (absorption coefficient, scattering coefficient, phase function). Measurements are reported for polyurethane foam and glass fiber insulation at 9.64 microns wavelength. The results are used to quantify the error in the simple technique for the extinction coefficient. The P-1 approximation is compared against the exact solution for both the foam and glass fiber data. Finally, recommendations are provided for improvement of the simple technique.

4.3.1 Purpose

The experiment was carried out to determine whether or not nonisotropic scattering plays a significant role in the radiation heat transfer through foam insulation. The experiments permitted quantification of the error in the simple extinction coefficient measurement technique. In addition, a more fundamental understanding of the heat transfer through foam has been reached.

4.3.2 Method and Apparatus

A technique was developed to measure the absorption coefficient, scattering coefficient and phase function in a direct manner. Measurements of total hemispherical transmissivity or reflectivity were inadequate because they could not provide direct measurements of these important radiation parameters. Instead they rely on assumed phase functions and scattering coefficients and thus only provide overall

checks. The approach taken was to attempt to measure the scattering from a sufficiently thin sample so that the test could be treated as a single scattering event. As will be seen, it was not possible to obtain samples optically thin enough for this approximation while maintaining the integrity of the foam. Hence, the scattering coefficient, absorption coefficient, and the phase function were measured on the thinnest sample obtainable. The measurements were repeated with thicker samples of the same foam. An analytical solution to a simplified form of the equation of transfer (equation 3-8) was used to analyse the test results. The radiation parameters measured at different sample thicknesses were found to agree within the experimental uncertainty.

Optical Layout

The apparatus was simple in concept, but the aide of the people at the MIT Regional Laser Center was required for the set-up. A schematic diagram of the apparatus is shown in Figure 4-8. The beam was generated by a CO_2 laser. The laser is normally used for ultra high resolution infrared spectroscopy and therefore was monochromatic to within ± 1. MHz. The laser was grating tuned from line to line.

The laser beam was aimed at the first swing mounted mirror. When the mirror was up (away), the beam either hit a carbon block where it was absorbed, (this was a safety feature to prevent stray laser radiation from reflecting throughout the room) or the beam went to an Optical Engineering Company CO_2 Spectrum Analyser which determined the wavelength of the beam.
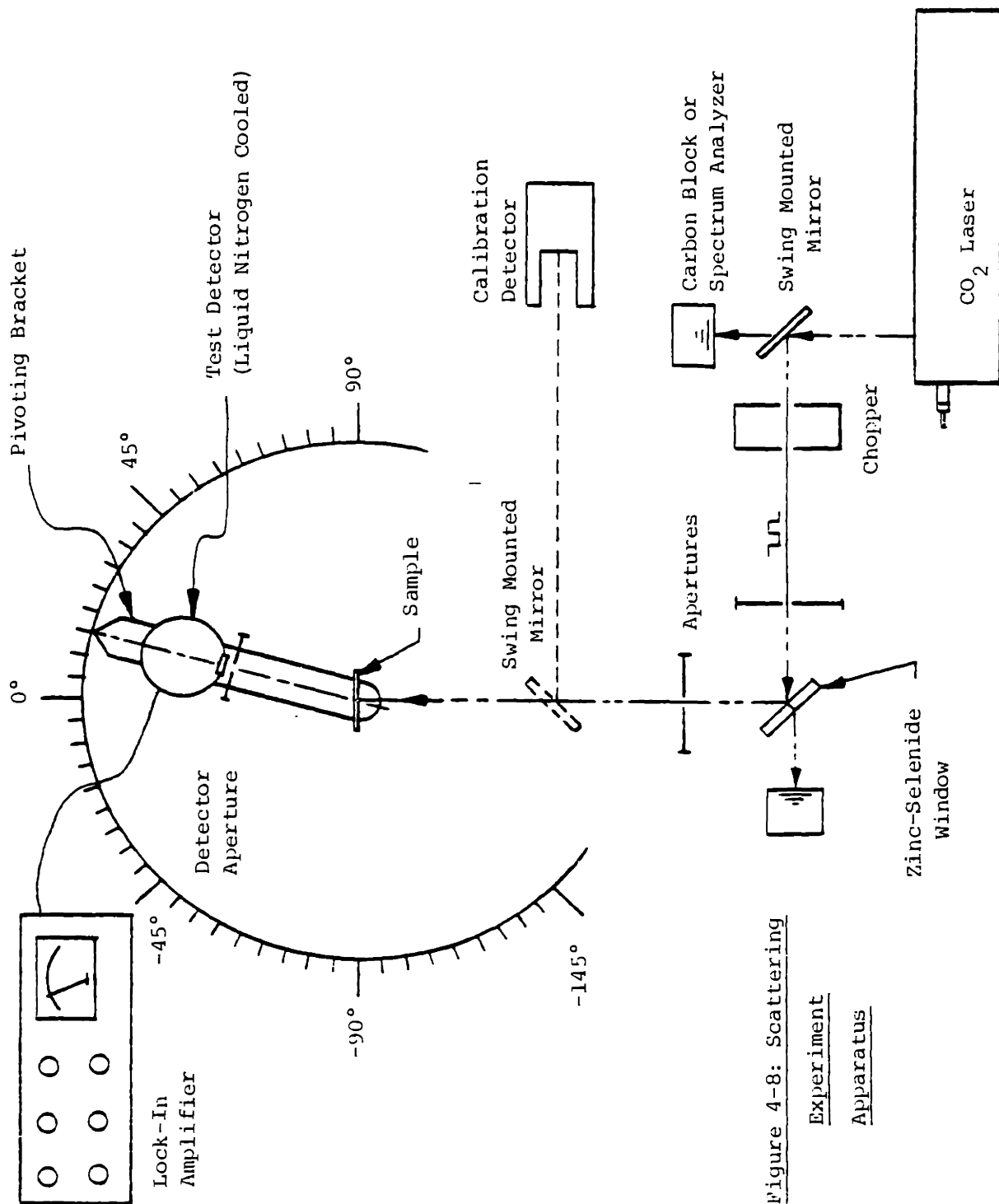
Figure 4-8: Scattering
Experiment
Apparatus

When the swing mounted mirror was in place, the beam was reflected and passed through the chopper. The chopper was a Newport Research Corporation Model 380 Frequency Programmable Light Chopper, Mk II. Line voltage powered a constant voltage transformer which fed a Variac transformer, the output of which powered the chopper control. By adjusting the Variac transformer, different chopping frequencies could be attained. The constant voltage transformer helped stabilize the chopping frequency even as the line voltage varied. The beam entered the chopper as a continuous source, and left the chopper as a square wave; one half of the time the beam was blocked and one half of the time it was transmitted. For all tests, the chopping frequency was maintained at 395 $\pm$10 Hz.

Since the chopper produced some scatter from the beam, an aperture was placed after the chopper to absorb this stray energy. This aperture opening was set at 0.141 inch (0.36 cm) with a plug guage. After this first aperture the beam was aimed at a zinc-selenide window. Most of the energy striking this window was transmitted into a block of absorbing material. Approximately 10% of the incident energy was reflected toward the sample. Since the laser power was approximately 1-2 W, and since 50 to 200 mW were needed in the tests, this window provided the proper beam attenuation. Prior to the use of this zinc-selenide window, an ordinary mirror was used and a methyl alcohol vapor attenuation cell was placed between the first mirror and the chopper. Small vacuum leaks in the system caused excessive power drift. The zinc-selenide window was perfectly stable and therefore solved the

attenuation drift problem. Unfortunately the zinc-selenide window provided two reflections, one off the front face and one off the back. Another aperture was used to absorb the back face reflection while transmitting the other. Alignment of this aperture was critical to obtaining an axially symmetric source beam at the sample. Unfortunately the goal of a perfectly symmetric source beam was never attained. Some asymmetry in the beam was therefore traded-off for better power level stability. This aperture was set at 0.070 inch (0.18 cm) with a plug guage.

A swing mounted mirror was placed in front of the sample. With this mirror in place, the beam was reflected to a thermopile calibration detector, Laser Power Meter Model No. 360001 made by Scientech Inc. Measured power output from this detector was read directly in milliwatts on a digital readout device by Analogic. The readout accompanies the thermopile detector.

When this swing mounted mirror was up, the beam struck the test specimen directly above the pivot point of the test detector bracket. By attaching a small aperture to the front of the test detector, it was possible to assure that most of the stray room radiation was blocked from the sensing element. The detector aperture was set small enough (0.0625 inch, 1.59 mm) so that all of the energy scattered from the sample which passed through the detector aperture was incident on the sensing element. By leaving the aperture opening fixed, the detected solid angle remained constant as the detector was moved around the

circle. Note that the radius of rotation was fixed by the bracket. The geometry of this system is given in Figure 4-9.

The bracket consisted of an aluminum plate 17 x 1.5 x 0.38 inches (43.2 x 3.8 x 0.97 cm) to which the detector was rigidly attached. The plate had a hole in one end through which passed a brass post. The post was screwed into the table so as to provide a secure pivot. The sample holder was mounted on top of this post, assuring that the samples were mounted at the pivot point of the detector. The other end of the plate had a scratch mark which was used to indicate the detector angle.

The detector aperture was connected directly to the body of the detector. This assured that the aperture alignment would not be affected as the bracket was moved about for the various tests. The detector aperture was set to 0.0625 inch (1.59 mm) with a plug gage.

Any components which could possibly receive direct laser energy were coated with Scotch tape number 5050 16P#410 4DSL. This tape is strongly absorbing in the infrared. The aperture frame, the aperture brackets, and the sample holder were all shielded with this tape, as a safety measure, and to reduce stray radiation which might affect the readings.

The entire apparatus was bolted to a rigid steel bench mounted three feet off the floor on Newport Research Corporation Pneumatic Isolation Mounts, Type XL-A. The room temperature was maintained at 65 F for improved laser power stability.
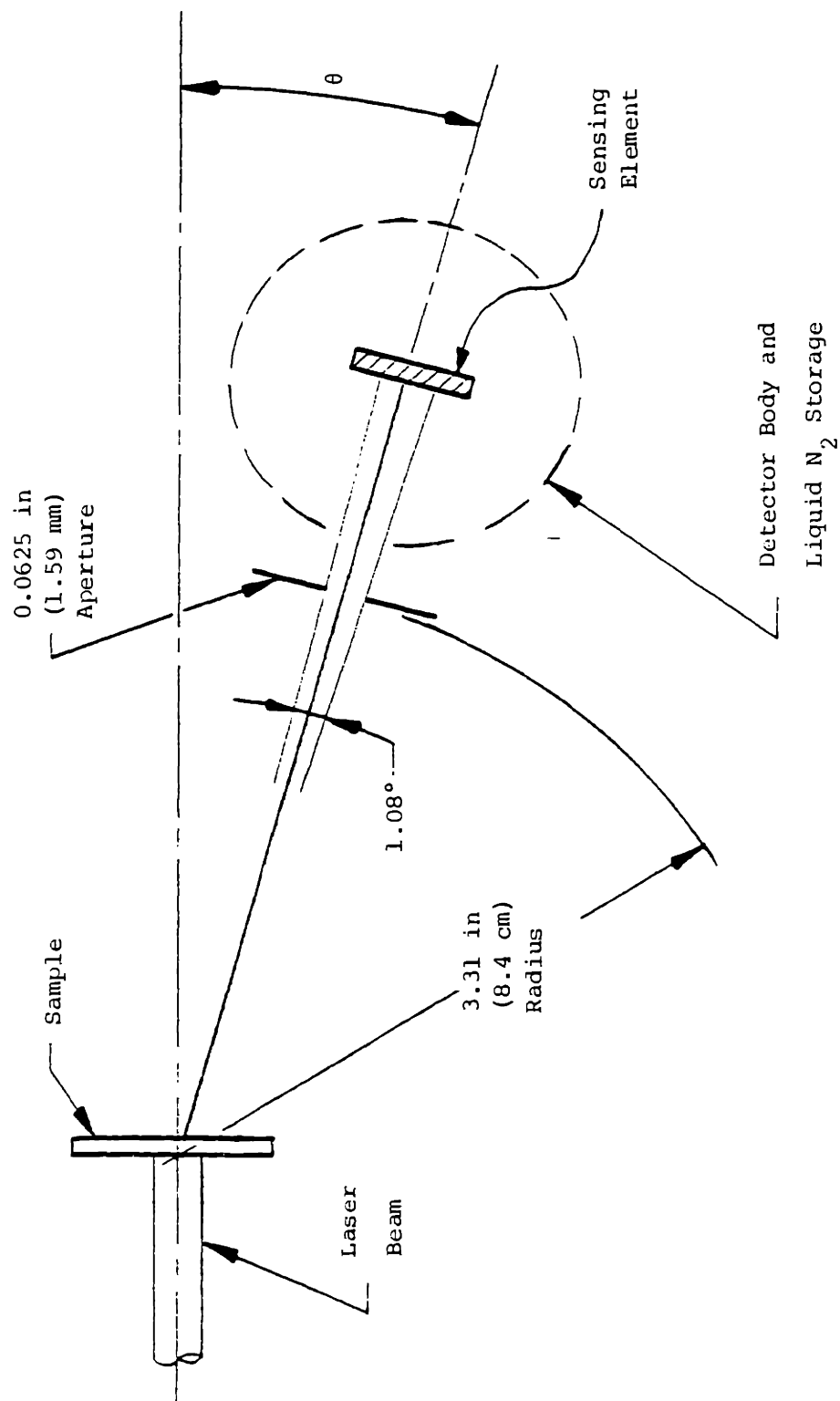
Figure 4-9 : Beam, Sample, Detector Geometry

Detection System

The detection system consisted of the test detector, the circuit, and the lock-in amplifier. The detector was a photoconducting type detector. The sensing element was gold doped germanium, and thus had a rapid enough response to produce a clean square wave output to the 400 Hz chopped laser input. The sensing element was approximately 0.1 x 0.1 inches (2.5 mm square) located 0.75 inches (1.9 cm) behind an NaCl window within a stainless steel container. The stainless steel container also acted as a storage flask for liquid nitrogen coolant. The flask liner was evacuated with a conventional vacuum roughing pump. Unfortunately the detector body was void of any markings indicating the manufacturer or model number. The detector output was read on the lock-in amplifier via the circuit shown in Figure 4-10. An Eveready battery was used for the 45 V d.c. source. The output voltage was input to a Princeton Applied Research Model 121 Lock-in Amplifier/ Phase Detector. The output voltage was also displayed on an oscilloscope for the purpose of verifying the rapid response of the detector. The chopper synchronization output signal was also input to the lock-in amplifier.

The lock-in amplifier compared the output voltage signal to the chopper signal and integrated out all signal components out of phase or not within 5% of the chopping frequency. The remaining signal was integrated and amplified to give an output voltage between zero and 10 V d.c. The maximum gain on the amplifier was 10^6. Thus a $10\mu V$ square
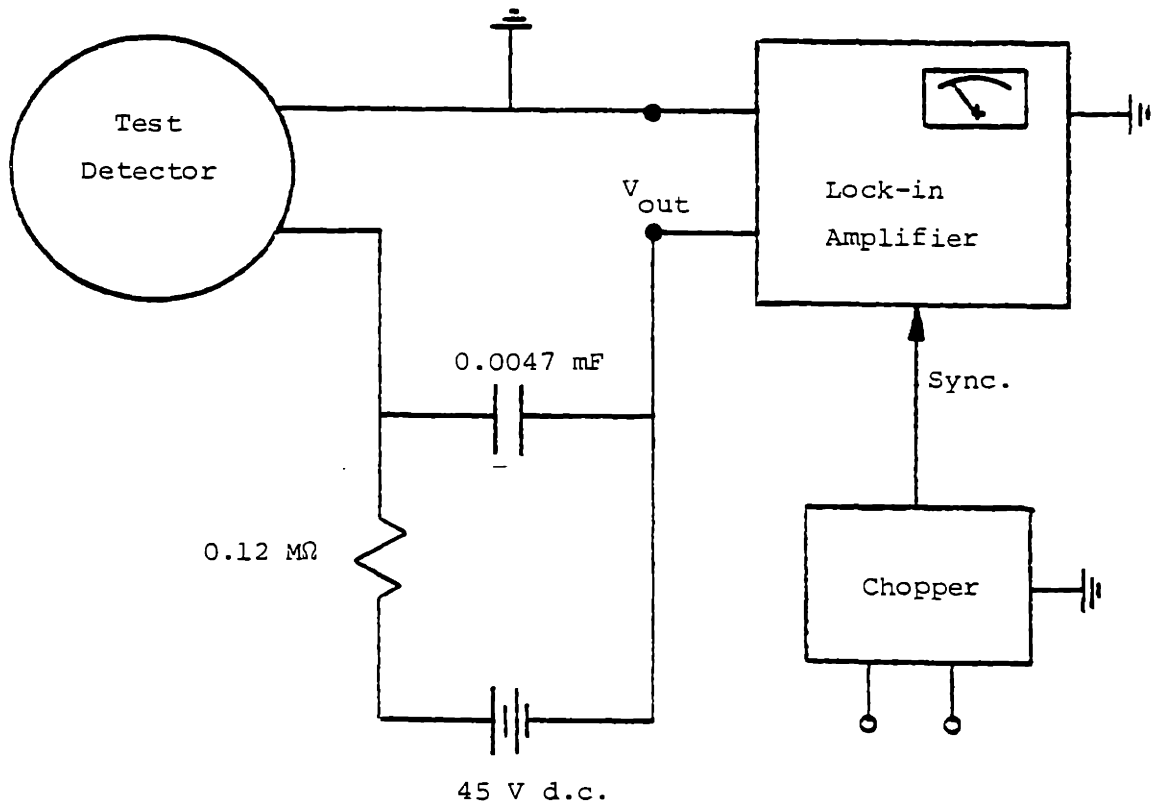
Figure 4-10 : Wiring Diagram for Detection System

wave input produced a 10 V d.c. output at maximum gain. The amplifier output voltage was measured within 1% at any amplification on a mirrored meter, built in to the amplifier. Alternatively one could use an oscilloscope or any other device to measure the lock-in amplifier output voltage.

The apparatus enabled accurate measurement of scattered energy from foam samples at any angle from 0 to 85 degrees and 95 to 160 degrees from the incident beam direction. Angles from 85 to 95 degrees were blocked by the sample holder. At angles greater than 160 degrees the detector body blocked the source beam.

4.3.3 Experimental Procedure

The overall experimental procedure follows. Details on various aspects of the procedure follow the general explanation. At the beginning of the day, the CO_2 laser was turned on and tuned to the operating line (wavelength). The chopper was set and the power level monitored until the laser stabilized. A sample was inserted in the holder and the detector bracket moved to the zero degree position. Laser power was recorded on the calibration detector. The mirror was flipped up so that the energy transmitted at zero degrees could be measured. The mirror was flipped down, the laser power was recorded, and the mirror was flipped up so that scattered energy could be measured at the next angle. This was repeated until the detector was moved from 0 to 85 degrees with measurements taken at small increments (0.5 degrees) near zero degrees, gradually increasing to five degree

increments from 25 to 85 degrees. Unfortunately, space limitations prohibited taking measurements all the way to 160 degrees in one continuous swing. Some measurements were taken from -90 to zero degrees to assure that the scattering was symmetrical. Where assymetry was significant, the measured value was taken as the average of positive and negative angle measurements (as defined in Figure 4-8).

In order to measure backscattering, the sample post was unscrewed from the table and moved to a position which allowed swinging from 90 to 160 degrees. Since the optical alignment process was tedious, all backscatter data was taken with one setup. Subsequently the apparatus was returned to the forward scattering setup for some final tests.

Despite all precautions, the laser power slowly drifted during testing. In order to relate scattered energy measurements to a consistent power level, laser power was measured on the thermopile calibration detector between scattering readings. After a scattering measurement was taken at a particular angle, the swing mounted mirror was dropped so as to reflect the beam to the calibration detector. Laser power was measured on the thermopile detector, and the mirror swung back up. The scattered energy was measured at the next angle, and so on. While the test detector had a rapid enough response to give a clean square wave output at 400 Hz, the calibration detector was a thermopile and therefore had a very slow response. The step response of this detector was tested and found to have a characteristic time constant of approximately ten seconds. For each measurement with this

detector, 45 seconds (4.5 time constants) were allowed between the time that the mirror was dropped and the time of the reading. This ensured a full response without causing such excessive delays as to exacerbate the laser power drifting problem.

Calibration of Test Detector

In all cases the test detector was calibrated against the same thermopile detector. The room temperature was maintained at 65 F (18 C) at all times so as to ensure consistency in the thermopile detector readings. During preliminary tests prior to completion of the apparatus shown in Figure 4-8, it was determined that the test detector calibration drifted considerably from one day to the next. It was also determined that at power levels higher than 25-30 mW, the test detector response begins to deviate from linearity. This corresponds to an output voltage measured with the lock-in amplifier of approximately 130-150 mV. At test detector output levels greater than 200 mV the deviation from linearity was 20%, as seen in Figure 4-11. This figure shows a typical detector response curve, measured prior to the installation of the small aperture in front of the test detector. The sensing lement was therefore receiving all of the incident laser power. (The beam was aimed directly at the sensing element.)

Later in the testing it was discovered that the calibration drifted by as much as 30% over a time period of two hours. Hence, the calibration had to be checked for each data point whenever possible.

Test
Detector
Output
Voltage
(mV)

Incident Laser Power (mW)
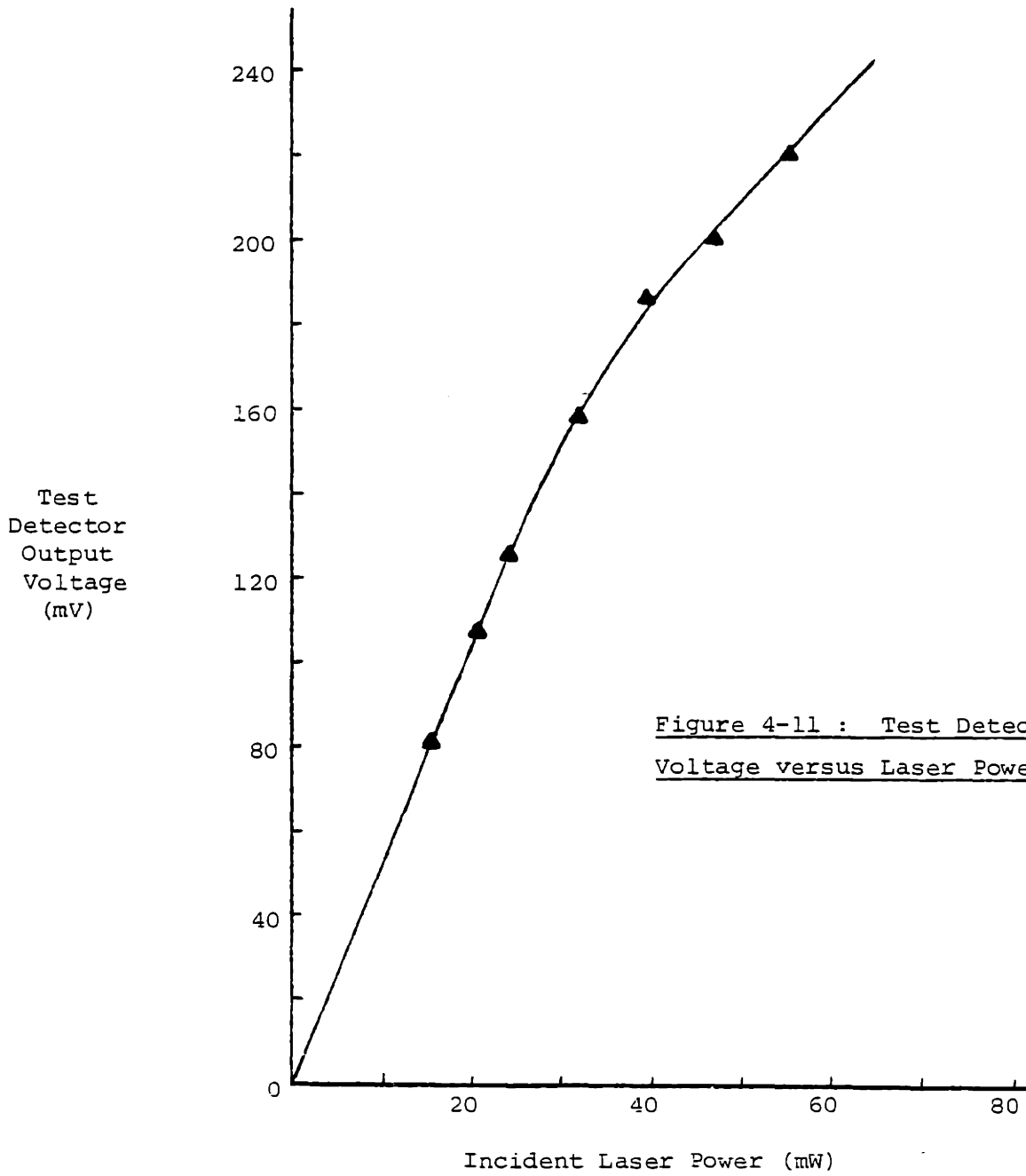
Figure 4-11 :   Test Detector Output
Voltage versus Laser Power

The calibrations were performed by one of two methods. In the first method, no sample was placed in the sample holder. The test detector was moved from -7 to +7 degrees with output voltage readings taken every degree from +5 to +7 and -5 to -7 degrees, and every half degree from -5 to +5 degrees. The laser power was measured on the calibration detector between readings on the test detector. The laser beam width was fully traversed by the test detector. The power level was assumed axially symmetric so the resulting voltages could be integrated over the appropriate portion of the sphere and compared to the power read on the calibration_detector. Table 4-1 illustrates this computational exercise for some typical calibration data. In this table, all test detector voltage readings have been normalized to a constant laser power of 62.12 mW, (the average of all laser power readings on the thermopile calibration detector). The calibration constant (C_c) is determined from equation 4-2 for $\theta_1 = 0$; $\theta_2 = 7.5$ degrees, r =8.4 cm, P_L = 62.12 mW. The readings at $+\theta$ and $-\theta$ are averaged to determine V_{avgi} . This value is assumed constant from θ_{1i} to θ_{2i} so that the integral in equation 4-2 may be evaluated.

$$P_L = C_c \cdot 2\pi r^2 \sum_{i=1}^{13} \int_{\theta_{1i}}^{\theta_{2i}} V_{avg\ i} \sin\theta\ d\theta \qquad (4-2)$$

Table 4-1 : Typical Calibration Data with No Sample

i Summation Index	1	2	3	4	5	6	7	8	9	10	11	12	13
θ Polar Angle	0	0.5	1	1.5	2	2.5	3	3.5	4	4.5	5	6	7
*Reading at + θ (mV)	199	120	23.9	4.42	2.54	.332	.438	.0859	.0421	.0400	.0318	.0073	.0035
*Reading at - θ (mV)	—	184	101	25.7	3.04	1.44	.466	.703	.343	.0973	.0897	.0118	.0060
V_{avgi} Avg. of +/- θ Readings	199	152	62.5	15.1	2.79	.886	.452	.394	.193	.0687	.0608	.0096	.0048
θ_{1i} Limits of	0	0.25	0.75	1.25	1.75	2.25	2.75	3.25	3.75	4.25	4.75	5.5	6.5
θ_{2i} Integration	0.25	0.75	1.25	1.75	2.25	2.75	3.25	3.75	4.25	4.75	5.5	6.5	7.5

Calibration Constant = 4.95

* Normalized to Laser Power of 62.12 mW

All energy passing through the aperture is assumed incident on the sensing element. (See Figure 4-9.) Hence the radius (r) is the distance from the sample holder centerline to the detector aperture. The limits of integration are zero to 7.5 degrees. This causes the test detector to traverse the same area as the sensing area of the thermopile detector.

The second calibration procedure is similar to the first. The primary difference is that the calibration is performed with a sample in the sample holder. After the measurements of scattered energy are taken from -90 to +90 degrees, the thermopile detector is placed behind the sample and the transmitted power is measured. This transmitted power measurement is compared to the integrated test detector readings using equation 4-2. When placed behind the sample, the calibration detector measures all energy within an 8.3 degree angle from incident. Hence the limits of integration in equation 4-2 must be changed to zero to 8.3 degrees so as to match detected solid angle with the new geometry.

This second calibration method has two advantages. A calibration may be taken with this method for every sample tested. Since the test detector calibration has been found to drift by 30% over a period of a few hours, and since a scan from -90 to +90 degrees normally required two hours, the frequency of calibration check was important. Second, since the peak test detector output voltage is lower (typically from 1 to 60 mV), one may see from Figure 4-8 that the measured readings will always be on the linear portion of the detector response curve. The

primary advantage of the first calibration method is due to the higher laser power level. At higher power levels, the thermopile detector measurement is more accurate. The finest subdivision on the thermopile display was 1.0 mW. One must therefore expect readings to be accurate to only 1-2 mW.

Table 4-2 presents a summary of several test calibrations. The date taken and the test method and power level are provided. The variation in detector calibration was the limiting factor in experimental accuracy of radiation properties measurement.

Before proceeding into the data analysis, consider the implications of the calibration procedure, and of equation 4-2. One may use equation 4-2 to calculate the detected scattered energy over any range of θ. If the sample were infinitesimally thin, then equation 4-2 could be used to determine the total scattered power, i.e.:

$$Q_{scat} = C_c \cdot 2\pi r^2 \int_0^\pi V_{arg}(\theta) \sin \theta \, d\theta \qquad (4-3)$$

If $I_M(\theta)$ is the scattered intensity measured at θ, based on the laser beam cross sectional area (A_b), we can also write:

$$Q_{scat} = 2\pi \int_0^\pi (I_M(\theta) \cdot A_b) \sin \theta \, d\theta \qquad (4-4)$$

Hence:

$$V_{avg}(\theta) = \frac{I_M(\theta) \cdot A_b}{C_c \, r^2} \qquad (4-5)$$

Table 4-2 : Summary of Detector Calibrations

Date	Test Method	Mean[*] Laser Power (mW)	Calibration Constant mW / cm^2mV
7/21/82	1	80.5	6.43
7/21/82	2	24.7	5.68
7/22/82	1	74.5	5.44
7/22/82	2	18.9	4.91
7/24/82	2	19.8	5.83
8/17/82	1	62.1	4.95
8/17/82	2	7.7	4.06
8/18/82	1	79.9	5.39
8/18/82	2	22.0	4.90
8/18/82	2	11.1	3.00

[*] Measured with thermopile calibration detector.

If the laser beam intensity is approximated as a constant over the beam area, we may write:

$$P_L = I_o \cdot A_b \cdot \Delta\omega_L \qquad (4\text{-}6)$$

where:

P_L = incident laser power

I_o = incident intensity (average)

A_b = laser beam cross sectional area

$\Delta\omega_L$ = solid angle of laser beam $\qquad (4\text{-}7)$

From equations 4-5 and 4-6 we find:

$$\frac{I_M(\theta)}{I_o \Delta\omega_L} = \frac{C_c \, r^2 \, V_{avg}(\theta)}{P_L}$$

The usefulness of equation 4-7 will become apparent in the next section.

4.3.4 Data Analysis

Using the apparatus described in section 4.3.2 and the procedure described in section 4.3.3, several tables of numbers were generated. Measured output voltages at detector angles from zero to 160 degrees were recorded for different thicknesses of various foam and glass fiber samples. This section presents the theoretical framework with which the phase function, absorption coefficient, and scattering coefficient are extracted from the data.

Measurement of scattered intensity around the sphere provides the information required to calculate the scattering coefficient and phase function. However, the calculations required to determine these properties from the data are not straightforward. Figure 4-12 presents the measured voltages normalized to a consistent laser power level as a function of detector angle with no sample in place, with a thin polyurethane foam sample, and with a thicker sample of the same foam.

One difficulty arises in the treatment of the data for angles close to zero degrees. The laser has a significant beam width and a small beam divergence. At angles between zero and ten degrees, the detector measures the sum of transmitted energy plus forward scattered energy. Forward scattering within the first ten degrees is therefore totally indistinguishable from transmission.

Figure 4-12 : Output Voltages versus Angle

0.0265 in. Sample (0.67 mm)

0.083 in. Sample (2.1 mm)

Laser No Sample

Detector Output Voltage (mV)

Angle (degrees)
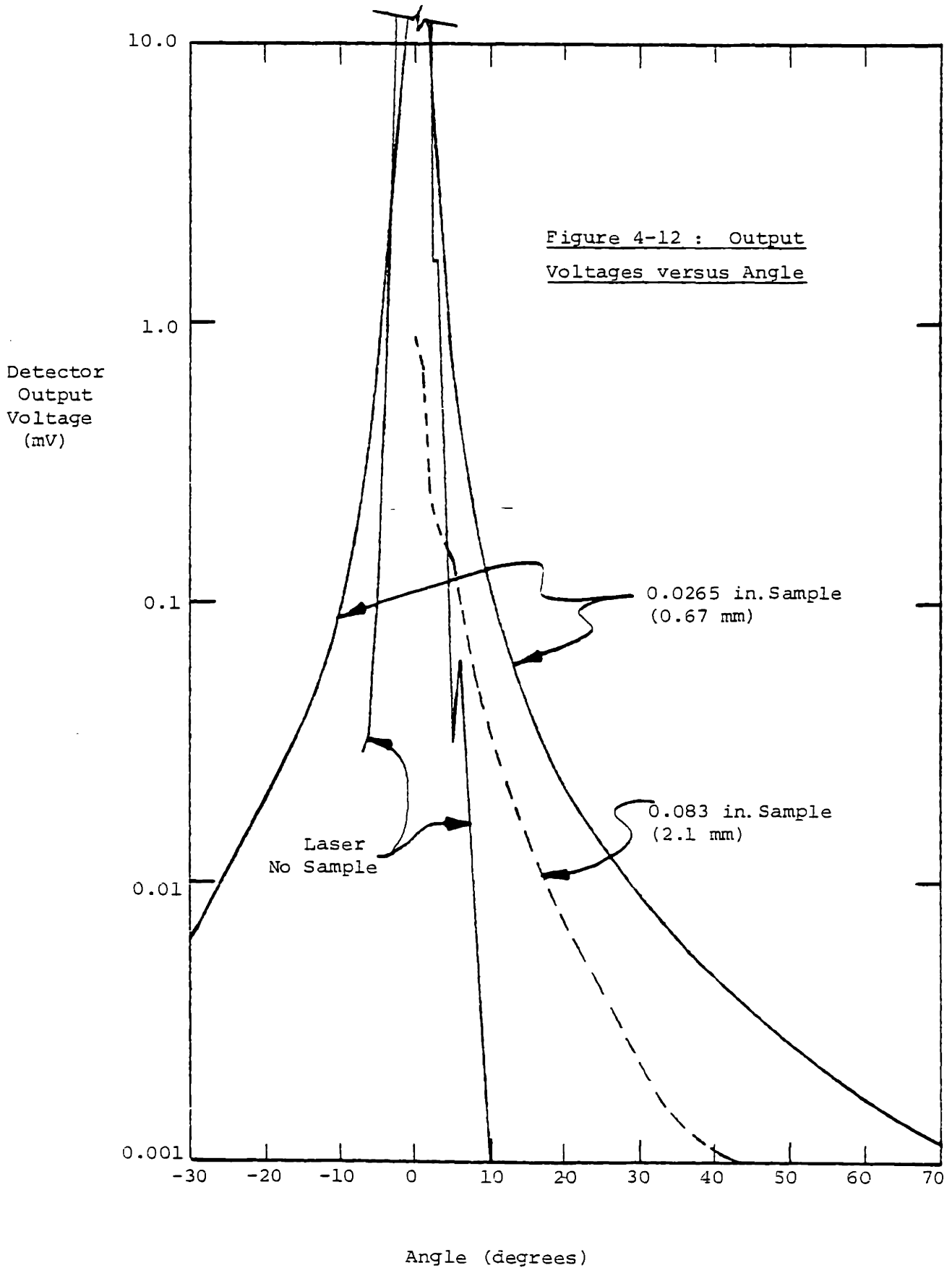
The second problem is the quantitative determination of the scattering and absorption coefficients. Initially, the problem was treated as a single scatter/absorption event. Therefore the scattering coefficient could be defined as the ratio of total scattered energy to total incident energy. The absorption coefficient could be defined as the ratio of total absorbed energy to incident energy. Unfortunately it was found that the values for scattering and absorption coefficients calculated in this way varied widely depending on the test sample thickness. The thicker the sample, the lower the calculated values of these properties.

The sum of the scattering and absorption coefficients (the extinction coefficient) could alternatively be determined from the percentage of incident energy which was transmitted. See equation 4-1. The extinction coefficient calculated via equation 4-1 did not agree with the sum of the scattering plus absorption coefficients previously determined via the single event model. Hence, the simple analysis inadequately represents the physical process taking place in the test.

Improved Model for Data Reduction

For the conditions present during the tests, it is possible to analytically solve a simplified form of the radiation equation of transfer. Equation 3-1 is repeated here for convenience:

$$\frac{dI_\lambda(s)}{ds} = -(a_\lambda + \sigma_{s\lambda}) \, I_\lambda(s) + a_\lambda I_{\lambda b}(s) \qquad (3-1)$$

$$+ \frac{\sigma_{s\lambda}}{4\pi} \int_{\omega' = 4\pi} I_\lambda(s,\omega') \, \phi_\lambda(\omega,\omega') \, d\omega'$$

We may omit the $a_\lambda I_{\lambda b}(s)$ term completely for the following reasons: Since the laser beam has a much higher intensity than the radiation emitted by the sample at room temperature, the emission will be negligible. Furthermore, since the the laser beam is chopped at 400 Hz, and the lock-in amplifier ignores D.C. signals, emission does not contribute to the measured signal.

The laser is monochromatic and therefore all radiation intensities are monochromatic. Since the test is performed at a single wavelength we drop the λ subscripts and use this notation change for the balance of this chapter. This simplifies the equation of transfer to equation 4-8.

$$\frac{d \, I(s)}{ds} = -(a + \sigma_s) \, I(s) + \frac{\sigma_s}{4\pi} \int_{4\pi} I(s,\omega') \, \phi(\omega,\omega') \, d\omega' \qquad (4-8)$$

One more simplification will be made to reduce equation 4-8 to a simple differential equation. First we must discuss the scattering coefficient and phase function and make an approximation which will streamline the derivation. Consider the phase functions plotted in Figure 4-13. The curve labeled Φ represents a hypothetical actual phase function while the curve labeled Φ^* is a modified phase function. The difference between these two functions is that up to a cutoff angle of θ_f, the modified phase function has a value of zero. Over the rest of the curve Φ^* was increased over Φ by a constant factor so as to keep the function Φ^* properly normalized. If we define F by equation 4-9:

$$F \equiv \frac{1}{2} \int_{\theta=0}^{\theta_f} \Phi(\theta) \, \sin\theta \, d\theta \qquad (4-9)$$

Then:

$$\left.\begin{aligned}
\Phi^*(\theta) &= \frac{\Phi(\theta)}{1-F} \quad \text{for } \theta > \theta_f \\
\Phi^*(\theta) &= 0 \quad \text{for } 0 \leq \theta \leq \theta_f
\end{aligned}\right\} \qquad (4-10)$$

Furthermore if σ_s is the scattering coefficient corresponding to the phase function Φ, we define σ_s^* as σ_s times the same constant factor which increased Φ to Φ^* for angles greater than θ_f. Thus the product $\sigma_s^* \Phi^*$ equals $\sigma_s \Phi$ for all angles greater than θ_f.

$$\sigma^* \equiv \sigma (1 - F) \qquad (4-11)$$
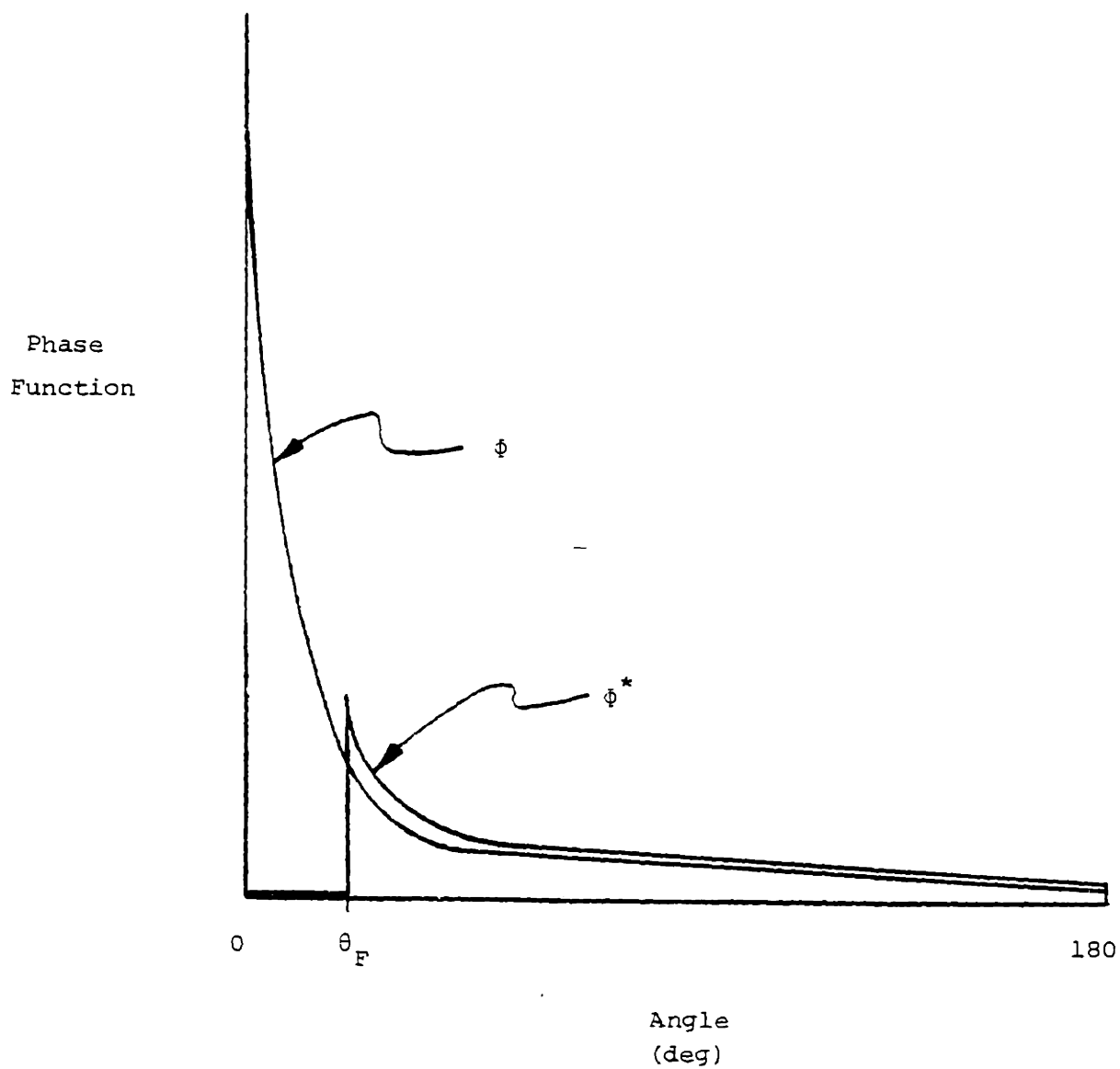
Figure 4-13 : Illustration of Phase Function
Modification for Scattering Data Analysis

For an beam of intensity I incident on an infinitesimal thickness of material, the scattered intensity at angles greater than θ_f would be the same regardless of whether the foam had σ_s and Φ or had σ_s^* and Φ^* as radiation properties. Hence the modifications described above will not affect the physics for angles greater than θ_f.

In this example, if the absorption coefficients were the same in both cases then the case with σ_s^* and Φ^* would have a higher transmissivity than the σ_s, Φ case. The difference in transmitted intensity would be exactly equal to the total scattered intensity from zero degrees to θ_f in the σ_s, Φ case. This illustrates that the scattering coefficient and phase function modifications cause some energy which was previously considered forward scattered at a small angle to be treated as transmitted energy.

Houston (14) has shown that this type of approximation results in no significant change in the calculated heat transfer results for strongly forward scattering phase functions, so long as θ_f is not too large. For his theoretically predicted phase functions the error was less than 5% at cutoff angles of 25 degrees and was negligible at cutoff angles under 10 degrees. Therefore, strongly forward scattered radiation can be equivalently considered as transmitted radiation. The inability to distinguish between the two in this experiment will have no bearing on radiant heat flux predictions based on experimentally measured properties. Indeed, the inability to experimentally distinguish between the two suggests that they are equivalent.

Assuming a phase function of the form of ϕ^* in Figure 4-13, and assuming a cutoff angle, θ_f, of 10 degrees, we may now simplify equation 4-8. Consider first the case where s is the laser beam incident direction (call this the x direction). We write I_L as the "laser" intensity in this direction. For this case, the integral on the right hand side of equation 4-8 will be negligible in comparison to the first term. Physically this means that the beam is attenuated by absorption and scattering as it passes through the sample. The intensity will also be increased if some of the energy which had previously been scattered away from the beam is re-scattered into the beam. For materials where ϕ decreases rapidly with θ, this re-scattering from angles greater than 10 degrees will be small. Furthermore, for thin samples where a limited number of scattering events occur, this effect will be so small that it may be neglected. Therefore we may write:

$$\frac{dI_L}{dx} = -(a + \sigma_s^*)\, I_L \tag{4-12}$$

Note that by using σ_s^* in equation 4-12, we are including the assumption that energy which is forward scattered within θ_f is not attenuated (i.e. it is transmitted). At x=0, I_L equals the incident intensity I_o. Integrating equation 4-12 from x=0 to x, I from I_o to I_L, we find:

$$\ln\left(\frac{I_L}{I_o}\right) = -(a + \sigma_s^*)\, x \tag{4-13}$$

or:

$$\frac{I_L}{I_o} = e^{-(a + \sigma_s^*)\,x} \qquad\qquad (4\text{-}14)$$

Therefore the transmitted intensity will follow the familiar exponential form, previously given by equation 4-1.

Consider now the case where the s-direction is at an angle θ ($\theta_f < \theta < 90$) to the x-direction, as shown in Figure 4-14. For this case we assume that the only appreciable contribution of scattering into the s-direction is scattering directly from the laser beam. Hence we may simplify equation 4-8 to:

$$\frac{d\,I(s)}{ds} = -(a + \sigma_s^*)\,I(s) + \frac{\sigma_s^*}{4\pi}\,(I_L \phi^*(\theta)\,\Delta\omega_L) \qquad (4\text{-}15)$$

where $\Delta\omega_L$ is the solid angle of the laser beam. Substituting equation 4-14 into equation 4-15 for I_L yields:

$$\frac{d\,I(s)}{ds} = -(a + \sigma_s^*)\,I(s) + \frac{\sigma_s^*\,\phi^*(\theta)\,\Delta\omega_L}{4\pi}\,I_o\,e^{-(a + \sigma_s^*)\,x} \qquad (4\text{-}16)$$

From geometry:

$$x = s\cos\theta \qquad\qquad (4\text{-}17)$$

And hence:

$$\frac{d\,I(s)}{ds} = -(a + \sigma_s^*)\,I(s) + \frac{I_o\,\sigma_s^*\,\phi^*(\theta)\,\Delta\omega_L}{4\pi}\,e^{-(a + \sigma_s^*)\,s\cos\theta}$$
$$(4\text{-}18)$$
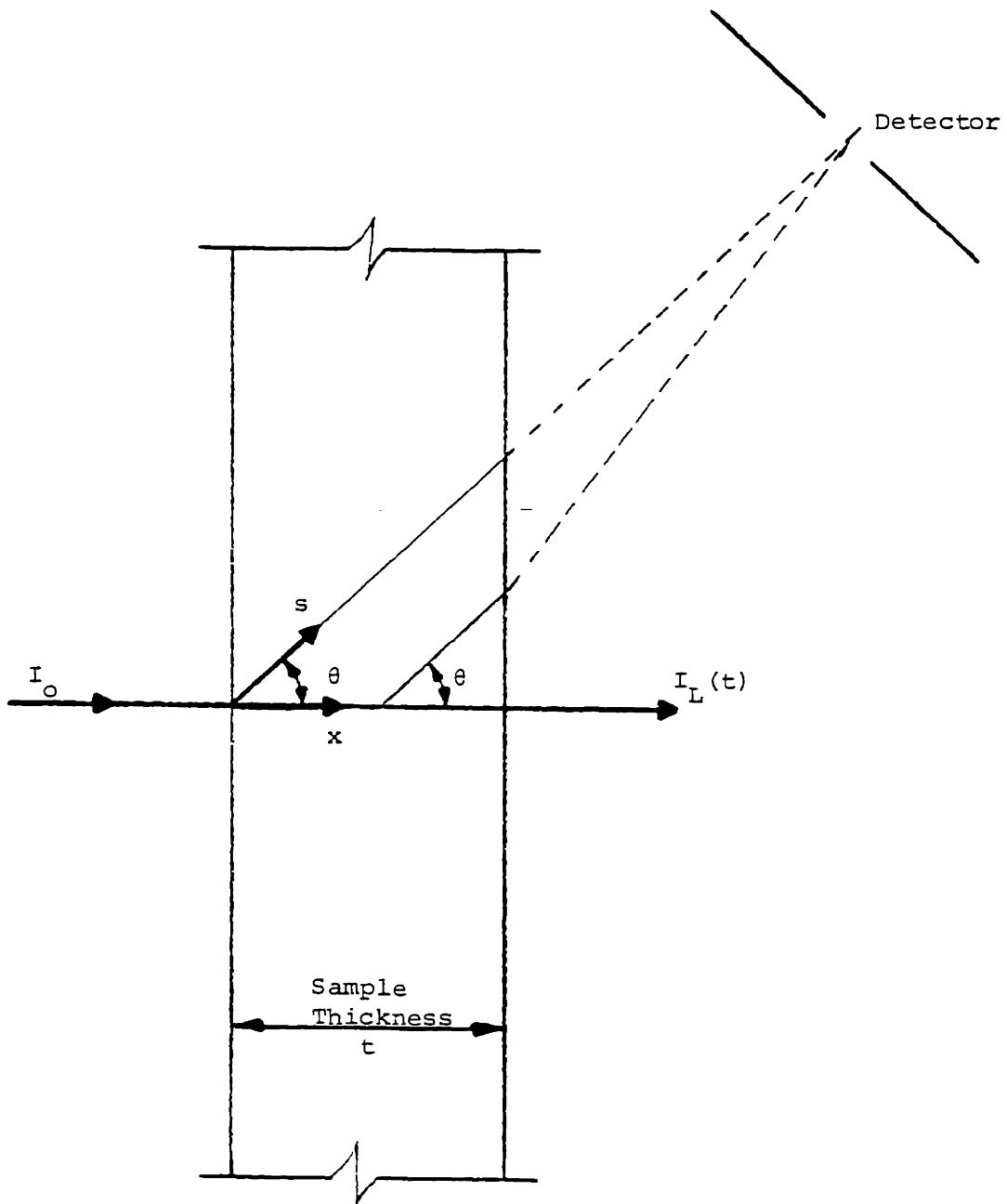
Figure 4-14 : Geometry for Scattering

The boundary condition required for this first order differential equation is just:

$$\text{at } s = 0 \quad ; \quad I(s) = 0 \tag{4-19}$$

And the solution is found to be:

$$I(s) = \frac{I_o \, \sigma_s^* \, \Phi^*(\theta) \, \Delta\omega_L}{4\pi(a + \sigma_s^*) \, (1 - \cos\theta)} \left(e^{-K^* s \cos\theta} - e^{-K^* s} \right) \tag{4-20}$$

where K^* is the modified extinction coefficient, $a + \sigma_s^*$. The solution may be verified by substituting into equation 4-18, and by checking equation 4-20 at the boundary condition. Note that there is a singularity at θ = 90 degrees where $\cos\theta$ equals zero. This came about from equation 4-17 which makes no physical sense at 90 degrees. Fortunately this does not affect the scattering test results. We may now apply equation 4-20 to our problem. At:

$$s = t / \cos\theta \tag{4-21}$$

the intensity $I(s)$ is just the intensity observed at the detector. Hence, if $I_M(\theta)$ is the measured intensity at θ, then:

$$\frac{I_M(\theta)}{I_o \Delta\omega_L} = \frac{\sigma_s^* \, \Phi^*(\theta)}{4\pi(a + \sigma_s^*) \, (1 - \cos\theta)} \left(e^{-(a + \sigma_s^*)t} - e^{-\frac{(a + \sigma_s^*)t}{\cos\theta}} \right) \tag{4-22}$$

The left hand side of equation 4-22 may be related directly to the detector output voltage and the incident laser power by equation 4-7. The right hand side is the product of the modified scattering coefficient (σ_s^*) times the modified phase function (Φ^*) times a complex function of angle (θ) and modified extinction coefficient ($a+\sigma_s^*$). Equation 4-22 is extremely convenient for data reduction. We proceed as follows. Since the modified phase function is zero from θ of zero to 10 degrees, we can integrate the energy detected in the first 10 degrees (using equation 4-2) to determine the percent transmission. Equation 4-14 yields the extinction coefficient. Given the extinction coefficient, equation 4-22 can be used to determine the value of $\sigma_s^* \Phi^*$ from the measured intensity at each θ. But σ_s^* is a constant. Therefore we may integrate the product over all solid angles and divide by 4π to obtain σ_s^*. (Recall that the integral of Φ^* over the sphere is 4π.)

$$\sigma_s^* = \frac{1}{4\pi} \int_0^\pi (\sigma_s^* \Phi^*) \cdot 2\pi \sin\theta \, d\theta \qquad (4-23)$$

Knowing σ_s^* we can determine the phase function from the product $\sigma_s^* \Phi^*$. Finally, the absorption coefficient is determined by subtracting the scattering coefficient from the extinction coefficient. Thus, the computational routine requires no iterations.

Note that equation 4-22 is only valid for $\theta_f < \theta < 90$ degrees. It is simple to repeat the analysis which led to equation 4-22 for the backscattering case. For brevity the analysis is omitted but the result is given. For $90 < \theta < 180$ degrees we find:

$$\frac{I_M(\theta)}{I_o \Delta \omega_L} = \frac{\sigma_s^* \Phi^*(\theta)}{4\pi(a + \sigma_s^*)(1 - \cos\theta)} \left(1 - e^{-(a + \sigma_s^*)t(1 - \frac{1}{\cos\theta})}\right) \tag{4-24}$$

The data reduction procedure is summarized below. The percent transmission is first determined by integrating the measured voltages over the first 10 degrees. Equation 4-2 is used to determine the transmitted power, except the limits of integration are zero and ten degrees. Equation 4-14 is used to find the modified extinction coefficient. Knowing the modified extinction coefficient, equations 4-7, 4-22, and 4-24 are used to determine the product $\sigma_s^* \Phi^*$ at each angle θ from the measured voltage at θ. Integrating this product over all solid angles and dividing by 4π provides σ_s^* (equation 4-23). The absorption coefficient is just the extinction coefficient minus σ_s^*. The phase function at θ is just the product $\sigma_s^* \Phi^*$ at θ divided by σ_s^*.

4.3.5 Experimental Results

In order to test the validity of the data analysis discussed in the previous section, the scattered energy was measured at 42 points around the circle for four different thicknesses of a single polyurethane foam. The slices were taken from a slab supplied by the Society of Plastics Industry via Dynatech R/D Co. They were cut so that the laser beam direction corresponded to the heat flow direction in the Dynatech measurement. The same slab was previously tested by Stern (37). He measured a mean extinction coefficient of 623 ft^{-1} using the simple technique of section 4.2.

The phase function, scattering coefficient and absorption coefficient is given for each of the four samples in Table 4-3, along with an average of the four results. It is clear from the data that there is no trend with sample thickness, a fact which testifies to the validity of the data analysis model of section 4.3.4. The magnitude of the scatter in the data is considerable and is probably from two sources. The first source of scatter is simply due to local variations in density, cell size, etc. which may give rise to local variation in radiation properties. The second and probably larger source is the experimental uncertainty itself, particularly in the calibration constant. Note that calibration checks were not performed on samples 1 and 4; on 1 by error of omission and on 4 because the transmitted power was too low to accurately measure on the thermopile detector. For these two samples a value of 4.8 (mW/cm^2-mV) was assumed for the calibration

Table 4-3 : Measured Radiation Properties at 9.64 microns for

Four Thicknesses of a 1.76 pcf Polyurethane Foam

sample	1	2	3	4	average
thickness (in)	0.0215	0.0265	0.0403	0.083	---
absorption coefficient (ft^{-1})	389.	461.	492.	368.	427.
scattering coefficient (ft^{-1})	148.	191.	156.	208.	175.
angle	phase	phase	phase	phase	phase
0 - 9.5	0	0	0	0	0
9.5 - 10.5	31.09	28.24	24.03	37.41	29.95
10.5 - 13.75	15.99	21.22	13.43	21.17	17.81
13.75 - 16.25	10.90	12.67	7.34	11.52	10.52
16.25 - 18.75	10.07	8.08	7.72	10.79	10.32
18.75 - 21.25	5.07	4.05	4.81	7.02	5.20
21.25 - 23.75	3.08	3.65	3.40	5.71	3.93
23.75 - 27.5	3.63	2.39	2.28	4.35	3.14
27.5 - 32.5	1.46	2.45	1.43	2.29	1.89
32.5 - 37.5	1.13	1.16	1.35	1.50	1.28
37.5 - 42.5	1.72	0.89	0.98	1.34	1.22
42.5 - 47.5	1.26	0.79	0.70	1.26	1.00
47.5 - 52.5	1.23	0.51	0.83	0.85	0.85
52.5 - 57.5	0.80	0.47	0.76	0.49	0.62
57.5 - 62.5	0.54	0.41	0.58	0.38	0.47
62.5 - 67.5	0.45	0.30	0.37	0.43	0.38
67.5 - 72.5	0.41	0.29	0.41	0.25	0.34
72.5 - 107.5	0.38	0.37	0.41	0.27	0.36
107.5 - 112.5	0.36	0.45	0.41	0.30	0.38
112.5 - 117.5	0.46	0.67	0.97	0.25	0.58
117.5 - 122.5	0.46	0.55	0.52	0.38	0.47
122.5 - 127.5	0.63	0.58	0.63	0.53	0.59
127.5 - 132.5	0.56	1.27	0.54	0.46	0.70
132.5 - 137.5	0.57	1.26	1.09	0.57	0.87
137.5 - 142.5	0.84	0.80	1.24	0.59	0.86
142.5 - 147.5	0.94	0.59	1.76	0.59	0.96
147.5 - 152.5	0.95	0.79	1.79	0.77	1.07
152.5 - 157.5	1.26	1.09	1.31	1.14	1.19
157.5 - 180.0	0.72	1.36	1.51	0.76	1.08
asymmetry factor $\langle \cos \theta \rangle$	0.3877	0.3094	0.1850	0.4991	0.3501

constant (C_c), based on an average of several other calibrations. This could easily be in error by 20%, based on the data in Table 4-2. Note also that due to difficulties with optical alignment it was not possible to perform a detector calibration check during the backscatter measurements. Again a value of 4.8 was assumed for C_c.

A similar set of results is presented in Table 4-4 for two glass fiber insulation samples supplied by Dr. Koram of the Owens Corning Fiberglas Co. (33). For sample number 2 the transmission was too small to permit accurate measurement on the thermopile detector. Hence, a calibration constant of 4.8 was assumed for this case, as for the two foam samples without direct calibration checks.

Comparison to Simple Test Results

In order to quantify the error in the simple test procedure described in section 4.2, one must know exactly what is being measured via the simple procedure. From the beam and sample geometry in the Perkin-Elmer 283B, it is not clear exactly how close to zero degrees energy must be scattered in order to be included as transmission. We can answer this question by comparing the transmission value as measured on the Perkin-Elmer 283B to the forward scattering data. The measured voltages were integrated from zero degrees to a collection angle (θ_c) for four different samples. The total transmitted plus forward scattered energy from 0 to θ_c equals the measured value from the Perkin-Elmer 283B. These particular cases were chosen because a calibration check was performed for the test detector against the

Table 4-4 : Measured Radiation Properties at 9.64 microns

for Two Thicknesses of a 0.63 pcf Glass Fiber Insulation

Sample	1	2	Averaged
Thickness (in)	0.1258	0.1544	----
Absorption Coefficient (ft^{-1})	105	90	98
Scattering Coefficient (ft^{-1})	93	120	106
Angle	Phase	Phase	Phase
0 - 9.5	0	0	0
9.5 - 10.5	24.33	21.82	23.07
10.5 - 13.75	18.57	17.66	18.11
13.75 - 16.25	16.55	7.98	12.27
16.25 - 18.75	6.73	9.23	7.98
18.75 - 21.25	10.66	9.28	9.97
21.25 - 23.75	7.48	6.23	6.85
23.75 - 27.5	4.64	5.71	5.18
27.5 - 32.5	2.93	3.33	3.13
32.5 - 37.5	2.48	3.96	3.22
37.5 - 42.5	1.49	2.20	1.84
42.5 - 47.5	1.15	1.52	1.33
47.5 - 52.5	0.85	0.61	0.73
52.5 - 57.5	0.75	0.82	0.78
57.5 - 62.5	0.53	0.63	0.58
62.5 - 67.5	0.32	0.59	0.46
67.5 - 72.5	0.36	0.33	0.34
72.5 - 107.5	0.25	0.20	0.23
107.5 - 112.5	0.14	0.08	0.11
112.5 - 117.5	0.22	0.14	0.18
117.5 - 122.5	0.18	0.22	0.20
122.5 - 127.5	0.29	0.22	0.25
127.5 - 132.5	0.38	0.31	0.34
132.5 - 137.5	0.41	0.37	0.39
137.5 - 142.5	0.48	0.36	0.42
142.5 - 147.5	0.55	0.47	0.51
147.5 - 152.5	0.53	0.53	0.53
152.5 - 157.5	0.56	0.48	0.52
157.5 - 180.0	0.56	0.37	0.47
Asymmetry Factor $<\cos \theta>$	0.5920	0.6267	0.6094

thermopile detector in all four cases. The results are given in Table 4-5. From the table it appears that the Perkin-Elmer 283B cannot distinguish between transmission and forward scattering out to approximately 5 degrees. In fact, the collection angle may be less than 5 degrees. Recall that a small amount of incident energy would be detected beyond 5 degrees with no sample. Hence some of the energy beyond 5 degrees with a sample is actually transmitted energy.

As another check between the two techniques, the same samples used in the scattering test (plus one more from the same foam slab) were tested in the Perkin-Elmer 283B for transmission at 9.64^{μ} wavelength. The results are plotted in Figure 4-15. The spectral extinction coefficient computed via this simple technique is found to be 638 ft^{-1} (20.9 cm^{-1}), from Figure 4-15. Using the asymmetry factor for the averaged phase function from Table 4-3, the scattering coefficient (determined by the scattering experiment) was modified according to equation 3-13 and found to be 114 ft^{-1} (3.74 cm^{-1}). Since the absorption coefficient was 427 ft^{-1} (14.0 cm^{-1}), the modified spectral extinction coefficient at 9.64 microns was found to be 541 ft^{-1} (17.8 cm^{-1}), as compared to 638 ft^{-1} determined by the simple technique, as noted above. Thus, the simple technique for extinction coefficient determination is found to overestimate the appropriate extinction coefficient at 9.64 microns by approximately 18%. In other words, the appropriate extinction coefficient is 15% below the approximate method value. However, this may be somewhat misleading because we are not taking into consideration the uncertainty in the scattering experiment

Table 4-5 : Comparison of Perkin-Elmer 283B Transmission

to Scattering Experiment Test Results

Sample	Transmission from Perkin-Elmer 283B	Collection Angle (θ_c) Which Causes Scattering Data to Agree with Perkin-Elmer 283B Result
polyurethane	23.	3.3
polyurethane	10.9	8.1
polyisocyanurate	25.6	7.8
glass fibers	5.7	1.0

Average : 5.0

Figure 4-15 : Scattering Test Samples -
Transmission at 9.64 microns versus
Thickness - from Spectrometer
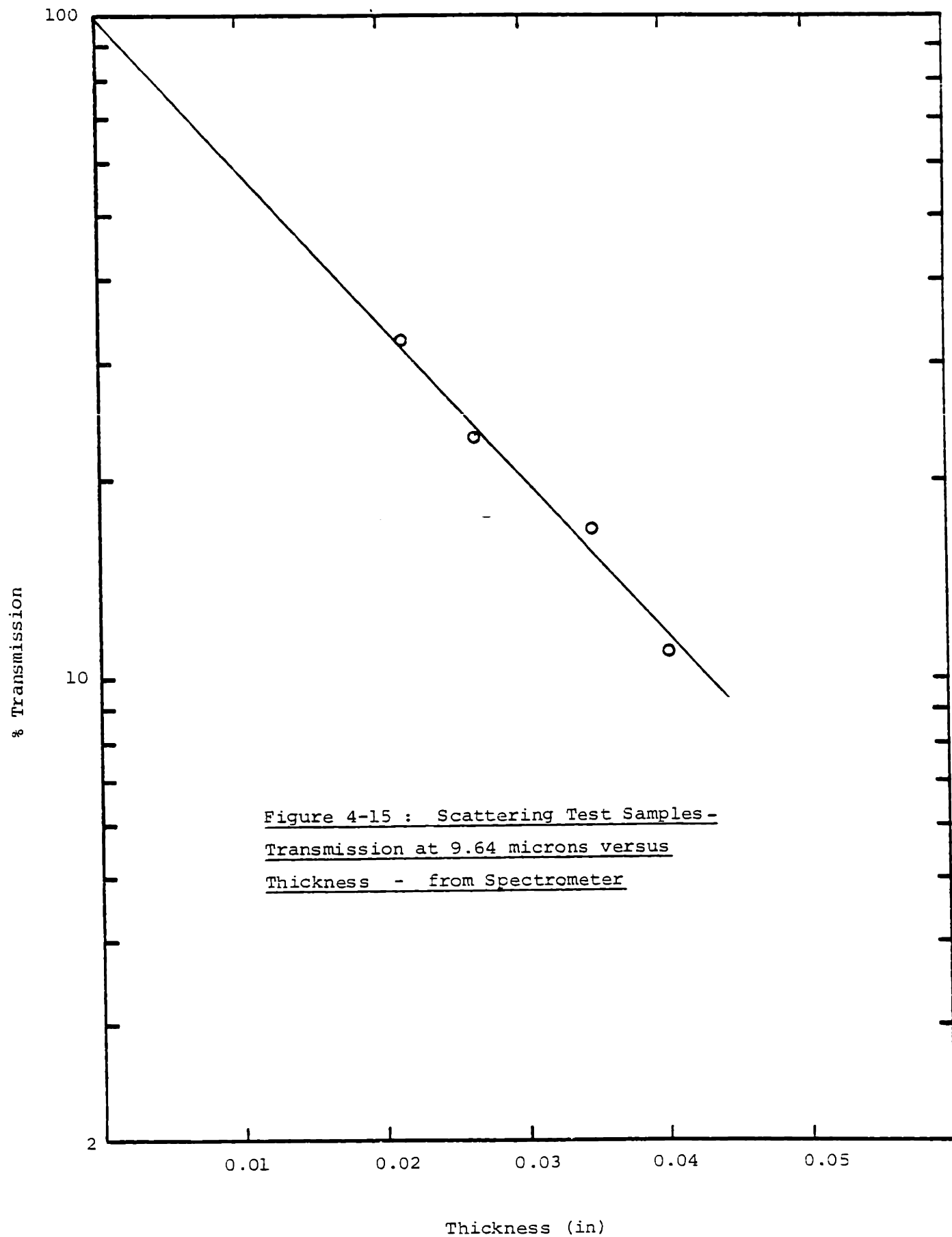
measurement. This will be discussed further in the next section.

Results for Other Foams

The forward scattering was measured for several other foam samples. Because of the lack of backscattering data it is not possible to compute the phase function, scattering and absorption coefficient for these foams. Considering the sample to sample variation in Table 4-3, it is not clear that tests from one sample alone would be sufficient to determine these parameters. Some of the raw data for various foams is presented in Appendix A, where the measured voltages have all been normalized to a consistent incident power level and may thus be directly compared to the same data for the foam whose radiation properties are given in Table 4-3. Qualitative similarities in the forward scattering behavior are apparent.

Scattering By Films

In an attempt to understand the scattering phenomenon on a more basic level, a thin film of polyurethane obtained from a "free rise bun" was tested for forward scattering. While it is difficult to describe the results in a quantitative way, it was qualitatively found that the membranes do not cause significant scatter. The measured voltages at each angle are presented in Table 4-6 for the laser with no sample and for the free rise bun film. The voltages have been normalized to a consistent laser power of 74.51 mW and a detector calibration constant of 4.81 mW/ cm^2 - mV. At angles less than 8 degrees with the sample in

Table 4-6 : Scatter Data for Thin Film of Polyurethane

Angle (deg)	Measured Output Voltages (mV)		
	No sample	Thin Film	Ratio
0	229	99	2.31
0.5	235	106	2.22
1	186	85.6	2.17
1.5	83.8	42.0	2.00
2	12.9	6.75	1.91
2.5	1.53	0.778	1.97
3	1.52	0.634	2.40
3.5	0.434	0.149	2.91
4	0.114	0.0643	1.77
4.5	0.080	0.0407	1.97
5	0.0308	0.0203	1.52
6	0.0576	0.0077	7.48
7	0.0322	0.0047	6.85
8	0.0069	0.0035	1.97
9	0.0019	0.0022	0.86
10	0.0011	0.0026	0.38
12.5	0.0005	0.0014	0.36
15	0	0.0010	0
17.5	0	0.0008	0
20	0	0.0005	0
22.5	0	0.00035	0
25	0	0.0002	0
30	0	0.0002	0
35	0	0.0002	0
40	0	0.0001	0
45	0	0.0002	0
50	0	0.0001	0
55	0	0.0001	0
60	0	0.0001	0
65	0	0	0

detector radius   =   5.8 cm
laser power   =   74.5 mW
calibration constant =   4.81 mW/cm^2 - mV

place, the voltage is approximately one half the corresponding value when the sample is removed. At angles greater than 8 degrees the incident power is zero. Some scattering due to the film becomes apparent. If the scattered energy from angles of 9.5 to 90 degrees are integrated (equation 4-2), the total forward scattered energy is found to be 0.25 mW. This is just 0.3% of the incident power level. For comparison, a foam sample approximately 1.5 bubble diameters thick (sample 1 in Table 4-3) scatters approximately 20% of the incident energy over these same angles.

The data of Table 4-6 is for the sample mounted normal to the beam. In order to determine whether sample angles other than normal to the beam would behave differently, the sample was angled at 90, 75, 60 and 45 degrees to the incident beam. The detector voltage was checked at detector angles of 0, 1.5, 3, and 5 degrees. The measured values all agreed to within the measurement uncertainty regardless of sample orientation.

4.3.6 Application to Radiation Theory

In order to use these results to check the approximate radiation models, arrangements were made with Dr. Koram (33) of the Owens Corning Fiberglas Co. to run his finite difference program which solves the exact equations, described in section 3.2. The experimentally determined phase function, absorption coefficient and scattering coefficient were used in the program, assuming that the medium is gray. This allowed us to compare the exact results to those calculated via the simpler methods of section 3.3.

The phase function had to be expressed as the sum of a series of Legendre polynomials in order to perform the exact computation. In order to facilitate the Legendre polynomial expansion, the phase functions of Tables 4-3 and 4-4 were modified so as to eliminate the sudden drop to zero at 10 degrees. This is easily accomplished by reversing the modification process depicted in Figure 4-13 and discussed in depth by Houston (14). For our purposes the phase functions were assumed to have a constant value from zero to 16.25 degrees, where this constant value is determined by the value of the unmodified phase functions at 15 degrees (from Tables 4-3 and 4-4). The new phase function is integrated over the sphere and divided by 4π to define a normalization factor (F_n), as given by equation 4-25.

$$F_n = \frac{2\pi \int_0^\pi \Phi^*(\theta) \sin\theta \, d\theta}{4\pi} \tag{4-25}$$

A new modified phase function is defined by equation 4-26:

$$\Phi_{mod}(\theta) \equiv \frac{\Phi^*(\theta)}{F_n} \qquad (4\text{-}26)$$

and a new scattering coefficient is defined by equation 4-27:

$$\sigma_{s\ mod} = \sigma_s^* F_n \qquad (4\text{-}27)$$

Hence the product $\sigma_{smod}\Phi_{mod}$ is equal to the product $\sigma_s^*\Phi^*$ for all angles greater than 15 degrees. The physics are therefore unchanged. At angles under 15 degrees, energy which had previously been considered transmitted would now be considered scattered at a small angle. As noted in section 4.3.4, (and documented by Houston), this type of modification will have a negligible effect of the calculated heat flux.

The new modified phase function may be accurately expressed by a 20 term Legendre polynomial expansion. Dr. Koram supplied the author with the coefficients required for the expansion, where the expansion is given by equation 4-28:

$$\Phi_{mod} = \sum_{n=0}^{19} A_n P_n(\mu) \qquad (4\text{-}28)$$

where:

A_n = coefficients

P_n = nth Legendre Polynomial of μ

μ = cos θ

The coefficients and the values of the phase function calculated using those coefficients in equation 4-28 are given in Tables 4-7 and 4-8 respectively, for both the foam and glass fiber data. The asymmetry factors given on the bottom of Table 4-8 were calculated by breaking the sphere into increments of 5 degrees and using the values in Table 4-8 as an average over each increment, thus evaluating the integral of equation 3-12.

The results of the exact calculations were compared to the results using the P-1 approximation in the three zone model. This comparison is presented in Table 4-9. As can be seen in the table, the P-1 approximation agrees closely with the exact results, so closely in fact that we could in the future use the P-1 approximation as an "exact" model.

Comparison to Isotropic Scattering Model

We would also like to draw some conclusions regarding the accuracy of the simple technique for the extinction coefficient measurement described in section 4.2. So far we have shown that the three zone model is essentially exact for sufficiently optically thick media if the extinction coefficient is determined via the P-1 approximation. If the

Table 4-7 : Coefficients Used in Legendre Polynomial

Expansion of Modified Phase Function

n	An	
	Foam	Glass Fibers
0	0.999983	1.0002
1	1.05164	1.8908
2	2.18705	2.6316
3	1.86944	2.3493
4	1.85876	2.0354
5	1.71955	1.5964
6	1.33609	1.02168
7	1.15337	0.75243
8	0.776737	0.386027
9	0.415310	0.061876
10	-0.0316162	-0.051829
11	-0.364278	-0.132697
12	-0.553221	-0.27966
13	-0.643506	-0.453012
14	-0.673393	-0.504900
15	-0.646322	-0.533731
16	-0.478317	-0.411578
17	-0.496727	-0.178707
18	-0.288212	0.0023427
19	-0.106336	0.137843

Table 4-8 : Modified Phase Functions Used in Exact Solution

Angle	Phase	
	Foam	Glass Fibers
0	9.09	11.32
5	10.10	11.70
10	11.33	12.02
15	10.04	10.88
20	6.44	8.15
25	3.15	5.23
30	1.71	3.44
35	1.43	2.70
40	1.23	2.07
45	0.97	1.28
50	0.82	0.77
55	0.68	0.69
60	0.47	0.67
65	0.35	0.47
70	0.36	0.29
75	0.37	0.26
80	0.34	0.25
85	0.35	0.20
90	0.38	0.21
95	0.36	0.25
100	0.33	0.24
105	0.36	0.17
110	0.44	0.15
115	0.49	0.16
120	0.52	0.17
125	0.59	0.22
130	0.71	0.31
135	0.83	0.36
140	0.90	0.38
145	0.97	0.44
150	1.06	0.50
155	1.15	0.46
160	1.14	0.41
165	1.06	0.43
170	1.04	0.46
175	1.12	0.40
180	1.18	0.34

| $<\cos\theta>$ Asymmetry Factor | 0.35140 | 0.63122 |

Table 4-9 : Comparison of Exact

Computations to the P-1 Approximation

Conditions: k_{s+g} = 0.186 Btu-in/hr-ft^2-F

                     T_1 = 555.9 °R

                     T_2 = 513.4 °R

                     ε_1 = 0.86

                     ε_2 = 0.86

                     L   = 1.5 inch

	Foam	Glass Fibers
Absorption Coefficient (ft^{-1})	427.44	87.72
Scattering Coefficient (ft^{-1})	175.44	134.16
Heat Flux – Exact (Btu/hr-ft^2)	6.15	8.55
Heat Flux – P-1 Approximation and 3 Zone Model	6.14	8.54

extinction coefficient is determined via the simple experimental technique of section 4.2, we wish to know the error.

The absorption coefficient, scattering coefficient, and phase function were measured and reported in section 4.3.5. The P-1 approximation was applied to the results, and an appropriate extinction coefficient of 541 ft^{-1} (17.8 cm^{-1}) was calculated. At the same wavelength, the extinction coefficient was measured using the simple technique and found to be 638 ft^{-1} (20.9 cm^{-1}). This is 18% higher than the appropriate value for exact heat flow calculations. However this is a direct comparison of the two experimental techniques and thus, all of the uncertainty should not be assigned to only one or the other technique.

A better way to estimate the error in the simple technique would be to compare the calculated result via the P-1 approximation against what would hypothetically by measured via the Perkin-Elmer 283B if all the energy scattered within the first 5 degrees is considered transmitted. Using the modified phase functions in Table 4-8 one may calculate that 1.9% and 2.2% of the total scattered energy is within the first 5 degrees for foam and glass fibers respectively. Using the absorption and scattering coefficients of Table 4-9 one may show that the simple technique would yield extinction coefficients of 599 ft^{-1} and 219 ft^{-1} for foam and glass fibers respectively. The appropriate extinction coefficient using the data in Tables 4-9 and 4-8 are 541 ft^{-1} and 137 ft^{-1} for foam and glass fibers, respectively. Comparing 541 to 599, and

137 to 219, the simple technique overestimates the appropriate extinction coefficient by only 10.7% for foams while for glass fibers the error is 60%. This corresponds to an underestimate of the radiation contribution (equation 3-22) for foams of 9.7% while for glass fibers the underestimate is 37.4%. Hence, one may conclude that the simple technique will be quite useful in foams but will probably not be extremely useful for glass fibers unless the accuracy can be improved.

Improvement of Simple Technique

The previous computational exercise suggests a possible improvement in the simple technique. If the detector optics of the Perkin-Elmer 283B could be changed to include a greater percentage of the forward scattered energy as transmission, then the technique would be even more accurate than the figures previously quoted. This improvement may even allow the technique to be used for measurement of extinction coefficients in glass fiber insulation.

Consider an infinitesimal thickness of insulation with an incident beam of intensity I_0 striking the insulation. The fraction of energy absorbed will be aI_0, the fraction scattered will be $\sigma_s I_0$ and the fraction transmitted will be $(1 - a - \sigma_s)I_0$. Consider first the case where the phase function is of the form of Φ in Figure 4-13, and the asymmetry factor is $<\cos \theta>$. The appropriate scattering coefficient for heat transfer purposes is $\sigma_s (1 - <\cos \theta>)$. If a spectrometer measured only the energy strictly transmitted, then the "error" in the extinction

coefficient measurement would be given by equation 4-29:

$$\% \text{ error } = \frac{a + \sigma_s - [a + \sigma_s (1 - <\cos \theta>)]}{a + \sigma_s (1 - <\cos \theta>)} \cdot 100 \qquad (4-29)$$

which may be simplified to:

$$\% \text{ error } = \frac{\sigma_s <\cos \theta>}{a + \sigma_s (1 - <\cos \theta>)} \cdot 100 \qquad (4-30)$$

If instead of only detecting transmitted energy, the optics were arranged so that the detector measured the transmitted energy plus all scattered enery between zero degrees and a collection angle of θ_c, then the calculated scattering coefficient would be decreased. The decrease in the calculated scattering coefficient will correspond directly to the fraction of the total scattered energy which is scattered at angles less than θ_c. Hence the "improved" scattering coefficient (σ_s') would be:

$$\sigma_s' = \sigma_s \left(1 - \frac{1}{2} \int_0^{\theta_c} \Phi(\theta) \sin \theta \, d\theta \right) \qquad (4-31)$$

The error in the improved extinction coefficient measurement technique would be:

$$\% \text{ error } = \frac{\sigma_s \left[(1 - \frac{1}{2} \int_0^{\theta_c} \phi \sin \theta \, d\theta) - (1 - <\cos \theta>) \right]}{a - \sigma_s (1 - <\cos \theta>)}$$ (4-32)

And the error goes to zero when:

$$<\cos \theta> - \frac{1}{2} \int_0^{\theta_c} \phi \sin \theta \, d\theta \rightarrow 0$$ (4-33)

Now that we have both experimental and theoretical estimates of the phase function, it is possible to determine the collection angle which would give zero error in extinction coefficient measurement.

For the experimentally determined foam phase function (given in modified form in Table 4-8), the collection angle θ_c for zero error is 23.74 degrees. For the measured glass fiber phase function (given modified in Table 4-8), the zero error collection angle is 38.11 degrees. The value in this approach is that the error introduced is not large, even at large deviations from the zero error collection angle.

For the foam data of Tables 4-8 and 4-9, the error is +7.2% and -3.8% at collection angles of 7.5 degrees and 37.5 degrees respectively. For the glass fibers data of Tables 4-8 and 4-9, the error in the measured extinction coefficient would be +24% and -8.9% at collection angles of 22.5 degrees and 47.5 degrees, respectively.

What is more, as the phase function changes the optimum collection angle changes only slowly. This is evident when one considers the three phase functions presented by Houston (14). The phase functions are said to be representative of the phase function for glass fibers in the near, mid and far infrared. The asymmetry factors may be found to be 0.8242, 0.7323 and 0.4166, respectively. The optimum collection angles may be found from equation 4-33 to be 42.17, 38.27, and 37.83 degrees respectively. In all cases if the collection angle is set at 40 degrees, the error is less than 2.2% if the values of 134.16 and 87.72 ft^{-1} are used for the scattering and absorption coefficients, respectively.

Hence one may conclude from this argument that if the collection angle was set at 24 degrees for foamed materials and 40 degrees for fibrous materials, the measured extinction coefficient would be within approximately 5% for the complete spectrum.

However, this analysis is only strictly valid for an infinitesimal sample thickness. For finite sample thickness, energy which is scattered must pass through a portion of the sample before reaching the detector. The scattered energy would of course be attenuated along the way. Hence the simple analysis would tend to underestimate the optimum collection angle. Furthermore, if collection angles of 24 and 40 degrees were used for foams and glass fiber insulations, respectively, the error might be more than 5% due to the attenuation of scattered energy. Therefore a more accurate analysis is required.

The analysis described earlier for data reduction (see section 4.3.4) is suitable for this problem. In order to determine the optimum collection angle one would have to integrate equation 4-22 and determine the limit of integration which would cause equation 4-14 to predict the correct extinction coefficient. This exercise has not yet been performed.

—

5. OVERALL HEAT TRANSFER MODEL

While the information for the combined conduction-radiation model has all been presented in Chapters 2 and 3, it was felt that a short summary which repeats the conclusions would be useful for most readers. This chapter does that, reiterating the assumptions, approximations and error estimates which go along with the model. We also present some thermal conductivity data for comparison to the model's predictions.

5.1 Model

The following model is proposed for heat transfer through planar foam insulation bounded by gray isothermal walls, where the gas composition is constant throughout the foam. The effects of variable gas conductivity are discussed in the next chapter, Aging Model.

The first step is to compute the effective conductivity of the medium in the absence of radiation. Equation 5-1 is used when 100% of the solid is in the form of membranes.

$$k_{s+g_1} = k_g + \frac{2}{3}(1 - \delta) k_s \qquad (5-1)$$

Equation 5-2 is used when 100% of the solid is in the form of struts.

$$k_{s+g_2} = k_g + \frac{1}{3}(1 - \delta) k_s \qquad (5-2)$$

In real foams there is some material in struts and some in membranes. The distribution must be experimentally determined. If P_S is the percentage of solid material in struts, and $100 - P_S$ is the percentage of solid in membranes, then the effective conductivity of the medium is given by:

$$k_{s+g} = \frac{(100 - P_s)\, k_{s+g_1} + P_s\, k_{s+g_2}}{100} \qquad (5-3)$$

which after some algebra reduces to:

$$k_{s+g} = k_g + \left(\frac{2}{3} - \frac{P_s}{300}\right)(1 - \delta)\, k_s \qquad (5-4)$$

Equation 5-4 represents an <u>upper limit</u> to conduction. The actual conduction will be less than that predicted by equation 5-4. The difference between the actual and the predicted conductivities will be less than 20% of the second term on the right hand side of equation 5-4, i.e., the <u>lower limit</u> is given by:

$$k_{s+g \atop LL} = k_g + 0.8\left(\frac{2}{3} - \frac{P_s}{300}\right)(1 - \delta)\, k_s \qquad (5-5)$$

While the actual conductivity could be as low as that given by equation 5-5, it is believed that the actual value will be closer to that of equation 5-4 than that of equation 5-5. Hence, equation 5-4 is recommended for predictive purposes. In the absence of experimental data on P_s for a particular foam, a value of 75% is recommended. Recall from chapter 2 that Reitz's preliminary measurements indicate 85% of the solid in struts. We will see later in this chapter that a value of 75% tends to help correlate the data better than do lower values.

In order to predict the radiation heat transfer, the extinction coefficient must be experimentally determined. A simple method is described in section 4.2. A more accurate but also more complex technique is described in section 4.3. If the sample thickness times the extinction coefficient (dimensionless optical thickness) is greater than 100, equation 5-6 may be used with good accuracy.

$$k_f \simeq k_{s+g} + \frac{16 \, \sigma \, T_m^3}{3K} \tag{5-6}$$

The second term on the right hand side may be called the "radiation conductivity" (k_r). At lower optical thickness (30), the error in equation 5-6 will be aproximately 7% of the radiation conductivity for typical values of material properties found in foam insulations.

If the optical thickness is less than 100, it therefore becomes necessary to solve the following three simultaneous algebraic equations for T_a, T_b and q:

$$q = k_{s+g} \left(\frac{T_1 - T_a}{L_a} \right) + \varepsilon_1 \sigma (T_1^4 - T_a^4) \tag{5-7}$$

$$q = k_{s+g} \left(\frac{T_a - T_b}{L_c} \right) + \frac{4\sigma}{3KL_c} (T_a^4 - T_b^4) \tag{5-8}$$

$$q = k_{s+g} \left(\frac{T_b - T_2}{L_b} \right) + \varepsilon_2 \sigma (T_b^4 - T_2^4) \tag{5-9}$$

where the nomenclature was previously defined in Figure 3-1. Using q, calculated from the solution to these equations, the foam conductivity is given by:

$$k_f = \frac{q(L_a + L_b + L_c)}{T_1 - T_2} \tag{5-10}$$

Using this calculated foam conductivity one may calculate the "radiation conductivity" (k_r) from equation 5-11:

$$k_r \equiv k_f - k_{s+g} \tag{5-11}$$

The error in this radiation model is less than 1% for optical thicknesses greater than 15, for typical insulation properties. If the simple technique of section 4.2 is used to determine the extinction coefficient, the total radiation induced error in equation 5-10 will be approximately 10% of the radiation conductivity or approximately 2.5% of the overall conductivity for low density foams. This simple technique always underestimates the actual radiation heat transfer because it always overestimates the extinction coefficient. For higher density foams, i.e. for foams with high extinction coefficients ($K > 1000$ ft^{-1}) the radiation induced error will be considerably less than 2.5% overall.

Summary of Uncertainties in the Model

For purposes of summary we group the uncertainties into the following two categories: uncertainties due to approximations in the model, and uncertainties in experimental determination of properties of materials. Both uncertainties affect the overall model predictions.

In the first category we have two uncertainties. The first is the spread between the upper and lower limits to solid conduction. As noted in equations 5-4 and 5-5, the uncertain range of possible results is 20% of the solid contribution. The second uncertainty lies in the prediction of the radiation heat flux. For optical thicknesses greater than 15, the theoretical maximum uncertainty is approximately 6.5% (3% in P-1 approximation, 3.5% due to neglecting effect of albedo). In

practice the error between the approximate solution and the exact solution is less than 1% for typical values of material properties.

The heat transfer model requires experimental knowledge of the following material properties: δ, k_s, k_g, P_s, ϵ_1, ϵ_2, K. It is easy to determine the effect on the overall conductivity due to uncertainty in any of these properties. The extreme values of the property in question are used in equations 5-4 through 5-10 to determine the range of possible values for overall conductivity. Three of these properties deserve note. The solid polymer conductivity (k_s) appears to vary by approximately a factor of two from foam to foam. The extinction coefficient may be determined within approximately 11% via the simple technique of section 4.2. The percentage of solid in struts is currently unknown. Reitz (38) is developing an accurate technique for measurement of this property. A value of 75% is tentatively suggested.

5.2 Comparison of Model to Data

The comparison of this model to measurements of thermal conductivity of real foams is hindered by three factors. First, all the available data is for foams where some air is introduced into the foam during mixing of the polyol and isocyanate. Without a gas chromatagraph measurement of actual cell gas composition, there is no way to accurately predict the conductivity of the cell gas. Second, the technique for accurate determination of the percentage of solid in struts versus membranes is still under development by Mr. Reitz at MIT at the time of this writing. Thus, no measurements of this parameter

were performed on the foam samples tested. Finally, the thermal conductivity of the pure polymer is highly uncertain. If a middle value is chosen from the available data for polyurethane, the uncertainty is 35%.

In an attempt to overcome these difficulties, a series of foams with identical chemistry but varying density were prepared by Dr. Brotzman of the Owens Corning Fiberglas Corporation. The density was changed by simply adding more or less blowing agent to the mix. The hope was that if all three of these problem areas remained constant, then we should be able to use the model to predict the trend in overall conductivity. The foam density, measured conductivity (for one inch thick samples), measured extinction coefficient, and calculated conductivity are presented in Table 5-1 for each of the five samples. As seen in the table, the difference between the highest and lowest conductivity foam is only 6%, a small difference considering the three uncertainties noted earlier. While it is possible to juggle the various constants in any number of ways within the realm of possible values so that the calculated value fits the measured value within the 3% uncertainty band, it is not possible to obtain the sudden drop and rise on each side of the 1.98 pcf sample while predicting reasonable values for the higher densities.

One should note that the measured overall conductivity changes by only 2% from the lowest density to the highest density material. The radiation term decreases by 42% while the conduction term increases by

Table 5-1 : Comparison of Theory to Data

ρ_f* (Measured) (pcf)	K (Measured) (ft^{-1})	k_f** (Measured)	k_f*** (Calculated)	k_r (Calculated)	k_{s+g} (Calculated)
1.85	432.	0.145	0.1434	0.0379	0.1055
1.98	449.	0.141	0.1435	0.0365	0.1070
2.31	479.	0.149	0.1451	0.0343	0.1108
2.84	629.	0.148	0.1431	0.0263	0.1168
3.45	754.	0.146	0.1458	0.0220	0.1238

Units for thermal conductivity : Btu -in / hr-ft²-F

* Average of 4 samples

** Average of 4 samples, mean temperature 75°F, 3% uncertainty, measured one day after foaming

*** Assumptions

k_g = 0.088 Btu-in / hr-ft²-F

k_s = 2.1 Btu-in / hr-ft²-F

P_s = 75% in struts

10%. In order to match both the magnitude and the change in conduction with density, it was necessary to assume a high value for the gas conductivity (implying that air is mixed in during foaming). If the conductivity of pure R-11 were assumed (0.059), then the solid conduction would have to assume a higher polymer conductivity or lower percentage in struts in order to bring the total back up to the measured value. Either of these changes would lead to a much stronger change in conduction with density, causing the predicted overall conductivity to vary more strongly with density than the measured overall conductivity.

The author recommends that the test be repeated in approximately six months time. This will allow time for Reitz to complete development of his technique for accurate determination of the percentage of solid in struts. This should also allow sufficient time for Sinofsky (16) to complete development of a technique for measurement of solid polymer conductivity in foams. At the time of the thermal conductivity measurement, the cell gas composition should be determined by gas chromatography. The extinction coefficient should be measured by the simple technique of section 4-2. The foam will thus be fully characterized and the accuracy of the theory may be experimentally determined.

Some extinction coefficients were measured and reported by Stern (37). He also used the simple technique for extinction coefficient measurement. The thermal conductivity of the test foams was measured on samples as old as three weeks at the time of measurement. The reported

conductivity therefore represents a value with considerable aging already taken place. Nonetheless, as may be seen in Table 5-2, the conductivities are substantially lower than those noted in Table 5-1 while the extinction coefficients are generally much higher for equal density. However, the difference in conductivity between the foams in Table 5-1 from those in Table 5-2 may not be explained by the difference in extinction coefficients alone, but rather, other factors are also at work.

One encouraging aspect of the foam data in Table 5-1 is that the measured extinction coefficient ⁻follows the density very closely. Figure 5-1 through 5-5 present the plots of percent transmission versus sample thickness which were used to obtain the extinction coefficients. Figure 5-6 gives a typical spectrograph of a foam slice. Due to the small variation in transmission versus wavelength, it was felt that the more accurate technique for obtaining the true Rosseland mean extinction coefficient described in section 3.3.2 was unnecessary. It was quicker to use the mean transmission from 5 to 25 microns wavelength and assume that the medium is gray. The error is not significant due to the nearly gray behavior of the foam. Figure 5-7 presents the measured extinction coefficient plotted against density. Since the extinction is absorption dominated, it is not surprising that the plot for constant foam chemistry varies linearly with density.

Table 5-2 : Data of Stern (37)

Material	Density (pcf)	K (Measured) (ft^{-1})	k_f (Measured)	k_r* (Calculated)	$k_{s+g} = k_f - k_r$ (Calculated)
polyurethane	1.77	623.	0.124	0.027	0.097
polyisocyanurate	1.89	658.	0.127	0.026	0.101
polyurethane	2.68	1294.	– 0.105	0.013	0.092

Thermal conductivity units: Btu-in / hr-ft^2-F

$$* \ k_r \ \simeq \ \frac{16 \ \sigma T_m^{\ 3}}{3K} \qquad ; \qquad T_m \ = \ 535 \ R$$

Figure 5-1 : Transmission Versus
Thickness for 1.85 pcf
Polyurethane Foam

Thickness (in)

Figure 5-2 : Transmission Versus Thickness for 1.98 pcf Polyurethane Foam

Figure 5-3 : Transmission Versus
Thickness for 2.31 pcf
Polyurethane Foam

Figure 5-4 : Transmission Versus
Thickness for 2.84 pcf
Polyurethane Foam

Figure 5-5 : Transmission Versus Thickness for 3.45 pcf Polyurethane Foam

Figure 5-6 : Typical Spectrograph of Polyurethane Foam Slice

Sample Thickness = 0.031 in
(0.79 mm)
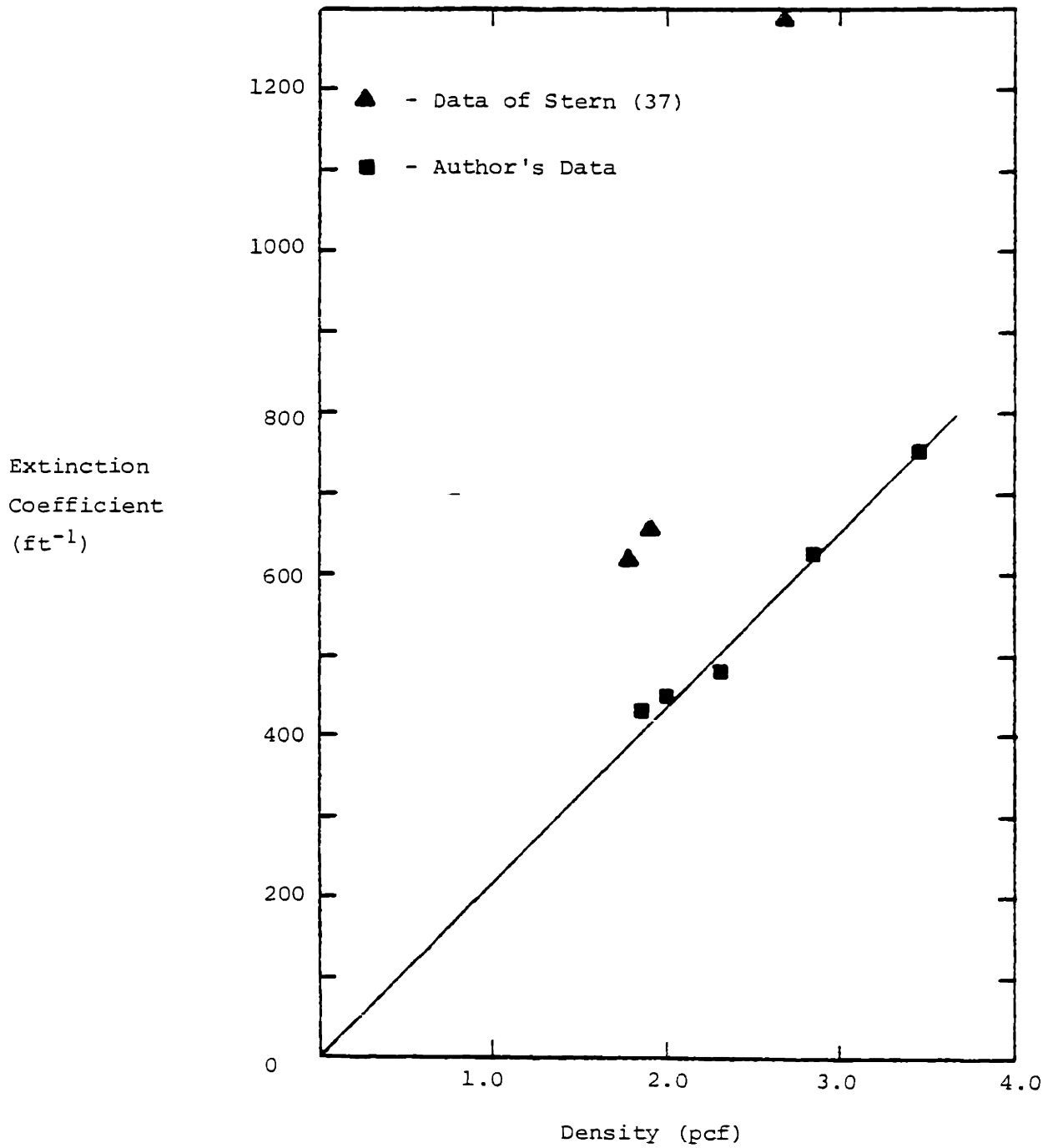
Figure 5-7 : Measured Extinction Coefficient versus Density

6. AGING MODEL

The previous chapter developed the heat transfer model for foam insulation for the case where the gas composition is constant throughout the foam. This chapter extends the model to include the case where the gas conductivity varies across the foam thickness. This variation occurs in aging foams which may have a high conductivity mixture near the surface and a low conductivity mixture in the core. This chapter is also relevant to predicting conductivities for cryogenic applications where over some regions of the foam the gas conductivity may be zero.

6.1 Background

As noted in Chapter 1, the approach taken by most authors in the foam literature has been to find an effective diffusion coefficient for each of the diffusing gases, and to apply the mathematical results of Newman (25), (19) to predict gas concentration profiles during aging for each of the diffusing gases. In this work, we have assumed that by this approach (or any other), the gas composition may be determined at all points in the foam. This chapter is concerned with calculation of the effective conductivity given this information.

It is tempting to simply jump to the conclusion that the space mean gas conductivity may be treated as a constant in the heat transfer model. This is easily shown to be incorrect by considering the limiting case of no radiation, no solid conduction, where the gas conductivity is a constant value everywhere except zero over a thin section. Under

these conditions the heat flow would be zero, thus the effective conductivity would be zero. This is significantly different from the conductivity which would be calculated via the space mean gas conductivity.

This example illustrates that we must be careful about the method of determining the "gas conduction". Considering the same example but allowing solid conduction plus radiation to occur, the effective conductivity would no longer be zero. Furthermore, the gas would play some role over the bulk of the foam and so it would also be incorrect to say that the effective conductivity of the medium is simply the solid plus radiation contributions (the gas contribution being zero).

A better model is required to handle these limiting cases. The question arises whether or not these affects are important in aging of foams. If they are important, what is the error associated with the simple-minded view that the gas, solid and radiation act separately? What is the error under typical aging conditions if one simply computes the space mean gas conductivity for the gas contribution? This chapter will address these questions.

6.2 Thermal Conductivity of Gas Mixtures

Before proceeding with the aging model, it is important to establish some facts concerning the thermal conductivity of the gas. This section is restricted to computation of the thermal conductivity of homogeneous gas mixtures of carbon dioxide, freon, oxygen, nitrogen and

water vapor. In the case of aging foams where the composition varies with position, the results of this section apply only on a local basis, i.e. within a single bubble where the gas mixture is homogeneous.

Under most conditions the carbon dioxide rapidly diffuses out of the foam (approximately one day) leaving only freon, oxygen, nitrogen and water vapor. For most practical purposes we need not be overly concerned if the gas mixture conductivity model is less accurate when CO_2 is present in the mixture. Water vapor also has a high diffusion coefficient and therefore rapidly reaches atmospheric concentration in the cells. While the freon, oxygen and nitrogen are not highly polar, water vapor is highly polar, and as will be seen shortly, this causes some concern as to the validity of the gas mixture conductivity model. Fortunately the atmospheric concentration of water is small relative to that of oxygen and nitrogen. Errors in model predictions for most aging conditions would therefore be small.

In this heat transfer study we ignore the effects of water condensation within the foams as well as any possible changes in the solid polymer conductivity during aging. Separately quantified, these effects could be included within the framework used in this work.

For lack of a better model, a summation of component mole fraction times pure component conductivity is sometimes used to estimate the conductivity of gas mixtures. Bretsznajder (8) points out that this model is valid when the gases have similar molecular weights and are nonpolar. The molecular weight of R-11 gas is 137.4 while that of O_2

and N_2 are approximately 32 and 28 respectively. None of these gases are highly polar, but clearly the ratio of molecular weights is greater than 4:1.

One correlation which is valid in this case was developed by Lindsay and Bromley, and is presented by both Reid (6) and Tsederberg (7). The general form of the relation is called the Wassiljewa equation. It is an empirical relation which also applies to viscosity of gas mixtures. Equation 6-1 applies to an n component mixture.

$$k_{mix} = \sum_{i=1}^{n} \frac{y_i k_{gi}}{\sum_{j=1}^{n} y_j A_{ij}} \tag{6-1}$$

where y_i is the mole fraction of the ith component, and k_{gi} is the thermal conductivity of the pure i^{th} component. The constants A_{ij} are determined from the following relation originally proposed by Lindsay and Bromley:

$$A_{ij} = 0.25 \left\{ 1 + \left[\frac{\eta_i}{\eta_j} \left(\frac{M_j}{M_i} \right)^{0.75} \frac{T + S_i}{T + S_j} \right]^{0.5} \right\}^2 \frac{T + S_{ij}}{T + S_i} \tag{6-2}$$

where:

η = pure component viscosity

T = absolute temperature

M = molecular weight

The remaining constants, S_i, S_j and S_{ij} are called Sutherland constants. For a pure component, if T_{bi} is the normal boiling point of component i, then:

$$S_i = 1.5 T_{bi} \qquad (6-3)$$

The remaining constant is determined from:

$$S_{ij} = S_{ji} = C_s (S_i S_j)^{0.5} \qquad (6-4)$$

where S_i and S_j are determined from equation 6-3, and C_s is assumed unity for nonpolar gases. Reid (6) reports the use of a value for C_s of 0.73 for the case where one gas is highly polar. For our case we use 1.0 when both i and j are oxygen, nitrogen or freon. We use 0.73 when only one of two (i or j) is water. When performing the summation in equation 6-1, A_{ij} is always equal to 1.0 when i=j.

No data is available in the literature on thermal conductivity of freon, oxygen, nitrogen and water vapor mixtures. However, data is available for freon nitrogen mixtures. Peters, et al. (5) measured the thermal conductivity of nitrogen freon mixtures at freon mole fractions of 0.0, 0.25, 0.5, 0.75, and 1.0. The Lindsay - Bromley correlation overestimated the mixture conductivity by approximately 5.0% in the

worst case, while the summation of mole fraction times pure component conductivity overestimates the data by 35% in the worst case. For both correlations, the largest percentage error occurs at 50% freon, 50% nitrogen. Based on this data, it is imperative to use the Lindsay - Bromley correlation rather than the simple linear model.

By a simple numerical exercise , it was found that the Lindsay - Bromley correlation predicts essentially the same effects for oxygen freon mixtures as for nitrogen freon mixtures. Thus, the lack of data with oxygen is not a cause for alarm since the effects of oxygen should theoretically be similar to the effects of nitrogen. The same cannot be said for water vapor. It is highly polar and therefore behaves very differently from nitrogen. Fortunately however, the water vapor concentrations are normally low, and thus the magnitude of any errors in gas mixture conductivity would normally be small.

6.3 Separation of Gas, Solid, Radiation Contributions During Aging
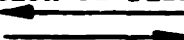
As noted in section 6.1, the heat transfer contributions of solid, gas and radiation during aging may not be separated a priori. In this section we will develop a more exact model, show where this model deviates from the simple model, and thereby show where the simple model is applicable.

6.3.1 General Model

The most accurate approach to this problem would be to determine the local thermal conductivity at every point in the foam. With this information the effective resistance to heat flow would be determined at each point. For the one-dimensional case (no edge diffusion), the local resistance would be integrated from one side of the foam to the other for the total resistance. In the general case, the variation of material properties and radiation contribution with temperature would be accounted for. For three dimensional diffusion cases, one would perform the one dimensional integration for an infinitesimal area element, then integrate the heat flow through each area element over the surface of the insulation. Note that resistance would be integrated across the thickness, but heat flow would be integrated over the area.

The one dimensional integration process may be approximated by breaking the foam into several thin layers over which the overall conductivity is assumed constant. For the purpose of illustration, only the one-dimensional diffusion case is considered (no edge diffusion). Consider the case where there is a small enough temperature difference across the foam (relative to the absolute value of temperature) so that changes in material properties and changes in the local "radiation conductivity" may be neglected. (See equation 5-6.) Under these conditions the heat flow through the foam can be calculated with the resistance network given in Figure 6-1. The overall foam conductivity (k_f) for each layer is calculated using the heat transfer model
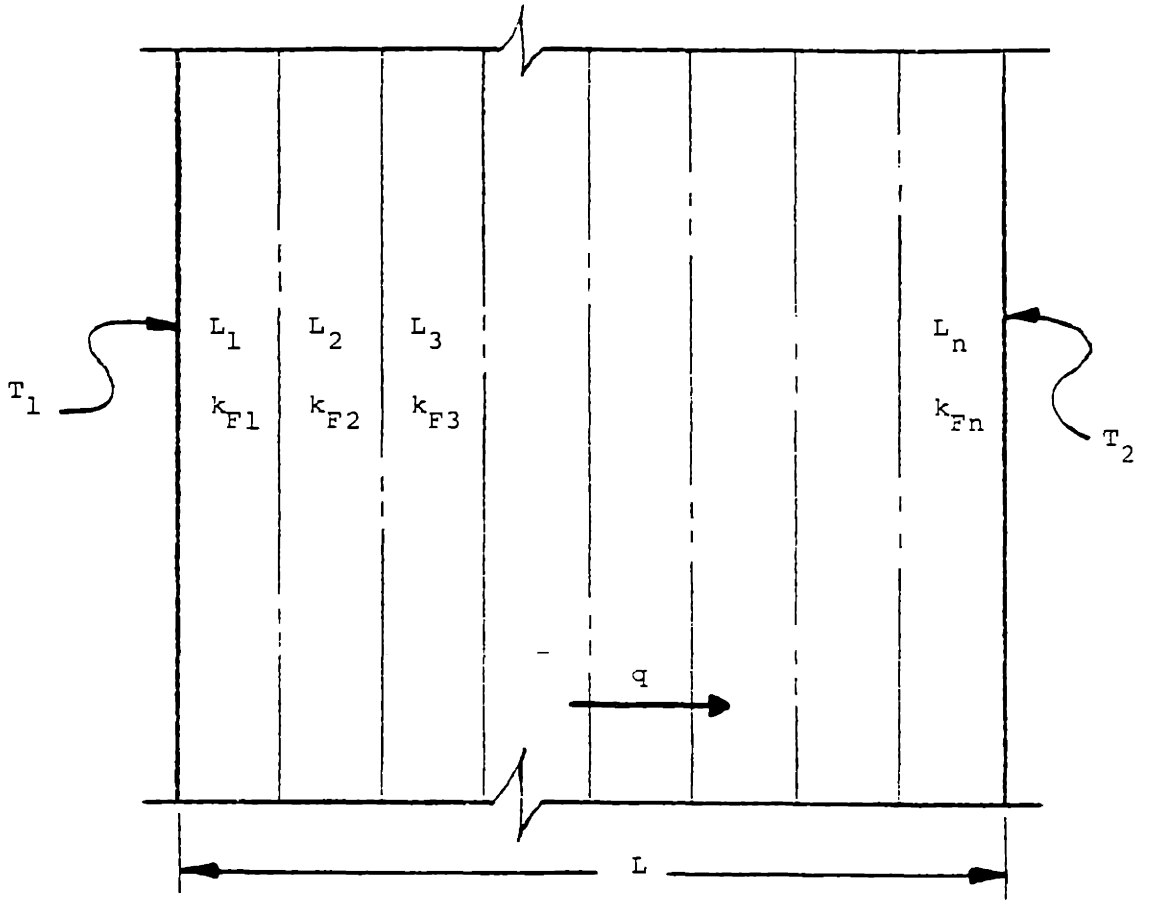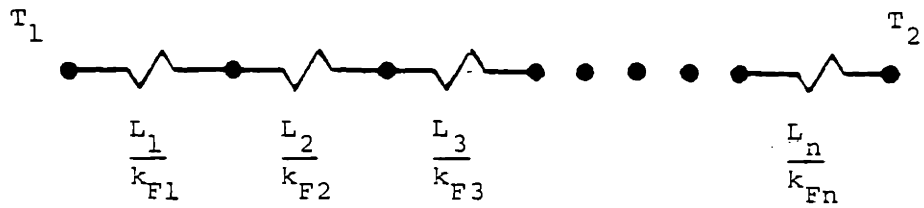
Figure 6-1 : Resistance Network for Heat
Flow Through Aging Foam Slabs

summarized in Chapter 5; i.e. using equations 5-6 and 5-4. Summing all resistances we may derive the following formula for the overall conductivity of the aging foam sample:

$$k_{aged} = \left(\frac{1}{L} \sum_{i=1}^{n} \frac{L_i}{k_{fi}} \right)^{-1}$$

(6-5)

For the case where all sections are of the same thickness L_i, n times L_i is equal to the sample thickness and equation 6-5 reduces to:

$$k_{aged} = \left(\frac{1}{n} \sum_{i=1}^{n} \frac{1}{k_{fi}} \right)^{-1}$$

(6-6)

Note that this expression is valid even for the case where the gas conductivity is zero at some location. Since k_{fi} includes gas, solid, and radiation contributions, k_{fi} is never zero for real foam. In the limiting cases mentioned at the beginning of this chapter, this expression gives the correct answer.

In section 6.3.2 a simpler aging model is presented and compared to this accurate model. These two models are compared to models based on calculation of a mean "gas conductivity". The error in these models is given for some typical aging conditions as well as some extreme cases.

6.3.2 Simple Aging Model for Foams

While the aging model described in the previous section certainly may not be described as excessively complex, it does require knowledge of the parameters which determine the conductivity of the foam prior to aging. The parameters required include the extinction coefficient, percentage of solid in struts, and so on. It would be desireable for many purposes to be able to predict aging without having to measure these parameters. The simple model allows us to do this with only a negligible sacrifice in accuracy.

Recall that the "solid contribution" was defined as the effective conductivity in the absence of radiation minus the gas conductivity. In section 2.3.7 it was shown that the "solid contribution" changed by less than 2.5% even as the gas conductivity varied from that of pure freon 11 to that of pure nitrogen. (See Table 2-2 for reference.) Also, for the case of foams with optical thicknesses greater than 100, equation 3-22 shows that the radiation conductivity is independent of the conduction terms. From these two observations it may be inferred that the foam conductivity may be expressed by equation 6-7 for the case of uniform gas conductivity:

$$k_f \simeq k_g + k_{r+s} \tag{6-7}$$

where k_{r+s} equals the radiation plus solid contribution (which is independent of k_g). This approximation results in a loss of accuracy

during aging of 2.5% of the solid conduction contribution. This amounts to an error of less than 0.5% of the overall conductivity of an aging foam. Unfortunately equation 6-7 applies only to the case of uniform gas conductivity and thus may only be applied on a local basis for foams with varying gas composition.

At this point any number of approaches are possible. The most common approach in the literature, is to find a mean gas conductivity to be used in equation 6-7. Norton (17) apparently uses the conductivity of the mean gas composition. The space mean value of the local gas conductivity is a more intuitively appealing model to use. Both of these models will be shown to be incorrect.

If the initial gas composition and initial foam conductivity are known, the best approach would be to use equation 6-7 for the local heat transfer model during aging, and use the exact formulation of section 6.3.1 for the purposes of determining the overall foam conductivity. This eliminates the need for knowledge of the various material properties (extinction coefficients, etc.). The overall thermal conductivity at the time of foaming, and the initial gas composition provide all the required information. The initial gas composition is also required to predict the gas composition over time. Hence, other than the initial conductivity no measurements are required for heat transfer purposes other than those which would already be measured for diffusion purposes. Given the initial gas composition and initial thermal conductivity, one simply subtracts the initial gas conductivity

from the initial overall conductivity in order to obtain the "local radiation plus solid contribution" (k_{r+s},local). This local value is assumed to remain constant throughout the foam over all time.

$$k_{r+s \atop local} = k_{f_{initial}} - k_{g_{initial}} = constant \qquad (6-8)$$

During aging, this local value is added to the local gas conductivity (k_{gi}) for each small region over which the gas composition is constant. This sum is the local conductivity of the foam (k_{fi}).

$$k_{fi} = \bar{k}_{gi} + k_{r+s \atop local} \qquad (6-9)$$

The values of k_{fi} from equation 6-9 are used in equation 6-5 or 6-6 to obtain the overall thermal conductivity of the aging foam. The uncertainty in this approach would be 0.5% due to the actual change in solid contribution during aging. Experimental uncertainty in the determination of initial foam and gas conductivities will cause a larger overall uncertainty. Knowledge of the solid conduction or radiation parameters are not required, so long as the solid polymer conductivity remains constant. If future research proves that the solid polymer conductivity changes during aging, then one could not use equation 6-9 during aging. Instead, the overall model of chapter 5 would have to be used to determine k_{fi}.

Errors in Approximate Methods

In order to estimate the error in the approximate methods, the aged overall thermal conductivity was calculated four different ways for some typical aging conditions. The results are given in Table 6-1. In all cases the diffusion coeficients reported by Brandreth (24) were used in the series solution for one dimensional diffusion through a two inch thick, unfaced slab. See Newman (25) for details. Using this solution, the gas composition was calculated at 16 points in the slab, as indicated in Figure 6-2. By symmetry only half of the slab need be analysed. The core centerline is impermeable by symmetry. In all cases the solid plus radiation contribution was assumed constant (0.06 Btu-in/hr-ft^2-F). The aging condition was 25 C, 0% relative humidity.

The conductivity calculated by method one was the standard against which the other methods were evaluated. Equation 6-1 was used to compute the gas conductivity at each point shown in Figure 6-2. Equation 6-9 was used to compute the values of k_{fi}, which were used in equation 6-5. We showed analytically that this approach is accuate to within 0.5% of the exact solution, neglecting the small error in equation 6-1.

In method two the gas conductivity was also calculated at each point in Figure 6-2. These values were averaged over space, thus determining the space mean gas conductivity. This gas conductivity was used in equation 6-7 directly.

Table 6-1 : Comparison of Aging Results

Using Four Different Computation Methods

	Time (yr)	0.5	0.5	0.5	1	5
computation method	initial R-11 pressure (atm)	1	0.7	0.3	0.3	0.3
1.	k_F - proposed model	0.1235	0.1259	0.1336	0.1432	0.1731
2.	k_F - space mean conductivity (% Error)	0.1260 (2.0)	0.1287 (2.2)	0.1380 (3.3)	0.1470 (2.7)	0.1742 (0.6)
3.	k_F - mean gas composition (% Error)	0.1244 (0.7)	0.1283 (1.9)	0.1431 (7.1)	0.1517 (5.9)	0.1744 (0.8)
4.	k_F - linear gas conductivity model (% Error)	0.1362 (10.3)	0.1435 (14.0)	0.1664 (25.)	0.1773 (24.)	0.2000 (16.)

units: Btu-in/hr-ft^2-F

k_{s+g} = 0.06 Btu-in/hr-ft^2-F

Diffusion Coefficients:

Gas	Assumed Value
Oxygen	4×10^{-8} cm/sec^2
Nitrogen	1×10^{-8} cm/sec^2
R-11	1×10^{-8} cm/sec^2
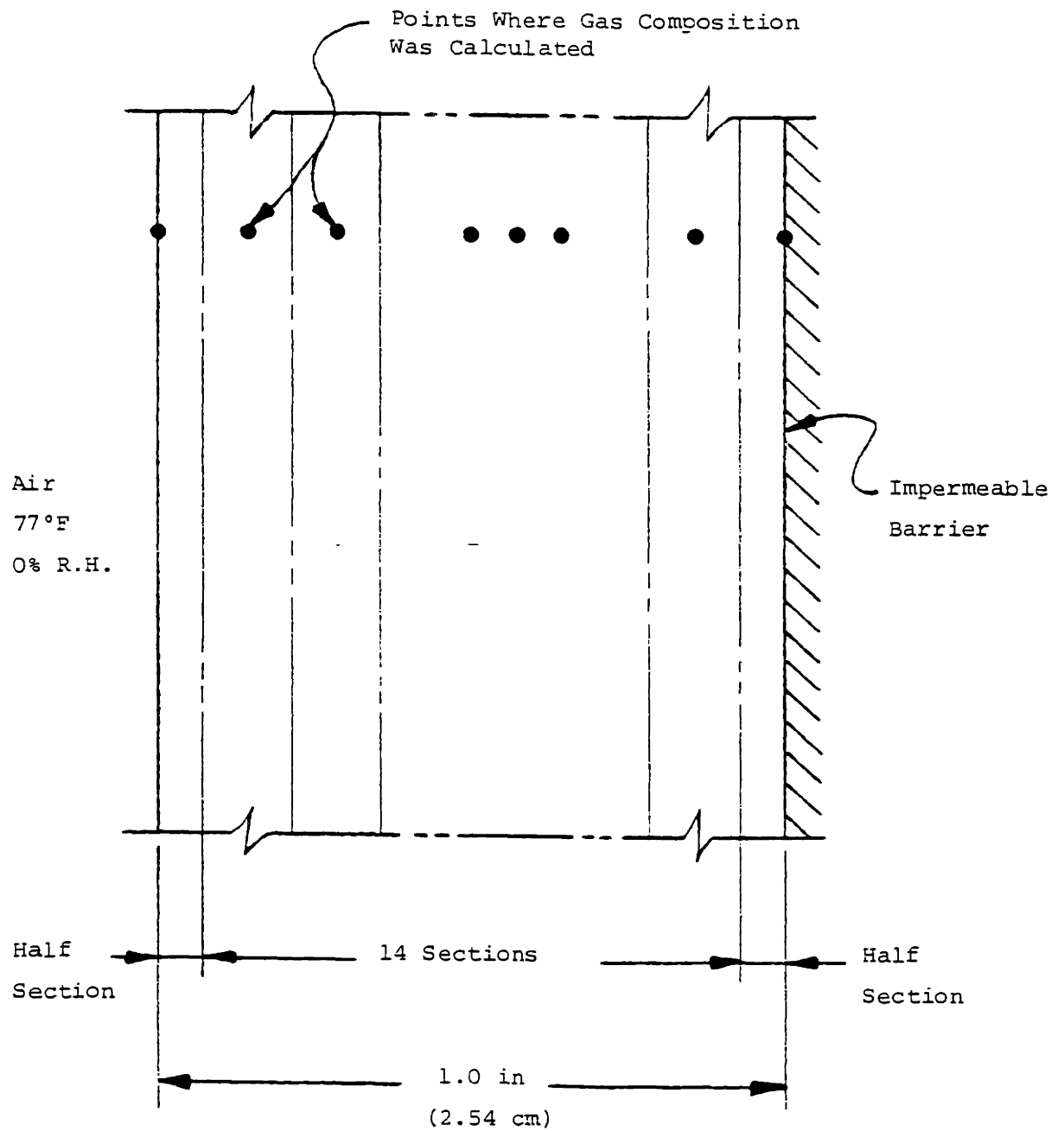
Figure 6-2 :   Geometry for Example Diffusion Calculation

Method three differs from the first two in that the conductivity was not calculated at each point. Instead Newman's solution for the average gas concentrations was used to compute the average gas composition. The conductivity of this composition was computed with equation 6-1, and used directly in equation 6-7.

Method four is equivalent to method three except the gas mixture conductivity was not calculated with equation 6-1. Instead, the mixture conductivity was taken to be the summation of component mole fraction times pure component conductivity. The mixture thermal conductivity was therefore assumed linear with gas component mole fraction.

From Table 6-1 it is clear that the linear gas conductivity model (method four) is excessively inaccurate. The space mean conductivity model (method two) and the mean gas conductivity model (method three) are both within 7% for these cases. However, since the computation effort required by method one is no greater than the effort required for the other two, there is no reason to compromise on accuracy. Note also that the errors shown in Table 6-1 are not generally applicable. If other aging conditions, sample thicknesses, or diffusion coefficients are used, the errors might be higher or lower. With method one, the error is never greater than 0.5% for any aging conditions.

The analysis which led to equations 6-5 and 6-6 had two inherent assumptions. We considered only one-dimensional diffusion and small temperature difference. The analysis will now be generalized.

Multi-dimensional Diffusion

When a planar sample of insulation is cut to a finite size, there will be gas diffusion from the sides as well as from the faces, leading to a three dimensional variation in gas conductivity. An accurate treatment of the heat transfer problem would use the one dimensional analysis previously described for regions over which the concentration profiles are similar. An area-weighted average of the calculated aged conductivities for each region would result in an accurate estimate of the total heat flow. This estimate would be exact for the case of one dimensional heat flow with isothermal faces and adiabatic edges. Thus, the actual error would not be excessive in most practical applications. However, this approach is somewhat tedious. In the future it would be worthwhile to perform the calculation for some typical shapes and typical diffusion coefficients. These results could be compared to those using the space mean gas conductivity for the "gas contribution". Based on the 3% error obtained in the one-dimensional case, it would not be surprising to get 5% error via the space mean conductivity approach.

Effect of Temperature Difference

This analysis loses accuracy as the temperature difference increases primarily because the local radiation conductivity varies with T^3. For typical aging tests the thermal conductivity is measured over time at the same hot and cold plate temperatures, and at small temperature differences (typically 50 F, 28 C). Therefore, in most cases the error will be small. For cryogenic applications where the material properties change considerably with temperature, and where the radiation conductivity will change considerably with temperature, a more refined analysis than that of section 6.3.1 is required. One would solve n simultaneous algebraic equations for the temperature at each node (point between regions of constant k_{ri}). Using the heat transfer model of chapter 5 (equations 5-4 and 5-6), the gas, solid and radiation terms would be modified within each region of constant k_{ri}. This most general analysis has not been performed. However, limiting cases have been examined where the gas contribution goes to zero in some locations (assuming contant solid polymer properties and constant radiation conductivity). For the cases examined, the space mean gas contribution calculation was found to be in error by up to 60% overall in comparison to this more accurate approach. See Table 6-2 for some hypothetical cases. Clearly the accuracy of the space mean approach depends strongly on the solid plus radiation contribution, and on the specific values of gas conductivity.

<u>Table 6-2</u> : <u>Illustration of Error in Extreme Cases Using</u>

<u>the Space Mean Gas Conductivity Approach</u>

Case	1	2	3	4	5
k_{r+s}	0.06	0.06	0.06	0.06	0.03
k_{g1}	0.180	0.072	0.072	0.180	0.18
k_{g2}	0.168	0.060	0.072	0.156	0.156
k_{g3}	0.156	0.048	0.072	0.132	0.132
k_{g4}	0.144	0.036	0.072	0.108	0.108
k_{g5}	0.132	0.036	0.072	0.084	0.084
k_{g6}	0.120	0.024	0	0.060	0.060
k_{g7}	0.108	0.024	0	0.036	0.036
k_{g8}	0.096	0.012	0	0.012	0.012
k_{g9}	0.084	0.012	0	0	0
k_{g10}	0.072	0	0	0	0
k_{approx}^{*}	0.1860	0.0924	0.0960	0.1368	0.1068
k_{aged}^{**}	0.1794	0.0875	0.0825	0.1077	0.0671
Error	3.7%	5.6%	16%	27%	59%

(Assumed Distribution — row label for k_{g1} through k_{g10})

*Determined from equation 6-7 where : $k_g \ = \ \dfrac{1}{10} \displaystyle\sum_{i=1}^{10} k_{gi}$

**Determined from equations 6-6 and 6-9.

Units : $Btu\text{-}in/hr\text{-}ft^2\text{-}F$

6.4 Summary of Aging Model

The heat transfer portion of an aging model has been developed which is both simple to use and accurate to within 0.5% for the case of one dimensional diffusion in a slab with reasonable temperature differences. It entails measurement of initial foam conductivity and gas composition in order to determine the local solid plus radiation contribution; which is then assumed constant for the life of the foam. The aged foam gas composition is computed at various points in the foam. The local gas conductivity is computed at each point, then added to the local solid plus radiation contribution (Equation 6-9). Finally, equation 6-5 or 6-6 is used to compute the aged foam overall conductivity.

For one dimensional diffusion this computation process is no more difficult but is more accurate than the computations required to calculate the space mean gas conductivity. If the aged foam conductivity is taken to be the radiation plus solid contribution plus the space mean gas conductivity, the uncertainty will be approximately 3% of the overall conductivity, assuming one dimensional diffusion with the diffusion coefficients reported by Brandreth (24). The error will be greater for multidimensional diffusion problems and may be even greater for different numerical values of diffusion coefficients. The technique of using the conductivity of the mean gas composition is inaccurate by as much as 7% for partially aged foams with typical diffusion coefficients. These approximate approaches will be grossly

inaccurate in cryogenic applications where the gas conductivity may approach zero in some portions of the foam.

If the initial gas composition is known but the initial conductivity is not known, other parameters are required for the prediction of aging. One must know the foam porosity, solid polymer conductivity, percentage of solid in struts and the extinction coefficient. These parameters are used to estimate the initial foam conductivity using the model in chapter 5. This process would introduce a much larger uncertainty than if the initial conductivity is measured. Therefore, all future aging studies should include measurements of initial foam conductivity. The initial gas composition should also be measured. Fortunately, any error introduced by not knowing the initial conductivity will be constant during aging. Hence it may be possible to predict the changes in foam conductivity with time, even when the initial foam conductivity is not measured.

7. IMPROVEMENT OF INSULATIONS VIA PARTICLE ADDITIONS

In the first six chapters we developed a heat transfer model for foams, presented data on the radiation properties, and applied the model to the aging problem. Table 5-1 shows that the radiation contribution is approximately 25% of the overall heat transfer for low density foams. In chapter 4 we showed that the simple model underestimates radiation in foams, hence radiation might account for up to 30% of the heat transfer in low density foams. While it is unlikely to find a method to substantially reduce conduction in foams, it may be possible to reduce the radiation contribution. This chapter describes one way to reduce radiation.

7.1 Theory

Given the radiation model of section 3.3, one may reduce radiation in foams by increasing the extinction coefficient. From Figure 5-7 we see that the extinction coefficient varies approximately linearly with density for one foam formulation. For equal foam densities other formulations have higher extinction coefficients. Hence there is some potential for increasing the extinction coefficient through chemical changes.

Another way to increase the extinction coefficient is to add opaque particles. Unfortunately, if the particles have a high conductivity, then their addition to the foam will also increase the conduction heat transfer. It is desirable to add particles which will provide the

greatest increase in the extinction coefficient with the lowest increase in conduction. Since most materials have conductivities much higher than that of the foam polymer, this is tantamount to increasing the extinction coefficient the greatest amount for a given volume fraction of particles in foam.

Decreasing Radiation

While it might be possible to solve Maxwell's equations for the behavior of various particles to infrared radiation, that process would require sophisticated computer programs along with experimental knowledge of the complex index of refraction. In contrast, our approach has been to use a published solution of the electromagnetic theory for spherical carbon particles as a rough guide (Hottel, reference 20, p. 406), and to use the simple experimental procedure for extinction coefficient measurement as our measure of success in reducing radiation.

The radiation behavior of dispersions of particles may be described with the same mathematical framework used throughout this work. That is, for a dispersion of particles in a medium it is possible to define the absorption coefficient, scattering coefficient, extinction coefficient and the phase function just as we have for foam and glass fiber insulations. When the particles are far enough apart so that no

interference occurs, the absorption, scattering and extinction coefficients are given by equations 7-1, 7-2 and 7-3:

$$a = N X_a C \tag{7-1}$$

$$\sigma_s = N X_s C \tag{7-2}$$

$$K = N X_T C \tag{7-3}$$

where:

N = number of particles per unit volume

C = geometric cross sectional area of a particle

X = efficiency factor

Recall that we wish to maximize the _modified_ extinction coefficient, $a + \sigma_s (1 - \langle \cos \theta \rangle)$, in order to minimize radiation. However, since any particle will most likely exhibit nongray behavior we must be careful to maximize the Rosseland mean modified extinction coefficient, given by equation 3-17.

Hottel (20) shows for spherical carbon particles that the total extinction efficiency (X_T) is a strong function of the ratio of particle circumference to radiation wavelength. At small values of this ratio, (<<1), the attenuation behavior may be described by the Rayleigh scattering solution. The extinction is absorption dominated ($X_a >> X_s$), and the total extinction efficiency (X_T) falls off. At higher values of circumference to wavelength ratio, (>1), the total extinction efficiency levels off at a value of approximately 2.5. This suggests that larger

particles are more efficient attenuators than small particles. However, Hottel also shows for spheres of infinite refractive index that the asymmetry factor $\langle \cos \theta \rangle$ increases with this ratio of circumference to wavelength. If carbon particles exhibit the same type of trend, the increase in the modified extinction coefficient with particle diameter would not be as dramatic as the increase in the extinction efficiency would suggest.

Note that the geometric cross section and the number of particles per unit volume play an equal role with the extinction efficiency in the determination of the extinction coefficient. It is the product of these three quantities (equation 7-3) which must be optimized. Smaller particle diameters have higher surface to volume ratios and hence favor more total cross section (N times C) per unit volume (or mass) of particles. Conduction in foams would be expected to increase with increasing volume fraction of particles. However, the magnitude of the affect on conduction is not easily quantified. Small particles might affect only the solid contribution term if the particle dimension is small relative to the thickness of membranes and struts. When the particle diameter is of the same order as the thickness of membranes (~ 0.5 microns) or the cross sections of struts, then this will no longer be true.

Powers (41) provides a comprehensive review of various exact and approximate solutions to the problem of thermal conductivity of aggregates. Unfortunately none of the correlations were found to agree

with the data provided in the next section. When the aggregate correlations were applied only to the solid polymer, the calculated results still could not explain the data reported in the next section.

The exact theory for the effects of additions of particles in foams is very complex. However, one would expect to find trends. As more particles per unit volume are added, the extinction coefficient should increase linearly (equation 7-3). The conduction contribution will be increased, but not necessarily linearly. For any one type particle in a fixed density foam, one would therefore expect to find a concentration of minimum overall foam conductivity.

As the particle diameter is decreased, improved performance would be expected since the extinction efficiency is relatively constant for circumference to wavelength ratios greater than 1. At some particle diameter, gains in surface to volume ratio would be offset by decreases in extinction efficiency. Hence, for any particle material in a fixed density foam, one would expect to find an optimum particle diameter which results in a minimum overall foam conductivity. Note also that as the extinction efficiency begins to decrease, the effects should first be seen in the far infrared portion of the spectrum where the circumference to wavelength ratio is the smallest.

Since the radiation conductivity is inversely proportional to the extinction coefficient, and since the extinction coefficient of a particlular foam is nearly linear with density, particles should exhibit stronger effects at lower foam densities than at higher foam densities.

At higher foam densities the extinction coefficient is already large and the radiation conductivity already small. Lower densities have lower extinction coefficients and therefore higher radiation heat transfer rates. There is therefore greater potential for radiation reduction at low densities than at high densities.

7.2 Data

In order to quickly determine whether or not a particle material has promise for this application, the extinction coefficient could be measured for a dispersion of particles. A dilute dispersion in a nonabsorbing liquid within a variable pathlength cell would probably provide the most accurate and rapid measurements of transmission versus pathlength, using only a conventional infrared spectrometer.

For the purposes of proof of concept such tests were unnecessary. Instead, some particles were simply sandwiched between KBr (potassium bromide) windows and the infrared transmission was measured. The weight of particles per unit area was also measured. This test qualitatively indicated that small (2-5 micron mean particle diameter) coal particles were better attenuators than large (325 mesh, 35 micron mean particle diameter) coal particles, which were better attenuators than small (1-10 micron) $CaCO_3$ particles.

Based on this qualitative evaluation, three foams were made with various concentrations of the small coal particles and one foam was made with some large coal particles. The particles were dispersed in the

polyol prior to foaming using a high speed laboratory mixer. A summary of the foams produced with the measured densities and measured thermal conductivities is given in Table 7-1. Sample A was the control foam, it had no particles added. Sample B, C and D had the small particles added, while sample E was foamed with the large particles.

The extinction coefficient was also measured for each of the five samples, via the simple technique described in section 4.2. Typical spectrographs of samples A, C and E are given in Figures 7-1 through 7-3. For the foam with small particles, (sample C), the curve exhibits higher transmission in the far infrared than over the rest of the spectrum. This trend is not seen in the same foam without particles, (sample A) nor is it seen in the foam with large particles (sample E). This may be due to the decreased extinction efficiency of the smaller particles at large wavelengths, as discussed in the previous section.

Measured values of average transmission versus thickness are given in Figure 7-4 for samples A and D. The data for the sample with no particles (sample A) converges around a straight line passing through 100% transmission at zero thickness. The data for foams with particles (sample D) exhibits much more scatter, probably due to incomplete particle dispersion. This behavior was also found for samples B, C and E. Nonetheless, the mean extinction coefficient is clearly higher with particles than without. In order to minimize the number of data points required for each sample with particles, the best line passing through 100% transmission at zero thickness was drawn, even if the least squares

Table 7-1 : Summary of Particles in Foam Experiment

	Foam				
	A **	B	C	D	E
Density (pcf)	1.99	2.26	1.98	2.01	1.99
Particle Type	none	2-5 micron coal	2-5 micron coal	2-5 micron coal	325 mesh coal
Particle Concentration lbm/ft^3 foam	0	0.2	0.2	0.4	0.2
Measured Extinction Coefficient ft^{-1}	481	766	676	805	664
*Radiation Conductivity (Calculated)	0.035	0.022	0.025	0.021	0.025
*Measured Conductivity	0.121	0.121	0.114	0.129	0.122

*Units : Btu-in/hr-ft^2-F

Tested on Dynatech "K-Matic".

T_1 = 95 F , T_2 = 55 F, 1 inch sample thickness
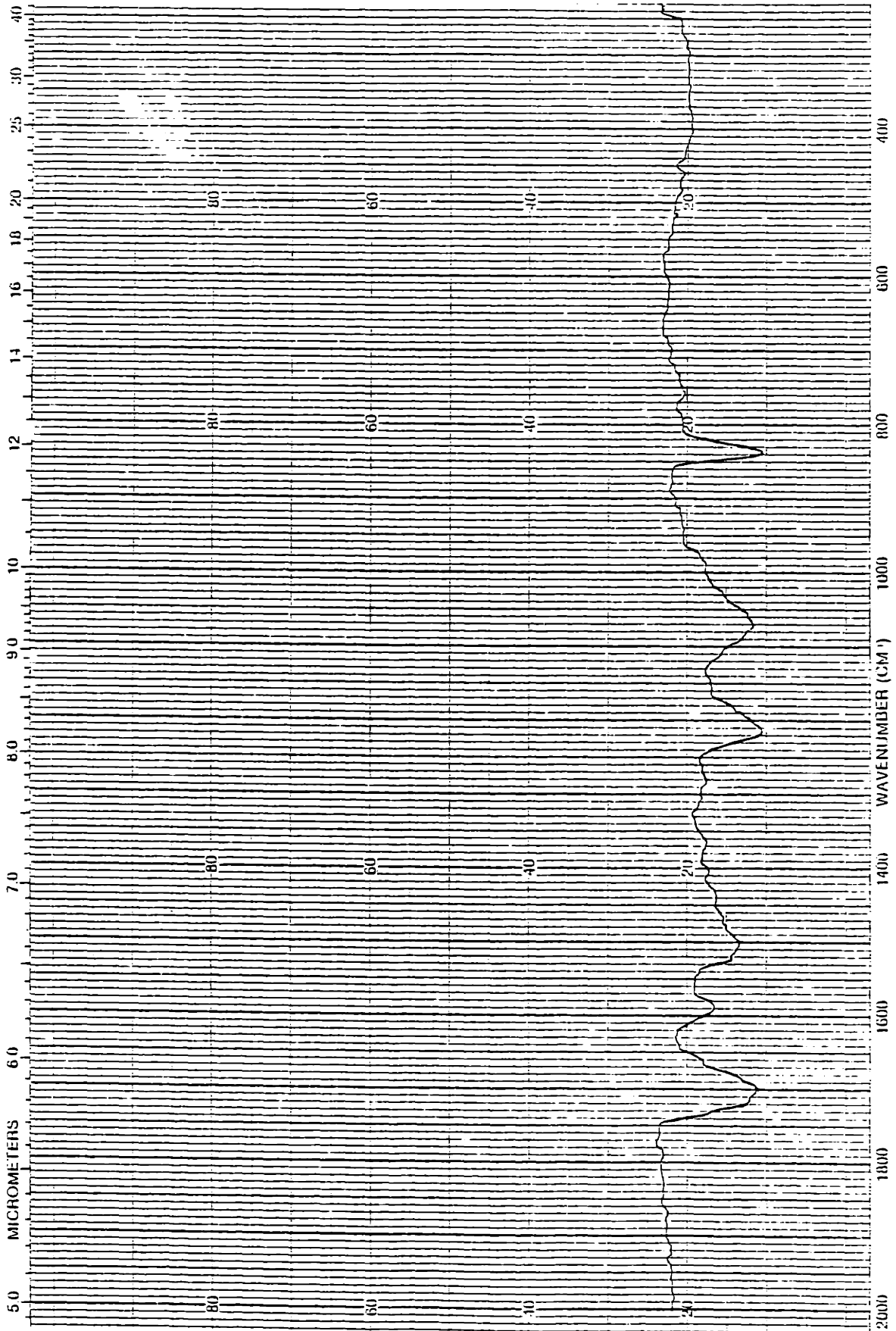
Estimated uncertainty ± 3%.

**Control Sample

248

Figure 7-1 : Transmission Through 0.042 in Thick Sample – Foam "A"
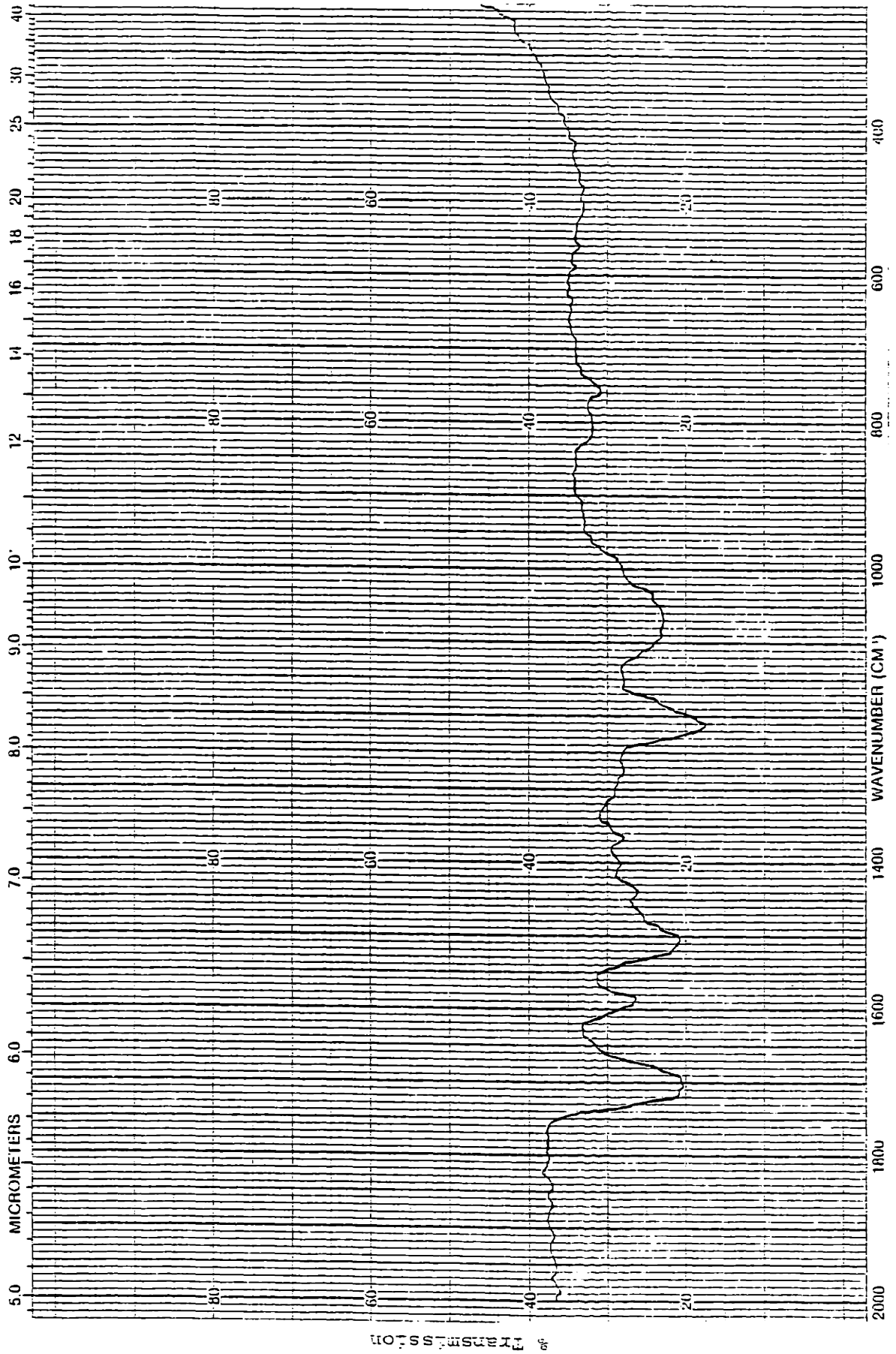
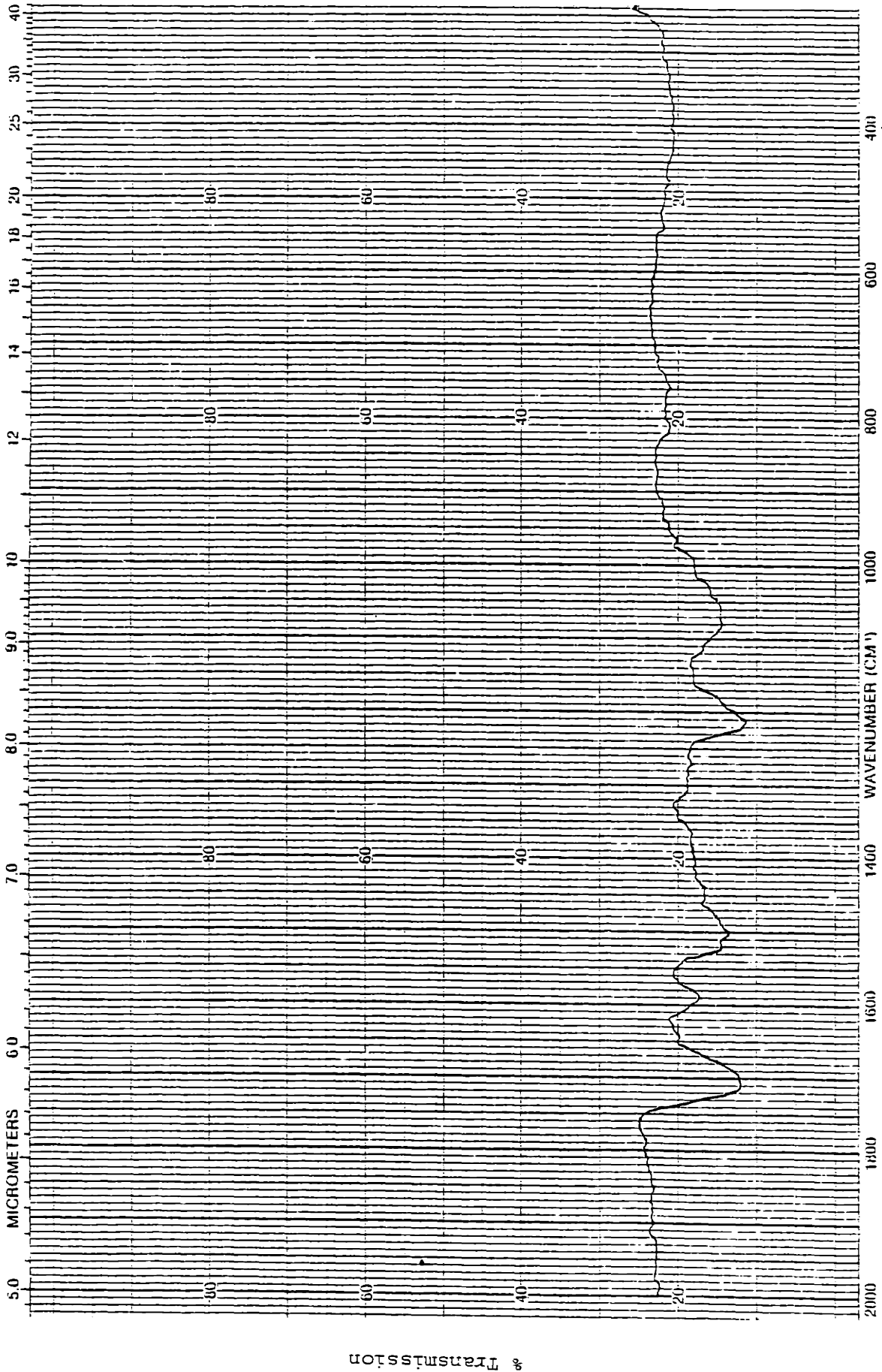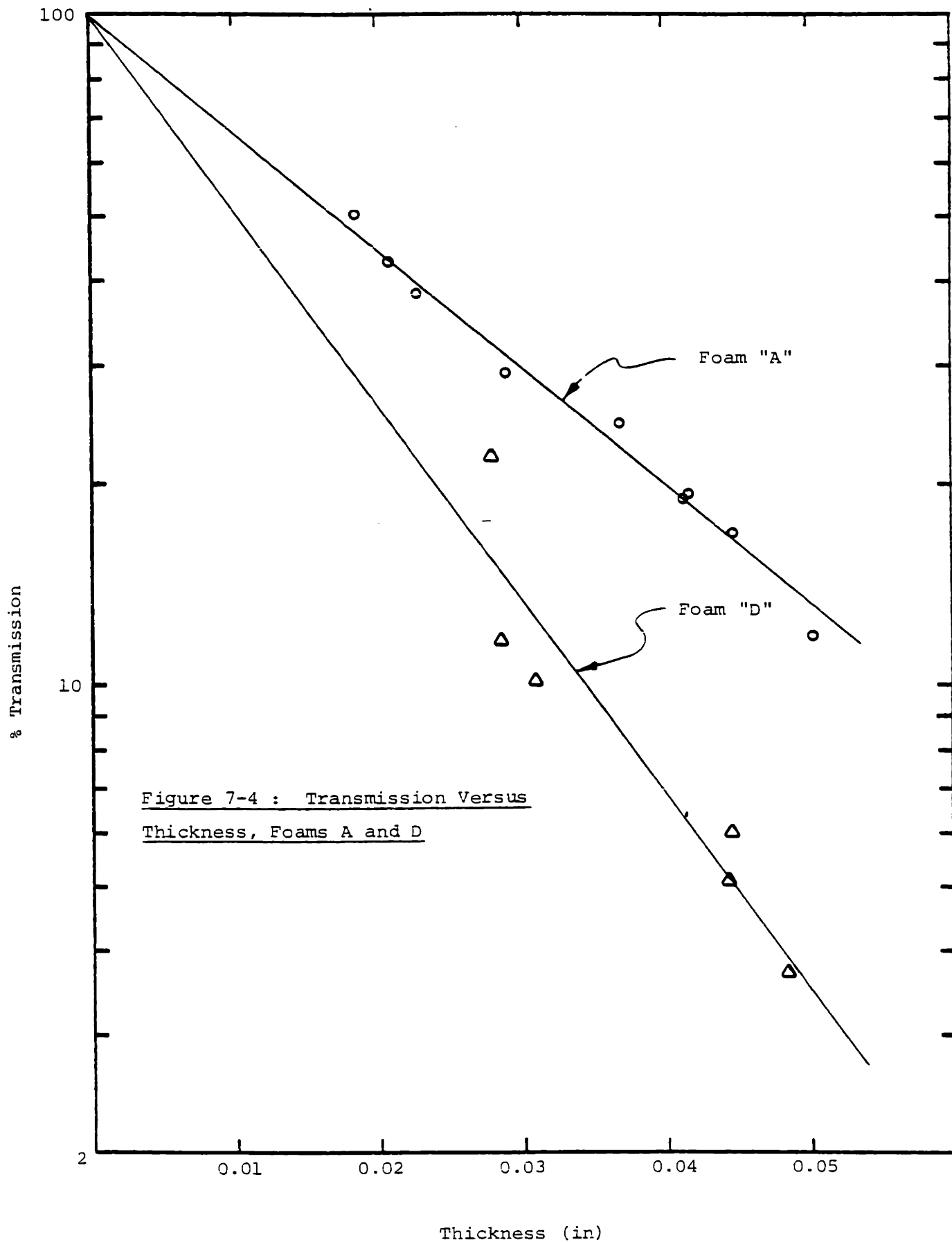Figure 7-2 : Transmission Through 0.019 in Thick Sample - Foam "C"

Figure 7-3 : Transmission Through 0.030 in Thick Sample - Foam "E"

Figure 7-4 : Transmission Versus Thickness, Foams A and D

regression would give a different line. The extinction coefficients determined in this way are given in Table 7-1 along with the calculated radiation conductivity. (See the radiation term in equation 5-6 for the radiation conductivity.)

Some of the expected trends may be seen in Table 7-1. Comparing samples A and B, the addition of particles caused a substantial increase in extinction coefficient, as well as an increase in foam density which increased conduction. The net effect on measured conductivity was zero. In foams A, C and D, the particle concentration is increased while maintaining constant foam density. Sample C had a decrease in radiation conductivity of 0.01 Btu-in/ hr-ft^2-F compared to sample A. This was partially offset by an 0.003 Btu-in/hr-ft^2-F increase in conduction. A net decrease in overall conductivity of 0.007 Btu-in/hr-ft^2-F (6%) resulted. The particle concentration was increased in sample D to twice the concentration in sample C. The extinction coefficient increase from C to D was approximately equal to the increase from A to C. The higher extinction coefficient results in a smaller radiation conductivity. A large increase in conduction also occured, causing the overall conductivity of D to increase dramatically in comparison to samples A and C.

Sample E provides an anomoly to this line of thought. The extinction coefficient is increased over that of A by almost the same amount as from A to C. Sample E is thus found to have essentially the same radiation conductivity as sample C. One would have expected the

smaller particles (in sample C) to have resulted in a larger increase in extinction coefficient than did the larger particles (in sample E). Note that samples C and E were produced with equal concentration of particles by mass (hence volume). The increase in conduction must have been greater for the large particles than for the small particles since the overall conductivity did not decrease from A to E as it did from A to C. Intuitively one might have expected the larger particles to increase the conduction to a lesser extent than the small particles.

7.3 Summary and Recommendations

The theory for the effects of particles on the overall conductivity of foams is not well understood. Nonetheless, some general trends which were expected from the theory agree with observations from the data. The proof of concept experiment has resulted in a foam with a 6% lower overall conductivity while at the same time replacing 10% of the polymer material with a less expensive filler. It is anticipated that a thorough screening of various inexpensive particles (fly ash, soot, glass, etc.) might result in superior performance to that achieved in this proof of concept experiment. For each test material, particles should be ground to different sizes so as to find the optimum particle size. The concentration must also be optimized. The extinction coefficient should be measured for each test foam so that effects on the radiation conductivity may be observed. It is anticipated that the beneficial effects of particles will be most substantial in low density foams, since they have the lowest extinction coefficients and the

highest radiation heat fluxes. Since the lowest conductivities presently achievable are in low density foams, it is anticipated that this technique will allow production of foams with conductivities lower than the current state-of-the-art.

8. SUMMARY AND CONCLUSIONS

A heat transfer model has been developed for foam insulation. The model is mathematically easy to apply and requires a minimum number of experimentally measured foam properties. If the required properties are accurately known, the overall uncertainty in the model is approximately 5% for foam densities below 5.0 pcf (80 Kg/m^3).

In order to predict the thermal conductivity of fresh foam, the model requires knowledge of the following foam properties: density of foam, percentage of solid in struts versus membranes, cell gas composition, and extinction coefficient. A simple technique for extinction coefficient measurement using a conventional infrared spectrometer has been presented. The technique has been found to be accurate to within 11% for foam insulations. This simple technique always overestimates the appropriate extinction coefficient, and hence underestimates the actual radiation heat transfer by approximately 10%. For low density foams this error causes a 2.5% underestimate of the overall heat transfer rate. The density of the foam and the cell gas composition are readily determined using conventional techniques. The percentage of solid in struts, however, is not as easy to measure. When no data is available, a value of 75% in struts, 25% in membranes is suggested, based on preliminary estimates by Reitz. Reitz's technique involves metallography and scanning electron microscopy technology in a polyhedra geometry mathematical framework. It is anticipated that the technique and some results will be published by Reitz within six months

from the time of this writing.

The proposed heat transfer model for foam places upper and lower limits on the conduction through the solid polymer. The actual conduction is expected to be closest to the upper limit result. Published conduction models are found to be accurate only for the case from 100% of the solid polymer is in membranes. Since preliminary measurements indicate up to 85% of the polymer residing in struts, previously published conduction models overestimate solid conduction by almost a factor of two.

The difference between the upper and lower limits for conduction is 20% of the solid contribution. This amounts to a plus zero, minus four percent uncertainty in the overall conductivity for a 2.0 pcf foam. For comparison, the variation in the thermal conductivity of pure polymer causes an uncertainty band of approximately 100% of the solid contribution. This is due to a factor of two variation in published values for polymer conductivity.

The overall heat transfer model has been used to show that the solid conduction and radiation contributions change by less than 2.5% during aging, so long as the polymer conductivity itself does not change. Using this result, an easy to use method was developed for predicting the overall conductivity of partially aged foam. Knowledge of the gas composition at all points in the foam was assumed. This method was analytically shown to be accurate to within 0.5%. Other methods often used in the foam literature were found to be in error by

up to 7% for typical aging conditions and 60% under extreme cases. The error in the published methods is due to improper treatment of conduction through a medium with varying conductivity.

An experiment was developed to directly measure the absorption coefficient, scattering coefficient and phase function. Using the experimentally determined radiation properties for foam and for fibrous glass insulation, the P-1 approximation (Lee and Buckius) was compared against the exact solution of Koram. The agreement was better than 1%. From the experimental results, the error in the simple technique for extinction coefficient measurement was estimated to be 11% for foams. These results are also useful for devising improvements to the simple technique for extinction coefficient measurement. Recommended improvements may increase the accuracy to 5% for foams, and furthermore enable use of the simple technique for fibrous glass and other insulation materials.

Comparison of the theory predictions to the overall conductivity data for fresh foam has been hampered by three factors: the lack of knowledge of the quantity of air entrained during foaming, the uncertainty in the conductivity of the solid polymer, and the nonavailability of test methods to measure the percentage of solid in struts versus membranes. Nonetheless, available data agrees with the model predictions for reasonable values of these parameters. Ongoing research at M.I.T. should eliminate these stumbling blocks in the near future.

The model predicts 25% of the heat transfer in low density foams by radiation. Using this knowledge, a method was devised for reducing the radiation in foams by adding strongly absorbing particles. A 6% reduction in overall heat transfer was observed in a high quality foam, where 10% of the solid polymer was replaced with a less expensive filler material.

REFERENCES

1.   Valenzuela, J.A., Glicksman, L.R. "Thermal Resistance and Aging of Rigid Urethane Foam Insulation". Proceedings of DOE-ORNL Workshop on Mathematical Modeling of Roofs, Nov. 3-4, 1981, Atlanta, GA.   CONF - 811179 pp. 261-262.

2.   Russell, H.W., "Principles of Heat Flow in Porous Insulators", Am. Ceramic Soc. J., v.18, 1935, pp. 1-5.

3.   Doherty, D.C., Hurd, R., Lester, G.R., "The Physical Properties of Rigid Polyurethane Foams", Chemistry and Industry, July 28, 1962, p. 1343.

4.   Schwartz, Abraham, Calculus and Analytic Geometry third ed., Holt, Rinehart and Winston, 1967, p. 722.

5.   Peters, H.C., Breunese, _J.N., Hermans, L.J.F., "Thermal Conductivity of Gaseous CFCl (Freon 11) and CF Cl (Freon 12) and Their Mixtures with N at 292K". International Journal of Thermophysics, Vol. 3, No. 1, 1982, pp. 27-34.

6.   Reid, R.C., Prausnitz, J.M., Sherwood, T.K., The Properties of Gases and Liquids third ed., McGraw-Hill, 1977, pp. 506-513.

7.   Tsederberg, N.V., Thermal Conductivity of Gases and Liquids, The M.I.T. Press, Cambridge, MA, 1965, pp. 153-157.

8.   Bretsznajder, S., Prediction of Transport and Other Physical Properties of Fluids, Pergamom Press, pp. 274-284.

9.   Deanin, R.D., Polymer Structure, Properties and Applications, Cahners Publishing Co., Boston, MA, 1972, p. 105.

10. Miller, M.L., The Structure of Polymers, Reinhold Publishing Corp., New York, p. 563.

11. Viskanta, R.   "Heat Transfer by Conduction and Radiation in Absorbing and Scattering Materials", Journal of Heat Transfer, Feb. 1965, pp. 143-150.

12. Fine, H.A., Jury, S.H., Yarbrough, D.W., McElroy, D.L., "Analysis of Heat Transfer in Building Thermal Insulation", Report Number ORNL/TM - 7481, Work performed under contract no. W-7405-eng-26, Dec. 1980.

13. Siegel, R., Howell, J.R., <u>Thermal Radiation Heat Transfer</u>, McGraw-Hill Book Co., 1972.

14. Houston, R.L., "Combined Radiation and Conduction in a Nongray Participation Medium that Absorbs, Emits and Anisotropically Scatters", Ph.D. Thesis, The Ohio State University, 1980.

15. Baxter, S., Jones, T.T., "The Physical Properties of Foamed Plastics and Their Dependence on Structure", Plastics and Polymers, April 1972, pp. 69-76.

16. Personal communication with Mark Sinofsky at M.I.T. during September - October, 1982.

17. Norton, F.J., "Thermal Conductivity and Life of Polymer Foams", Journal of Cellular Plastics, Jan. 1967, p. 24.

18. Skochdopole, R.E., "The Thermal Conductivity of Foamed Plastics", Chemical Engineering Progress, Vol. 57, No. 10, Oct. 1961, p. 57.

19. Newman, A.B., "Applying Diffusion Calculations to Drying Porous Solids", Chemical and Metallurgical Engineering, Vol. 38, No. 12, Dec. 1931, pp. 710-713.

20. Hottel, H.C., Sarofim, A.F., <u>Radiative Transfer</u>, McGraw-Hill, New York, 1967, pp. 326-342; 20-24.

21. Larkin, B.K., Churchill, S.W., "Heat Transfer by Radiation Through Porous Insulations", A.I.Ch.E. Journal, Vol.5, No.4, Dec. 1959, pp. 467-474.

22. Dayan, A., Tien, C.L., "Heat Transfer in a Gray Planar Medium with Linear Anisotropic Scattering", ASME Journal of Heat Transfer, Aug. 1975, pp. 391-396.

23. Lee, H., Buckius, R.O., "Scaling Anisotropic Scattering in Radiation Heat Transfer for a Planar Medium", ASME Journal of Heat Transfer, Vol. 104, Feb 1982, pp. 68-75.

24. Brandreth, D.A., Ingersoll, H.G., "Accelerated Aging of Rigid Polyurethane Foam", E.I. du Pont de Nemours and Co., Wilmington, Delaware.

25. Newman, A.B., "The Drying of Porous Solids: Diffusion Calculations", Transactions of American Institute of Chemical Engineers, Vol.27 (1931).

26. Rohsenow, W.M. and Choi, H.Y., Heat, Mass, and Momentum Transfer, Prentice-Hall, Inc., Englewood Cliffs, N.J., 1961, pp. 392-393 and pp.114-118.

27. Arpaci, V.S., Conduction Heat Transfer, Addison-Wesley Publishing Company, Reading, MA, 1966, pp.290-306.

28. Vdovin, N.A., "Thermophysical Properties of Some Polyurethanes and Filled Kaprolon", Plast.Massy.(USSR) (3), 48, 1977, p.48.

29. Personal communication with Dr. Sommerfeld of Mobay Chemical Corporation, Feb. 11, 1982.

30. Brochhagen, F.K., Schmidt,W., "Rigid Polyurethane Foam for Cold Insulation", Polyurethane Foams Proceedings of Symposium on Polyurethane Foams, ed. T.T. Healy, Iliffe Books, Ltd., London, 1964, p. 121.

31. Thermal Conductivity, Nonmetallic Solids, Vol.2 of Thermophysical Properties of Matter, TPRC Data Series, Y.S. Touloukian, ed., IFI/Plenum, New York, 1970, pp.949-966.

32. Schmidt, W., "Eigenschaften von harten Polyurethan- Schaumstoffen fur die Kalteisolierung", Kunstoffe, Vol.53, No. 7, July 1963, pp. 413-420.

33. Personal communication with Dr. Koram of the Owens Corning Fiberglas Corporation from August 1982 through October 1982.

34. Kerner, E.H., Proc. Phys. Soc. B69(1956) 802.

35. Viskanta, R., Grosh, R.J., "Effect of Surface Emissivity on Heat Transfer by Simultaneous Conduction and Radiation", International Journal of Heat and Mass Transfer, Vol.5, pp. 729-734, 1962.

36. Ozisik, M.N., Radiative Transfer and Interactions with Conduction and Convection, John Wiley and Sons, New York, 1973, pp. 24-25, 316-319.

37. Stern, C.H., "Radiation Characteristics of Rigid Foam Insulation", B.S. Thesis, Department of Mechanical Engineering, MIT, 1982.

38. Personal communication with Mr. Doug Reitz at the Massachusetts Institute of Technology, October 1982.

39. Personal communication with Mr. Frank Tyler of Building Products of Canada Ltd., April 1982.

40. Chu, C.M. and Churchill, S.W. Institute of Radio Engineers, Transactions on Antennas and Propagation, Vol. AP-4, No. 2, 142 (1956).

41. Powers, A.E., "Conductivity in Aggregates", Knolls Atomic Power Laboratory, Report Number KAPL-M-AXP-1, General Electric, Co., September 13, 1960.

42. Doyle, W.T., "The Clausius-Mossotti Problem for Cubic Arrays of Spheres", Journal of Applied Physics, Vol.49, No.2, February 1978, pp. 795-797.

APPENDIX A : RAW SCATTERING DATA FOR FOAMS

Table A-1 presents the raw forward scattering data for four foam samples. The first column (Sample A-1) is the same data (less backscattering data) used to compute the radiation properties presented as sample number 2 in Table 4-3. Using this column as a reference it appears that the other three samples are qualitatively similar to the first. One possible exception is polystryrene, which appears to scatter more energy at large angles.

Table A-1 : Raw Scattering Data

Sample	A-1	A-2	A-3	A-4
Foam	Polyurethane	Polyurethane	Polystyrene	Polyisocyanurate
Density (pcf)	1.76	2.74	2.20	1.86
Thickness (in)	0.0265	0.031	0.018	0.025
Deatector Angle (deg)	Output* Voltage (mV)	Output* Voltage (mV)	Output* Voltage (mV)	Output* Voltage (mV)
0	16.31	4.71	18.60	31.11
0.5	13.36	3.61	13.21	24.75
1.0	10.11	1.66	5.23	10.74
1.5	5.90	0.790	1.91	5.36
2.0	2.69	0.636	1.45	3.47
2.5	1.69	0.624	1.68	1.69
3.0	1.354	0.514	1.45	0.957
3.5	0.937	0.240	0.942	0.697
4.0	0.632	0.207	0.808	0.482
4.5	0.489	0.144	0.516	0.494
5.0	0.416	0.113	0.414	0.441
6.0	0.191	0.122	0.425	0.238
7.0	0.1397	0.0973	0.296	0.179
8.0	0.0939	0.0304	0.305	0.141
9.0	0.0634	0.0474	0.147	0.0833
10.0	0.0520	0.0404	0.147	0.0767
12.5	0.0445	0.0197	0.0952	0.0485
15.0	0.0219	0.0128	0.0595	0.0268
17.5	0.0171	0.00813	0.0416	0.0258
20.0	0.00920	0.00488	0.0435	0.0122
22.5	0.00777	0.00566	0.0405	0.0197
25.0	0.00572	0.00412	0.0331	0.0139
30	0.00410	0.00250	0.0319	0.00571
35	0.00212	0.00237	0.0154	0.00428
40	0.00219	0.00214	0.0132	0.00410
45	0.00133	0.00126	0.0149	0.00353
50	0.00117	0.00054	0.0110	0.00254
55	0.00124	0.00062	0.0100	0.00332
60	0.00091	0.00042	0.00826	0.00205
65	0.00065	0.00052	0.00759	0.00146
70	0.00060	0.00042	0.00478	0.00118
75	0.00021	0.00032	0.00245	0.00068
80	0.00021	0.00021	0.00154	0.00030
85	0.00011	0.00032	0.00052	0.00050

*Normalized to Incident Laser Power of 81.39 mW and Detector Calibration Constant of 4.91 mW/ cm^2 - mV.

Appendix B : Integral Solution Technique for
Boundary Problem in Simplified Radiation Analysis

One way to model the boundary radiation effects while utilizing the Rosseland diffusion approximation in the insulation core is to use a technique analogous to the integral technique for fluid flow boundary layer problems. The foam is divided into three regions, as shown in Figure 3-2. The Rosseland diffusion approximation is applied in the central region, from T_a to T_b (equation 3-25). Rate equations are derived for regions "A" and "B". The problem is thus reduced to solution of three equations in three unknowns, exactly as for the Optically Thin Limit Model of section 3.3.3.1.

Using the integral technique, the shape of the temperature profile is assumed from T_1 to T_a and from T_b to T_2. The rate equation for boundary "A" consists of an energy balance at the imaginary plane "A" in Figure 3-3, where the various contributions (Q_a, Q_b, Q_c, Q_d) are determined from the assumed temperature profile. The radiant flux from the core (Q_e) is determined from the Rosseland one-way flux. Conduction is assumed uncoupled from radiation in the boundary regions, and thus conduction heat flux (q_c) is assumed constant across the boundary region. If q is the net heat flux passing through the foam, the energy balance at "A" is given by:

$$q = q_c + (Q_a + Q_b + Q_c + Q_d - Q_e) \qquad \text{(A-1)}$$

and the conduction heat flux is given by:

$$q_c = k_{s+g} \frac{T_1 - T_a}{L_a} \qquad \text{(A-2)}$$

For brevity, the integrations required to determine Q_a, Q_b, Q_c, Q_d are omitted. The results are given below for the following assumed temperature profile:

$$T(x) = \left[T_1^4 - \frac{x}{L_a} (T_1^4 - T_a^4) \right]^{\frac{1}{4}} \tag{A-3}$$

This temperature profile leads to a minimum of algebra in the integrations. The scattering coefficient is assumed zero, thus the absorption coefficient and extinction coefficient are equal. Q_a is given by equation A-4:

$$Q_a = 2E_3(KL_a) \, \rho_1 \left[C_1 \sigma T_1^4 - C_2(T_1^4 - T_a^4) \right] \tag{A-4}$$

where:

$E_3(KL_a) = $ third exponential integral of KL_a

$\rho_1 = $ reflectivity of surface "1" (assumed diffuse)

$C_1 = 1 - 2E_3(KL_a)$

$C_2 = \frac{2\sigma}{KL_a} \left[\frac{1}{3} - KL_a E_3(KL_a) - E_4(KL_a) \right]$

$E_4(KL_a) = $ fourth exponential integral of KL_a

Q_b is determined from equation A-5:

$$Q_b = 2E_3(KL_a) \, \varepsilon_1 \, T_1^4 \tag{A-5}$$

where ε_1 is the emissivity of surface "1". Q_c is determined from equation A-6:

$$Q_c = C_1 \, T_2^4 + C_2(T_1^4 - T_2^4) \tag{A-6}$$

Finally Q_d is given by:

$$Q_d = Q_e \cdot \rho_1 \left[2 \, E_3(KL_a) \right]^2 \tag{A-7}$$

All that remains is determination of Q_e. From Hottel (20), the Rosseland one-way flux is given by:

$$Q_e = \sigma T_a^4 + \frac{8\sigma}{3K} T_a^3 \left(\frac{dT}{dx}\right)_a + \frac{2\sigma}{K^2}\left[T_a^3 \left(\frac{d^2T}{dx^2}\right)_a + 3T_a^2 \left(\frac{dT}{dx}\right)_a^2 \right] \qquad \text{(A-8)}$$

+ higher order terms...

Note that in the limit where K approaches infinity, the central core behaves as a blackbody at temperature T_a. Recall that in the optically thin limit model, the core was assumed to behave as a blackbody. The first derivative of temperature at boundary "A" may be estimated by:

$$\left(\frac{dT}{dx}\right)_a \simeq \frac{-q}{K_{s+g} + \frac{16\sigma}{3K}T_a^3} \qquad \text{(A-9)}$$

and by differentiation of equation A-9 with respect to x, it may be shown that:

$$\left(\frac{d^2T}{dx^2}\right)_a \simeq \frac{-T_a^2 \left(\frac{dT}{dx}\right)_a^2}{\left(\frac{k_{s+g}\, K}{16\,\sigma}\right) + \frac{1}{3}T_a^3} \qquad \text{(A-10)}$$

Using equations A-2 through A-10 in equation A-1 results in an implicit rate equation for q through boundary "A" in terms of T_1 and T_a only. A similar analysis was performed for boundary "B" but is omitted for brevity.

The resulting simultaneous equations were solved on a computer using a converging trial and error approach. The results were found to be slightly

less accurate than those of the optically thin limit model for the gray, pure absorption case, in comparison to the exact results of Fine, et al. (12). However, the integral solution was found to be less sensitive to the arbitrary selection of boundary optical thickness. In the case of highly non-gray materials this model might therefore be useful. Since foams were experimentally shown to be approximately gray, this model is felt to be unnecessarily unweildy.

END OF FILM

PLEASE REWIND